U.S. Department
of Transportation

**Federal Highway
Administration**

Impedance Spectroscopy for the Evaluation of Corrosion Inhibitors in Highway Deicers

FOREWORD

This report, *Impedance Spectroscopy for the Evaluation of Corrosion Inhibitors in Highway Deicers*, presents results of research on the corrosion-inhibiting potential of commercial deicers determined using electrochemical impedance spectroscopy (EIS). Results of the tests showed that EIS can be employed for the long-term study of corrosion in reinforced concrete and can be used for rating deicing formulations as to their corrosivity. The report is intended for researchers and technologists who have a general interest in deicers and, in particular, for persons responsible for highway deicing.

Charles J. Nemmers, Director
Office of Engineering
Research and development

NOTICE

1. Report No. FHWA-RD-96-178	2 PB97-142764	3. Recipient's Catalog No.

4. Title and Subtitle IMPEDANCE SPECTROSCOPY FOR THE EVALUATION OF CORROSION INHIBITORS IN HIGHWAY DEICERS		5. Report Date March 1997
		6. Performing Organization Code
7. Author(s) Ugo Bertocci		8. Performing Organization Report No.
9. Performing Organization Name and Address Office of Engineering R&D Federal Highway Administration 6300 Georgetown Pike McLean, VA 22101-2296		10. Work Unit No. (TRAIS) 3E4b0142
		11. Contract or Grant No. NAS/NRC RA Project Na 27.01.00.04
12. Sponsoring Agency Name and Address Office of Engineering R&D Federal Highway Administration 6300 Georgetown Pike McLean, VA 22101-2296		13. Type of Report and Period Covered Final Report February 1992 - July 1994
		14. Sponsoring Agency Code

15. Supplementary Notes

This work was performed while the author held a National Research Council/FHWA Research Associateship.
The FHWA Research Advisor was John W. Peart.   FHWA Contact: Robert A. Kogler

16. Abstract

Electrochemical impedance spectroscopy (EIS) measurements were carried out on steel bars embedded in concrete blocks that were immersed in aqueous solutions of commercial deicing salts, many of which had corrosion inhibitors added. The effectiveness of the inhibitors was assessed by monitoring the evolution of the EIS results for a period of 11 months. EIS was supplemented with open circuit potential and polarization measurements. From the results, a semiquantitative ranking of the commercial deicers tested as to their corrosivity could be derived.

17. Key Words electrochemical impedance spectroscopy, corrosivity, corrosion inhibitors, deicers, sodium chloride, calcium magnesium acetate, rebar corrosion	18. Distribution Statement No restrictions. This document is available to the public through the National Technical Information Service, Springfield, VA 22161.		
19. Security Classif. (of this report) Unclassified	20. Security Classif. (of this page) Unclassified	21. No. of Pages 82	22. Price

Form DOT F 1700.7 (8-72)   Reproduction of completed page authorized

This form was electronically produced by Elite Federal Forms, Inc.

SI* (MODERN METRIC) CONVERSION FACTORS

APPROXIMATE CONVERSIONS TO SI UNITS

Symbol	When You Know	Multiply By	To Find	Symbol
		LENGTH		
in	inches	25.4	millimeters	mm
ft	feet	0.305	meters	m
yd	yards	0.914	meters	m
mi	miles	1.61	kilometers	km
		AREA		
in²	square inches	645.2	square millimeters	mm²
ft²	square feet	0.093	square meters	m²
yd²	square yards	0.836	square meters	m²
ac	acres	0.405	hectares	ha
mi²	square miles	2.59	square kilometers	km²
		VOLUME		
fl oz	fluid ounces	29.57	milliliters	mL
gal	gallons	3.785	liters	L
ft³	cubic feet	0.028	cubic meters	m³
yd³	cubic yards	0.765	cubic meters	m³

NOTE: Volumes greater than 1000 l shall be shown in m³.

Symbol	When You Know	Multiply By	To Find	Symbol
		MASS		
oz	ounces	28.35	grams	g
lb	pounds	0.454	kilograms	kg
T	short tons (2000 lb)	0.907	megagrams (or "metric ton")	Mg (or "t")
		TEMPERATURE (exact)		
°F	Fahrenheit temperature	5(F-32)/9 or (F-32)/1.8	Celcius temperature	°C
		ILLUMINATION		
fc	foot-candles	10.76	lux	lx
fl	foot-Lamberts	3.426	candela/m²	cd/m²
		FORCE and PRESSURE or STRESS		
lbf	poundforce	4.45	newtons	N
lbf/in²	poundforce per square inch	6.89	kilopascals	kPa

APPROXIMATE CONVERSIONS FROM SI UNITS

Symbol	When You Know	Multiply By	To Find	Symbol
		LENGTH		
mm	millimeters	0.039	inches	in
m	meters	3.28	feet	ft
m	meters	1.09	yards	yd
km	kilometers	0.621	miles	mi
		AREA		
mm²	square millimeters	0.0016	square inches	in²
m²	square meters	10.764	square feet	ft²
m²	square meters	1.195	square yards	yd²
ha	hectares	2.47	acres	ac
km²	square kilometers	0.386	square miles	mi²
		VOLUME		
mL	milliliters	0.034	fluid ounces	fl oz
L	liters	0.264	gallons	gal
m³	cubic meters	35.71	cubic feet	ft³
m³	cubic meters	1.307	cubic yards	yd³
		MASS		
g	grams	0.035	ounces	oz
kg	kilograms	2.202	pounds	lb
Mg (or "t")	megagrams (or "metric ton")	1.103	short tons (2000 lb)	T
		TEMPERATURE (exact)		
°C	Celcius temperature	1.8C + 32	Fahrenheit temperature	°F
		ILLUMINATION		
lx	lux	0.0929	foot-candles	fc
cd/m²	candela/m²	0.2919	foot-Lamberts	fl
		FORCE and PRESSURE or STRESS		
N	newtons	0.225	poundforce	lbf
kPa	kilopascals	0.145	poundforce per square inch	lbf/in²

* SI is the symbol for the International System of Units. Appropriate rounding should be made to comply with Section 4 of ASTM E380.

(Revised September 1993)

TABLE OF CONTENTS

TABLE OF CONTENTS (continued)

LIST OF FIGURES

LIST OF TABLES

INTRODUCTION

The purpose of this work can be considered as twofold. On the one hand, it is to see if the addition of corrosion inhibitors to commercial deicing mixtures, which contain mainly chloride salts, can be shown to affect the corrosion behavior of steel in concrete. On the other hand, since the principal measurement method employed is electrochemical impedance spectroscopy (EIS), another purpose of the work is to evaluate EIS as a way to obtain information on the corrosion of steel in concrete under fairly realistic conditions. Some information on the effect of corrosion inhibitors added to deicing salts [1] or on the corrosion characteristics of alternate deicers [2] is available in the literature, but these studies were carried out in aqueous solutions rather than on steel embedded in concrete.

Several workers have applied EIS to the study of corrosion of steel in concrete [3-7], showing that valuable information on the electrochemical processes going on at the metal/concrete interface can be obtained with this method.

In order to simulate the conditions that are encountered in the field, the measurements were carried out on steel rods embedded in concrete and exposed to various solutions by immersion. The changes in electrochemical behavior were observed over a time period as long as practicable. Two batches of samples were cast, in one of which the concrete was contaminated with chloride by using water containing some NaCl. In this way, the effectiveness of corrosion inhibitors could be tested for reinforced concrete in which chloride was already present.

To speed up the penetration of the components of the solution into the concrete, this was cast so as to obtain high porosity, and the curing time in water was shortened, since, on the other hand, the requirements of mechanical strength were minimal. The thickness of the concrete separating the steel rods from the external surface was kept to a minimum (about 1 cm).

In order to facilitate the onset of corrosion by maintaining an oxygen-rich environment inside the concrete [4,8], the specimens were subjected to a regular regime of immersion in the solution from Monday to Friday, and were allowed to dry over the weekend. This regime was followed, with a few exceptions, for several months.

The deicers tested were commercial products, so that their exact composition and the exact nature of their inhibitors are not known. Two of the deicers were in liquid form, presumably because the chloride salt is mainly $MgCl_2$, while the others contained mainly NaCl. Another deicer tested was a mixture of magnesium and calcium acetates, generally known as calcium magnesium acetate (CMA). Since this material does not contain chlorides, it is considered to be much less aggressive and has some favorable properties from an environmental viewpoint [9]. These materials were tested for comparison against a sodium chloride solution, as well as against an alkaline solution saturated in $Ca(OH)_2$, which should approximate the composition of the liquid in the pores of concrete, and should tend to maintain the steel in the passive state. For all solutions containing chlorides, their concentration was close to 0.2 M.

EXPERIMENTAL PROCEDURES

SOLUTIONS EMPLOYED IN TESTS

Eight different solutions were used in the tests, as given in Table 1. In the following, the solutions will be referred to using the numbers given in the table. The chloride content of the deicer solutions was checked by chemical analysis; the results are shown in Table 2.

The schedule used in immersing the concrete specimens in solution is summarized in Table 3, from which one can see when the regular routine of immersion on Monday and removal on Friday was altered. Immersion of the specimens was done in 600-mL glass beakers, in which about 150 mL of solution was poured. The level of the liquid reached about 1 cm below the top of the concrete block, and care was taken to prevent the solution from wetting between the protruding rods. When the concrete samples were removed from solution, they were washed with distilled water in order to prevent surface accumulation of salts.

SAMPLE PREPARATION

The samples prepared for the measurements consisted of concrete cylinders, 5 cm in diameter and 12.7 cm in length, in which four rods of A36 steel, with millscale removed to a 32 finish, 0.635 cm in diameter and 11.4 cm in length, were embedded in a square pattern. About 2.5 cm of the rods extended outside the upper end of the concrete cast. To prevent corrosion at the exit points of the rods, 2.2 cm of them were coated with polyurethane paint. The top of the concrete cylinder, from which the rods protruded, was also coated with polyurethane paint. The bare part of the rods inside the concrete was 7.6 cm long, giving a surface area of 15.5 cm^2. The rods terminated about 1.3 cm from the bottom of the cast. Shape and size of the specimens are shown in Figure 1. The rods were marked with numbers from 0 to 3, clockwise starting from a rod painted red on top. When necessary to distinguish between rods in the same concrete block, these numbers will be used.

The concrete was made by mixing 1 part cement (by weight) and 3 parts fine sand with 0.5 parts water. Half of the casts were made with distilled water and half were made with a 0.6 percent solution of NaCl. All specimens were cured in water for 8 days and then left dry for about 2 months.

Twenty specimens were employed for the long-term tests. Table 4 gives the letters designating them, together with the type of concrete (chloride-contaminated or plain) and the solution number in which they were immersed. As the table shows, for two solutions (#2 and #4), duplicate specimens were used.

In order to promote uniform corrosion conditions for the four rods, they were kept short-circuited unless measurements were being performed. However, the short circuit was removed on day 144 of the long duration tests on the duplicate specimens PP, B, TT, and E to see how the open circuit potentials would vary when left to drift separately.

3

PRELIMINARY MEASUREMENTS

A number of measurements were taken prior to the start of the long-term tests. They are summarized in Table 5. From the impedance measurements carried out between two rods to a minimum frequency of 5 mHz on the dry specimens, a zero frequency resistance could not be extrapolated, but it was possible to determine the electrode capacitance as well as the resistance between two rods. The results show that the specimens are reasonably uniform and that their electrical resistance is not very high, even in the dry condition.

Repeated experiments showed that about 15 g of water could be absorbed by a dry concrete block. Some of them were weighed again after taking them out of solution on day 141 of the test and again before immersion 3 days later. Some more blocks were weighed after removal from solution on day 161 and were weighed again before immersion 11 days later. The data collected are given in Table 6.

MEASUREMENT METHODS

OPEN CIRCUIT POTENTIAL MEASUREMENTS

Open circuit potential (E_{oc}) measurements were carried out on the rods of a specimen, just before and after an EIS measurement. The E_{oc} of the four rods short-circuited, as well as that of the individual rods after the breaking of the short circuit, was measured versus a Saturated Calomel Electrode (SCE). It was noted that the E_{oc} of the various rods tended to drift apart immediately after breaking the short circuit, and that the voltage differences could become quite substantial. Since EIS measurements lasted several hours, the E_{oc} values read after an EIS run could be assumed to represent the true value that an individual rod tended to take. However, changes from measurement to measurement, with a time interval of about 10 days, indicated that the corrosion conditions varied significantly. More importantly, E_{oc} measurements showed that, in spite of all efforts to provide the same environment to the rods in a concrete block, this could not be maintained.

In order to learn how the E_{oc} of individual rods would behave when undisturbed by short-circuiting, on the 144th day of the long duration tests the short circuit between rods on the duplicate specimens B, PP, E and TT (solutions #2 and #4) was removed. From that day, E_{oc} measurements on these rods were carried out more frequently, more or less on a daily basis.

POLARIZATION MEASUREMENTS

To supplement the information provided by EIS, a number of potentiodynamic scans were carried out at sweep rates varying from 1 to 0.1 mV/s. The potential range examined went from +100 to -700 mV vs. SCE. The main purpose of these measurements was to help in estimating the value of the proportionality constant B between electrode resistance and corrosion current, but they also provided a useful comparison between the electrochemical behavior as presented by EIS and that shown by direct current methods.

The polarization curves were analyzed by mean of a commercial curve-fitting routine, from which polarization resistance, corrosion current density, and anodic and cathodic Tafel slopes could be obtained.

ELECTROCHEMICAL IMPEDANCE SPECTROSCOPY (EIS) MEASUREMENTS

Measurement Conditions

The frequency range employed in most EIS measurements was 1 kHz to 0.5 mHz. At the high-frequency end, indication of an additional time constant was observed, as shown in the Nyquist plot of Figure 2. Sagoe-Crentsil et al. [6] have attributed the presence of a high-frequency time constant to the dielectric response of the concrete matrix. However, the capacitance associated with this time constant was much larger than that found by the aforementioned authors. Considering the likelihood of instrumental artifacts at high frequency and the scant relevance that the dielectric properties of concrete have in the present work, it was concluded that no useful information could be obtained at frequencies higher than a few hundred hertz.

7

On the other hand, the EIS measurements had to reach very low frequencies in order to allow an estimate, however approximate, of the corrosion resistance. Keeping into account the availability of equipment and manpower, it was decided to strive to carry out two EIS measurements each working day in the frequency range of 1 kHz to 0.5 mHz, with a total duration of about 3 hours, plus an additional 14-hour (overnight) measurement in the range of 1 kHz to 0.1 mHz. Therefore, in a full week with no mishaps, 14 EIS measurements could be carried out. In some instances, the measurements were extended to even lower frequencies, but the results were not encouraging. The experimental points at the lowest frequencies showed a very high degree of scatter, so they did not afford a better view of the very slow electrochemical processes. This may be related to the tendency of the E_{oc} to drift with time, indicating a change in the corrosion conditions, and thus violating the stationary conditions necessary for EIS.

An SCE was always employed as a reference electrode (RE), so all electric potential values reported are referred to the SCE. As a counterelectrode (CE), initially another of the four rods (mostly rod 3) was used; but in order to keep the rods undisturbed unless unavoidable, two stainless steel rods immersed in the solution surrounding the concrete block were used, starting from day 153 from the start of the measurements. No differences in the results that were attributable to the change in CE could be noticed.

Most of the EIS data were collected at the open circuit potential, but measurements at potentials other than E_{oc} were carried out on a number of specimens. Such measurements can provide valuable information about the mechanisms that control the electrode kinetics [10].

Data Analysis

The EIS results were examined by fitting them to equivalent circuits, using commercially available software. The circuits that best simulated the experimental data were either a resistor R_{ct} (representing the charge transfer resistance of the electrode) in parallel with a capacitor C_{dl} (the double layer capacitance), followed by a resistor R_{sol} (the resistance of the electrolyte in the concrete), as shown in Figure 3a, or the one with an additional constant phase element (CPE) of slope 1 (45°) in series to the resistor, as shown in Figure 3b. In both cases, a significant dispersion had to be attributed to the double layer capacitor, which is described by an exponent n varying from 0.8 to 0.9. The CPE probably is the effect of diffusional transport in the concrete, as a Warburg impedance over a finite length diffusion layer. The fitting routine was able to provide an extrapolation to zero frequency, giving a value for the overall electrode resistance R_o. This value, which for the circuit in Figure 3a coincides with R_{ct}, is, in general, very inaccurate and may be regarded as an order of magnitude at best, since the scattering of the experimental points at the lowest frequencies was very large.

Some EIS spectra could be fitted only if a third equivalent circuit was used that contained a second resistor-capacitor (RC) combination, instead of a Warburg impedance, as shown in Figure 3c. Such spectra were observed only in the later stages of long-term tests, especially for electrodes exhibiting low resistance. This equivalent circuit is similar to that proposed by Wenger and Galland [11].

Examples of EIS spectra, together with simulated curves giving the best fit, are shown in Figure 4 for the cases with a single time constant (Figure 3a), and in Figures 5a and 5b for the circuit of Figure 3b for cases where the two time constants were close (Figure 5a) and well separated (Figure 5b). Figure 6 shows a spectrum where the third circuit (Figure 3c) gives the best fit. The spectra shown are among the best, extending to very low frequencies with a minimum of scatter. From many of the data obtained, however, the extrapolation to zero frequency is much more uncertain.

EXPERIMENTAL RESULTS

E_{oc} MEASUREMENTS

The E_{oc} values of the individual rods tended to drift away from each other when the short circuit between them was broken. Therefore, the only significant values were those taken at the end — rather than at the beginning — of an EIS measurement, 3 hours or more after breaking the short circuit. It should be kept in mind, however, that the rod employed as a working electrode (WE) for EIS, and also the one used as a CE before day 153, did not drift freely because they were connected to the potentiostat. Those specimens whose short circuit was removed on day 144 gave a better indication of the extent of the long-term E_{oc} fluctuations. The E_{oc} values were of particular interest because of the correlation found between electrode potential and electrode resistance that was detected by EIS.

Figures 7 and 8 show the E_{oc} values for the four specimens that were no longer short-circuited, while Figures 9 to 12 show the E_{oc} values of the rods that were not affected after an EIS measurement. The scatter among rods in the same concrete block, as well as large fluctuations with time, are quite evident. Also, it is almost impossible to find significant differences between the E_{oc} in Cl-free and Cl-contaminated concrete. Part of the record in Figure 8a is shown in an expanded version in Figure 13, where vertical lines mark the day in which the specimens were put back in solution after drying for a few days. It is evident that, in this specimen, E_{oc} fluctuated periodically in correlation with the dry-wet cycle, with potentials becoming more negative during the immersion period.

POLARIZATION MEASUREMENTS

Potentiodynamic scans on passive electrodes showed a pronounced hysteresis, a phenomenon also reported by Hakkarainen [12]. For specimen H in solution #6, the difference in the potentials at zero current is about 300 mV, even at low scan rates. The polarization resistance R_p, obtained from the tangent at I=0 varied by a factor of two depending on the direction of the scan, and tended to be smaller than R_o extrapolated from EIS. The values of the Tafel slope coefficients β_a and β_c obtained by curve fitting were unreliable, particularly β_a in the positive scan and β_c in the negative scan. The curve is shown in Figure 14. There is an indication of a second cathodic process in the negative scan, beginning at about -300 mV.

The difference between scans in the positive and negative directions can be seen clearly in Figures 15a and 15b, taken on specimen G in solution #5. The corrosion rate of this electrode, although low, is larger than that of specimen H, and, in this case, R_p is about 1.5 $M\Omega \cdot cm^2$, in reasonable agreement with R_o obtained from EIS, 2.2 $M\Omega \cdot cm^2$. In the negative scan (Figure 15a), conditions close to a limiting cathodic current of about 30 nA/cm^2 between -50 and -300 mV can be seen; in the positive scan, the limiting current is anodic, of about the same magnitude and voltage range. These curves with very steep slopes are probably the reason that no reliable values could be obtained for the Tafel coefficients by curve fitting.

Electrodes giving higher corrosion rates show less hysteresis in the potentiodynamic scans, with both potentials at I=0 more negative, as seen in Figure 16 for specimen C in solution #2. The evaluation of the Tafel slope coefficients is nevertheless difficult, in spite of the absence of

11

limiting currents, particularly on the cathodic side. Values of β_a and β_c vary by a factor of 4 (from 70 to 300 mV/decade), depending on the number of points used for the least-squares fitting. R_p, on the contrary, may vary less than 20 percent, depending on the direction of the scan (16 ± 3 kΩx cm^2), and agree well with R_{ct} obtained from EIS (15 ± 1 k$\Omega \cdot$ cm^2).

Similar results have been obtained on specimen D in solution #3 (Figure 17) and specimen NN in solution #1 (Figure 18). Table 7 collects some of the values obtained from polarization measurements.

EIS

Measurements at the Open Circuit Potential

Electrode Resistance

The evolution of the electrochemical behavior during the exposure tests was followed by carrying out EIS at E_{oc}. For each of the solutions examined, the EIS results are summarized in Figures 19 through 26. Each figure shows the value of the resistance R_o obtained by extrapolation of the experimental data to zero frequency, as well as the resistance R_{ct} associated with the first time constant when two time constants could be resolved. The first time constant is indicated by an open point; the second time constant is indicated by a solid point. If only one time constant could be obtained, R_o and R_{ct} coincide, and the solid point lies inside the open point. Circles are used for data from Cl-contaminated concrete and squares are used for Cl-free concrete. These data are plotted against time as well as against the electrode potential E_m, which was the E_{oc} of the rod used as WE at the time of the measurement.

All resistance data show a fairly clear correlation between the logarithm of the resistance and electrode potential E_m, and, with the exception of solution #8, the linear relationship is similar. Plotting the logarithm of the reciprocal of the resistance as a function of E_m, least-squares fit parameters are collected in Table 8, and plots for seven of the eight solutions combined are shown in Figure 27. Two sets of points are plotted, one corresponding to the zero frequency limit R_o, the other corresponding to R_{ct} when the equivalent circuit has two time constants. The linear least-squares fit for the two sets of points gives parallel lines — the admittance of the faster process (R_{ct}) being about one-half of an order of magnitude larger than that of R_o at each potential. The data for the eight solutions are shown separately in Figures 28 and 29.

To investigate if there were significant changes with time in the corrosion mechanisms, the combined sets of points were split in two for the first and the second half of the testing time. The resulting plots are shown in Figures 30a and 30b. As corrosion increased with time in many specimens, the plot corresponding to the second half has more points at lower potentials and larger admittances, which might explain a slight increase in the slopes of the linear least-squares fit. Altogether, however, no clear changes of behavior with time can be detected.

Double-Layer Capacitance

The double-layer capacitance C_{dl} obtained from EIS is, in most cases, of the order of 50 μF/cm^2, which would be compatible with a somewhat rough surface, either bare or covered by

a thin passive film. For three of the eight solutions (#7, #3, and #1), C_{dl} increases steadily with time, as shown in Figure 31a; however, in solutions #8, #5, and #2, it remains approximately constant, as shown in Figure 31b. The capacitance of electrodes immersed in solution #6 (CMA) exhibited a continuous decrease during the test period, going from 40-50 $\mu F/cm^2$ to about 25 $\mu F/cm^2$ (Figure 32a). Solution #4 (Figure 32b) showed a marked peak after about 2 months of testing, but later values were similar to the initial ones.

If all values are plotted together, there is an inverse relationship between electrode potential E_m and C_{dl}, as shown in Figure 33. Remembering that the electrode resistance R_o (or R_{ct}) decreases at lower E_m, R_o and C_{dl} appear to be inversely correlated. The dependence of the logarithm of C_{dl} on electrode potential, however, is much weaker than that of R_o and it is not linear.

The value of the exponent n is a measure of the frequency dispersion of the capacitance. Its departure from the limiting value of 1 signals the presence of a depressed semicircle in the Nyquist plot. In solid electrodes, the capacitance always exhibits a certain frequency dispersion, and n is always less than 1. The reason for this is not well understood, but it is believed that the smaller n is, the greater is the lack of uniformity of the electrode surface. The values of n obtained in this work are collected in Figure 34. It can be seen that n decreases when C_{dl} increases, in direct relation with the electrode potential E_m. Since this puts n in an inverse relationship with the corrosion resistance, its decrease is probably caused by an increase in surface roughness due to anodic attack.

Solution Resistance

Immersion in the different solutions also has an effect on the electrical resistance R_{sol} of the concrete. While both NaCl and the strongly alkaline "pore" solution had little effect on R_{sol} (as shown in Figure 35), all others seem to cause it to increase with time. Such an increase is rather small for solutions #1, #3, and #4 (as shown in Figure 36), but is very substantial for solutions #2, #5, and #6, particularly in the last month (as shown in Figure 37). Since these increases can be seen both in the Cl-free and Cl-contaminated specimens, they must be due to some components in the deicers. It is interesting to note that all of the ones that cause the greatest increases contain magnesium in fairly large amounts. Even solution #4, which, as seen in Figure 36, exhibits the largest R_{sol} increase among the intermediate group, contains about 10 percent magnesium salts.

It was necessary to confirm that the changes in R_{sol} are due to reactions with the deicing solutions and to investigate whether the resistance changes occur uniformly inside the concrete blocks. To do this, EIS measurements were carried out on specimen G in solution #5, which is mainly a 0.1 M solution of $MgCl_2$, and on specimen XX, solution #6, which is approximately 0.4 M in Mg^{++}; the embedded steel rods were used as RE, and the values were compared with those obtained with the SCE as RE placed, as usual, in the solution surrounding the block. Since the rods are in a square pattern (so the distance between rods on opposite corners of the square is $\sqrt{2}$ times that between adjacent rods), comparison between the value of R_{sol} obtained using either the adjacent rod or the rod farther away as RE provides an additional way to estimate the uniformity of the electrical resistance of the concrete. The results are shown in Table 9.

From the lack of dependence of C_{dl} on the RE, it appears that no artifacts are introduced by changing the position of the RE. Therefore, the differences in R_{sol} give an idea of how the resistivity of the concrete varies within the block. When the RE is the SCE, R_{sol} is at a maximum, indicating that most of the resistance is concentrated in the outer layer of the block where presumably the diffusing Mg^{++} ions have reacted with the concrete. The data from the inner rods give a much lower R_{sol}, showing that the resistivity increase is less inside, which supports the hypothesis that the resistivity is affected by diffusion from outside. The resistance ratio between the far rod (N. 2) and the adjacent rod (N. 3) is 1.14 ± 0.01 — less than the distance ratio of about 1.4 — further supporting the picture of the electrical resistivity increasing from the center to the surface of the block. These results are in agreement with chemical analysis of concrete exposed to CMA, which showed precipitation of magnesium products at the interface [13].

EIS Measurements on Polarized Electrodes

EIS measurements have been carried out at potentials other than E_{oc} on a number of specimens. The relationship between electrode admittance and measurement potential is shown in Figure 38. The straight line represents the linear fitting of the values of R_{ct} for all measurements carried out at E_{oc}. When polarized, electrodes otherwise showing little or no corrosion (more positive E_{oc}, high R_0 at E_{oc}) cathodically exhibit some of the characteristics of corroding electrodes, e.g., lower values of the corrosion resistance, larger capacitance, and more depressed semicircles (lower n). These electrodes, when polarized anodically, tend to show increased resistance along the line describing the average relationship between electrode resistance and potential for electrode measurements at open circuit. Only at the most positive potentials tested was there an indication of reversal in the resistance trends.

Electrodes that show indications of corrosion, on the contrary, when polarized do not appear to change their resistance by very much, as seen in Figure 38 for specimen J and rod 1 of specimen C. The resistance appears to decrease by anodic as well as by cathodic polarization. The capacitance increases on the cathodic side and decreases on the anodic side, following the general trend of the EIS data taken at E_{oc}. It must be mentioned that the measurements taken under anodic polarization show great scattering at the lowest frequencies, as shown, for instance, in Figure 39, so that estimation of R_0 becomes impossible.

The difference in behavior between corroding and non-corroding electrodes can even be seen in rods embedded in the same piece of concrete, as shown by the data pertaining to rods 1 and 0 of specimen C, whose results are presented in Table 10.

DISCUSSION

PROBLEMS ENCOUNTERED WITH THE MEASUREMENTS

The extremely long time constants for some of the processes are the main difficulty for EIS on reinforced concrete. These time constants require that the measurements be extended to very low frequencies. This is, in itself, a major problem because of the long timeframe involved, which limits the amount of data that can be reasonably acquired. Unfortunately, the problem cannot be easily overcome, even by extending the measurements to the microhertz range while increasing productivity by employing several measurement systems. This is because another factor — stability in the open circuit potential E_{oc} — produced unreliable results at low frequencies, as illustrated in Figure 40. Large changes in E_{oc} from day to day, but occasionally occurring within a much shorter timeframe, have been documented in Figures 7 and 8.

Because of the slow electrochemical processes that we attempt to measure, it should be kept in mind that the values of R_o, obtained by curve-fitting and extrapolation to zero frequency, are often little more than educated guesses. Figure 41, to illustrate this point, shows an EIS spectrum as well as that simulated with the values obtained by curve-fitting. The reader can infer a great deal of the curve from what can be considered only its beginning.

On the other hand, it should be remembered that these problems are present in polarization measurements, as shown in that section earlier in this report. Potentiodynamic scans slow enough to detect the slow processes would have durations comparable with EIS, so that the scattering of the data would not be less and the separation of the time constants of different processes, which EIS provides, would not be obtained.

The electrical resistance of the concrete, on the other hand, has never been a significant problem. This may be due to the relatively high porosity of the concrete, as well as to the small thickness separating the rods in a block from each other and from the surrounding electrolyte.

SIGNIFICANCE OF THE EIS MEASUREMENTS

For the interpretation of the experimental results, an important point is the relationship between EIS data and corrosion rates. The formula relating the differential resistance (provided by EIS) and corrosion rate i_{corr} (as expressed in current density terms) is:

$$i_{corr} = \frac{B}{R_p} = \frac{\beta_a \beta_c}{\ln 10 (\beta_a + \beta_c) R_p} \tag{1}$$

where β_a and β_c depend on the slopes of the anodic and cathodic polarization curves. These values cannot be obtained directly by EIS and have to be assumed or inferred from other kinds of measurements. Even if these values are not known, their range is not very wide, so that an order of magnitude of the corrosion current can be estimated with some confidence by taking 100 mV/decade for both β_a and β_c.

15

Polarization measurements are commonly used to obtain values for the anodic and cathodic coefficients β_a and β_c. The measurements taken in this work are described in detail in the section called "Polarization Measurements" earlier in this report. The values obtained from the potentiodynamic scans, however, are quite uncertain; they have not greatly improved the reliability of the estimates of β_c based on the slope of the charge transfer admittance $1/R_{ct}$ vs. potential as obtained from Figure 27 or Figure 30b, 110 mV/decade or 123 mV/decade, respectively. Examination of the values in Table 7 does not suggest that β_a is systematically larger than β_c. Therefore, the best estimate for $B=\beta_a\beta_c/(\beta_a+\beta_c)\ln 10$ is probably 0.026, corresponding to Tafel slopes of $RT/2F$, or 120 mV/decade. The error introduced by the uncertainty of β_a and β_c should not exceed 20 percent.

A problem arising in the EIS results is whether, when two time constants can be measured, the first (R_{ct}) or the second (R_o) is more relevant for estimating the corrosion rate of the steel rods. In general, the corrosion rate is considered to be given by the zero-frequency limit of the electrode impedance, i.e., R_o. Although this would be correct if one wanted to know how fast a given steel structure embedded in concrete would corrode, independently of which mechanism is rate-determining, R_{ct} is probably a better choice for laboratory measurements aimed at estimating the corrosion rate in a given environment, in the absence of hindering transport processes. It is desirable to know the effect of the inhibitor on the charge transfer reaction

$$Fe=Fe^{++} \tag{2}$$

when oxygen is in good supply and diffusion is rapid.

Under the assumption of uniform corrosion rate and an oxidation valency of 2 for iron, Figure 27 can be represented as a corrosion rate (R_{corr}):

$$R_{corr} = \frac{i_{corr}M_{Fe}}{zFd_{Fe}} = \frac{BM_{Fe}}{R_p zFd_{Fe}} \tag{3}$$

where $z=2$, according to (2), M_{Fe} is the atomic weight of iron and d_{Fe} is its specific gravity, and R_p is either R_{ct} or R_o. To obtain the corrosion rate in micrometers per year ($\mu m/yr$) the electrode admittance is multiplied by 0.30. The result is shown in Figure 42. When R_o is very large, only one time constant is measured and the corrosion rate is so small as to be completely negligible, no matter how uncertain the values may be. When the electrode impedance is relatively small, R_o and R_{ct} differ, and for the reasons given above, as well as to take the most conservative approach, the corrosion rate derived from R_{ct} should be considered.

As for the mechanisms that account for the electrochemical data, it appears that the steel is passive above -300 mV/SCE, with a cathodic limiting current of about 30 nA/ cm². When passivity breaks down, the current increases to 1 to 2 $\mu A/cm^2$. Such a current density corresponds to an admittance of roughly 100 $\mu S/cm^2$ for the charge transfer process corresponding to R_{ct}. Current densities of this magnitude are not those given by the zero frequency limit of the impedance R_o, which also accounts for some of the transport process. R_o is, in any case, rather poorly known because of low frequency data scatter, but it corresponds to current densities at least three times smaller — 200 to 500 nA/cm². The actual steady-state current that can be sustained by oxygen reduction is probably smaller, since the EIS data are

based on imprecise extrapolation. Also, the current density distribution may be distorted by uneven oxygen diffusion.

EFFECT OF THE INHIBITORS

NaCl and "Pore" Solutions

The samples immersed in NaCl and in the alkaline "pore" solutions, #7 and #8 respectively, form the reference points for the assessment of the effect of the corrosion inhibitors. For NaCl, Figure 25a shows a fairly steady decrease in corrosion resistance, although some of the rods (at least in the first 150 days) have exhibited passive behavior. A significant scattering is also seen in E_{oc} (Figure 12a), but the values tend to become more negative with time, particularly after 200 days. It is also not surprising that the differences between Cl⁻-free and Cl⁻-contaminated specimens tend to disappear.

The alkaline "pore" solution is supposed to provide a non-aggressive environment that maintains the steel in the passive state. Figure 26a shows that this is indeed the case, with no great change with time, except in the Cl⁻-contaminated specimen. This solution departs from the others in the relationship between E_m and electrode admittance. As seen in Figure 29d, the slope calculated from the least-squares fitting is much less than that for the other solutions, and the correlation coefficient is so low that the relationship is doubtful. The very large scatter may be only a consequence of the large values of R_0, which make EIS results unreliable. Polarization curves are also in agreement, as shown in Figure 43. The corrosion current is estimated as about 2 nA/cm², with an R_p of 10 MΩ·cm². The potential at which the current is zero can be shifted by 150 mV depending on the direction of the scan. The lack of corrosive attack is also indicated by the nearly constant value of the electrode capacitance with time (shown in Figure 31b).

The values of E_{oc}, with a few exceptions in Cl⁻-contaminated concrete, do not vary much with time, as shown in Figure 12b. These values, however, are lower than those for the other solutions for the same values of the electrode admittance. This is probably due to the high pH that was maintained by the very alkaline solution.

An interesting observation is that a completely different behavior, as far as corrosion is concerned, as that of solutions #7 and #8 is accompanied by a very similar behavior in the electrical resistance of the concrete (as shown in Figure 35). Both solutions do not seem to influence R_{sol} in any systematic way. Clearly, an increase in electrical resistance of the concrete is not a necessary condition for corrosion protection.

Alternative Deicer, CMA

Although CMA does not contain inhibitors, it was interesting to test its behavior in this study. The data obtained for this solution (solution #6) are shown in Figures 5a, 11b, 14, 24, 29b, 32a, 37, and 38. As shown in Figure 24a, the specimens immersed in CMA (solution #6) exhibit a decreasing corrosion rate with time. In the first couple of months of the long-term tests, a somewhat smaller resistance could be measured in Cl⁻-contaminated concrete, but later on the results became indistinguishable from those in Cl⁻-free concrete. In only a few instances

could two time constants be inferred from the data (see, for example, Figure 5a). In general, the extrapolated value of R_o, no matter how uncertain, was so large as to indicate that no corrosion was taking place. The electrode capacitance (Figure 32a) decreased steadily with time, probably because of a thickening of the passive layer. The open circuit potential (Figure 11b), apart from a few stray points, tends to become more positive with time. Very low corrosion rates also are estimated from potentiodynamic scans (Figure 14). EIS measurements that are several hundred millivolts negative from E_{oc} show a decrease of R_{ct} due to a higher rate of oxygen reduction, while polarization in the positive direction has only a very modest effect on the anodic reaction (Figure 38).

The electrical resistance of the concrete (R_{sol}) exhibited a steady increase over the whole testing time, with values in the last measurements being about 50 times the initial ones (Figure 20c) — consistent with the high magnesium content of the solution. The non-uniform resistivity of the concrete caused by Mg^{++} diffusion in the concrete block is illustrated by the R_{sol} values shown in Table 9 and discussed previously.

Deicer #1

The data for deicer #1 (NaCl with a phosphate inhibitor) are shown in Figures 9, 18, 19, 28, 31a, and 36. As shown in Figure 19a, in spite of considerable scatter and a countertrend towards higher R_o's for one rod in the first half of the testing period, the electrode resistance decreases with time and the difference between Cl-free and Cl-contaminated concrete disappears. E_{oc} also becomes more negative with time, while C_{dl} increases; this suggests increased roughening of the steel surface. The resistance of the concrete (R_{sol}) does not increase significantly. The corrosion behavior in this deicer solution is hardly distinguishable from that of NaCl alone, indicating that the inhibitor does not provide any detectable protection.

Deicer #2

The results for deicer #2, a liquid containing magnesium chloride with a citrate inhibitor, are shown in Figures 7, 9b, 16, 20, 28b, 31b, 37, and 39. This deicer has given contradictory results that are quite clearly illustrated in Figures 7a and 7b. In Cl-contaminated concrete (Figure 7a), the E_{oc} of all rods eventually reached values indicating passive behavior, while in Cl-free concrete the opposite occurred, so that the E_{oc} of all rods was in the active range. In the same concrete block, passive and corrosive behavior could be measured at the same time, as shown by rods 1 and 0 of specimen C (see Table 9 and Figure 38). In spite of having duplicate specimens for this solution, no clear trend can be found for either of the resistances (R_o or R_{ct}) obtained from EIS.

As shown in Figure 31b, the electrode capacitance does not increase with time, suggesting that little corrosion is taking place. Since noise measurements carried out on specimens immersed in this deicer had shown a pattern that is often associated with localized attack, it is possible that the results obtained can be understood as indicating a fair degree of corrosion inhibition, but with some pitting occurring intermittently. The only clear trend is in R_{sol} (Figure 37), which increases with time — a common feature of solutions containing magnesium.

A comparison with the results in uninhibited NaCl might lead to a conclusion that deicer #2 causes some slowing of the corrosion process.

Deicer #3

The results for deicer #3, a solid salt not yet on the market that is made mainly of NaCl, are shown in Figures 6, 10a, 17, 21, 28c, 31a, and 36. The trends that are demonstrated with time are: decreasing electrode resistance (see Figure 21a); disappearing differences between Cl⁻-free and Cl⁻-contaminated specimens; and E_{oc} becoming more negative (see Figure 10a). The only notable peculiarity of the EIS spectra in this solution is that they are better represented by the circuit in Figure 3c, as shown in Figure 6.

The general impression is that there is hardly any difference between the corrosion behavior in this solution and that found in the NaCl solution that is free of inhibitors. The electrical resistance of the concrete increases a little with time, but it is difficult to find a behavior that significantly differs from that of NaCl. The electrode capacitance increases with time (see Figure 31a), also indicating that the steel rods are corroding.

Deicer #4

The results for deicer #4, a solid containing 10 percent $MgCl_2$ in NaCl and with a proprietary lignosulfate polymeric inhibitor known as PCI™, are shown in Figures 5b, 8, 10b, 13, 22, 28d, 32b, 36, 40, and 41. Although one of the rods in Cl⁻-free concrete was able to remain in the passive state for more than 200 days (as shown in Figure 22a), eventually all of the electrodes exhibited a fairly low resistance. Also, the trend in E_{oc} is toward more negative values (see Figure 8).

The electrode capacitance, after a sharp increase in the first 2 months of testing, went back to rather low values, but with a tendency to increase with time. The electrical resistance of the concrete increased five or six times, less than for solutions containing large amounts of magnesium, but in agreement with the fact that magnesium is about 10 percent in the salt mixture. There is some evidence that corrosion is being slowed in this solution, but the protection afforded by the inhibitor appears to be insufficient over time.

Deicer #5

The results for deicer #5, a liquid containing $MgCl_2$ and also PCI™ as an inhibitor, are shown in Figures 11a, 15, 23, 29a, 31b, and 37. As with all solutions containing magnesium, the concrete resistance increases markedly with time, as shown in Figure 37. The rods embedded in Cl⁻-free concrete never indicated a deterioration in corrosion resistance, and even those rods in Cl⁻-contaminated concrete (although exhibiting lower R_{ct}) seemed to remain at about the same value or even better with time. A behavior consistent with little corrosion is also shown by the electrode capacitance (see Figure 31b). Because R_o and R_{ct}, as well as E_m, varied little with time, the plot in Figure 29a does not allow a good estimate of the relationship between electrode resistance and potential.

19

Keeping in mind that the lowest value of R_{ct} is 0.1 M$\Omega \cdot$cm^2, the corrosion rate appears never to have exceeded 1 μm/yr, and in general was 5 to 10 times less. Both the electrode resistance and the open circuit potentials have time trends suggesting that the inhibitor is much more effective in this deicer formulation than in deicer #4.

CONCLUSIONS

The tests carried out have shown that EIS can be employed for the long-term study of corrosion in reinforced concrete and can be used for ranking the deicer formulations as to their corrosion effects. Since the tests were carried out not on bare steel electrodes, but on rods embedded in concrete, the time required for obtaining meaningful results is quite long. This report describes about 1 year of testing, and yet, in some cases, it appears that a longer exposure would have been desirable in order to obtain more clear-cut results. On the other hand, the data collected should be more reliable than tests on bare metal because they probe the ability of the various inhibitors to penetrate the concrete, as well as the capability to counteract the deleterious effects of chloride salts that have already diffused into the material.

As could be expected when measuring a process such as corrosion that depends on a large number of variables — from metal surface inhomogeneities to variations in the permeability of the concrete cast — the data have shown a large amount of scatter, even for rods embedded in the same block. It was therefore very useful to have repeated data in what nominally were identical conditions. In this work, 80 electrodes were employed to study 8 different solutions. This lends some confidence to the conclusions drawn from the results, but a larger set of experiments would have been, at times, highly desirable.

Under the conditions employed in this study, a good correlation between electrode potential and corrosion resistance (and, by implication, corrosion rate) has been found. This correlation has been observed by many workers [14 -15], and has led to the suggestion that a simple and inexpensive way to monitor the corrosion conditions of steel in reinforced concrete is that of measuring E_{oc}. However, there are two caveats to be given on this point. The first is that in this research, the dry-wet alternation has always provided oxygen good access into the concrete, so that the reaction rates were presumably not limited by the cathodic reaction. The second is that although the correlation between E_m and electrode resistance is beyond question, it is largely of statistical nature, and there is substantial scatter in the points, which might entail an uncertainty of more than one order of magnitude in corrosion rate for the same value of E_m.

Taking into account the overall agreement between open circuit potential measurements and EIS data (whether electrode resistance or capacitance), as well as the results of the potentiodynamic scans, one can rank the six deicers from the least to the most corrosive. This can be done by choosing the most relevant of these quantities — the charge transfer admittance $Y_{ct} = 1/R_{ct}$ — and plotting its logarithm versus time and calculating a linear least-squares fit (as shown in Figure 44). The higher the slope of the straight line, the greater the corrosion rate becomes, indicating a failure to protect the steel on the part of the inhibitor. Using this value for a semiquantitative ranking, the results can be summarized in Figure 45, from the least to the most corrosive, as follows:

1. Solution #6 CMA.
2. Solution #5.
3. Solution #2.
4. Solutions #1 and #4.
5. Solution #3 and Solution #7 NaCl.

One should not attach too much meaning to small differences in the numerical value of the slopes. Therefore, it is doubtful that deicers #1 and #4 behave significantly better than plain road salt (#7). While CMA is clearly superior to all other deicers, deicer #5 and, to a much more limited extent, deicer #2, have been shown to be able to slow corrosion. Finally, it should be mentioned that the ranking of deicers #6, #5, and #4 is essentially similar to that given by other researchers who tested the same products on bare steel [2].
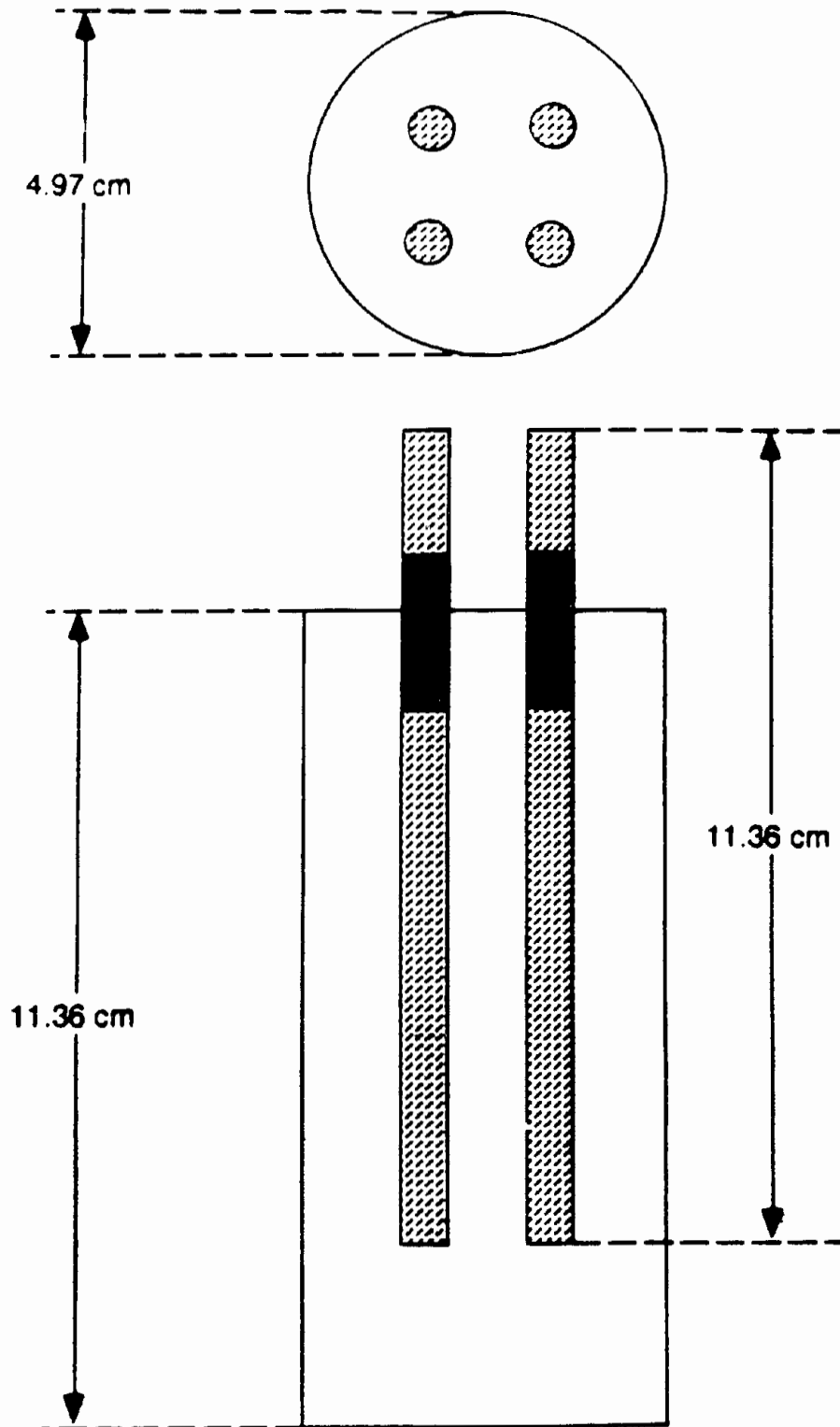
Figure 1. Shape and size of the cast concrete specimens.
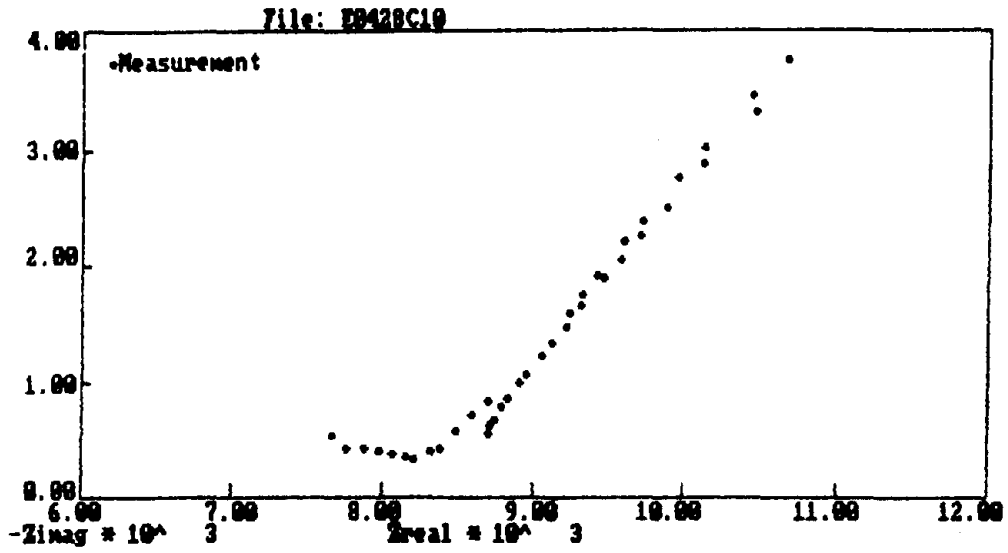
(a) Experimental results: specimen C, solution #2, E_m=-409 mV/SCE
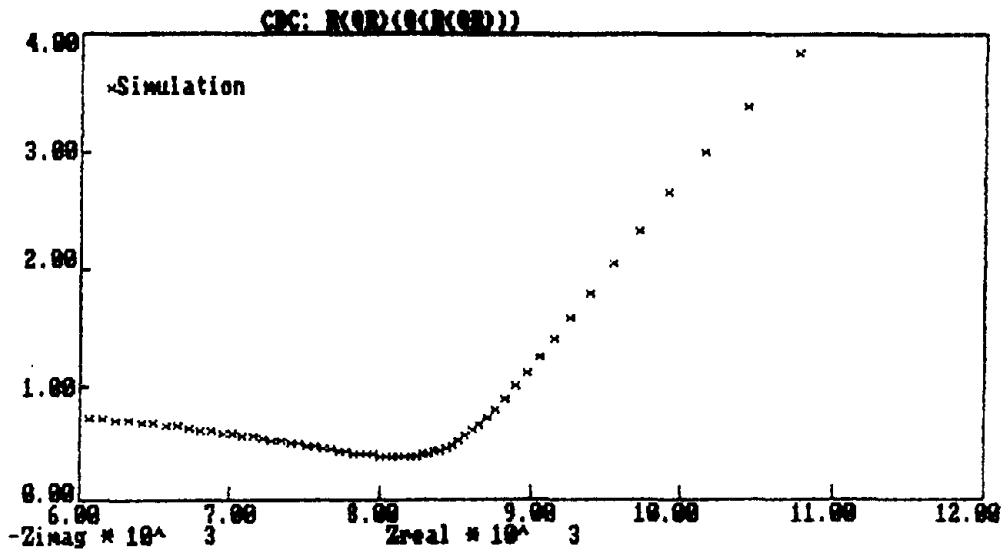
(b) Simulated curve: C=2.9 µF/cm , R=9 kΩxcm^2.

Figure 2. Nyquist plot of the high-frequency end of a typical EIS spectrum.
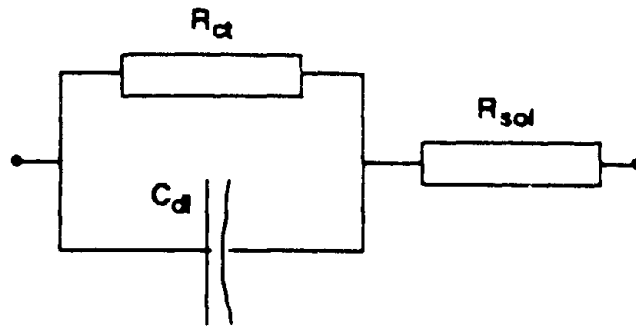
(a)
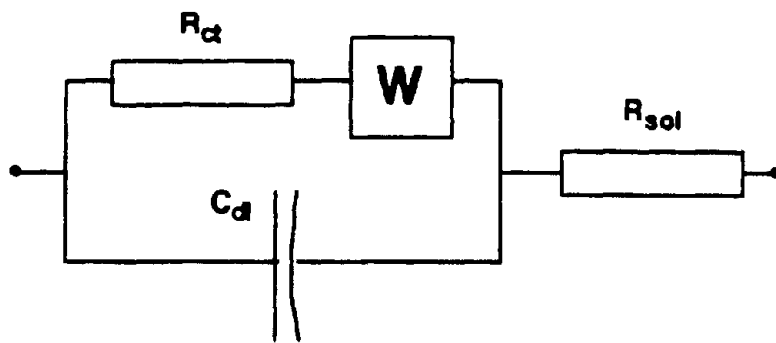
(b)
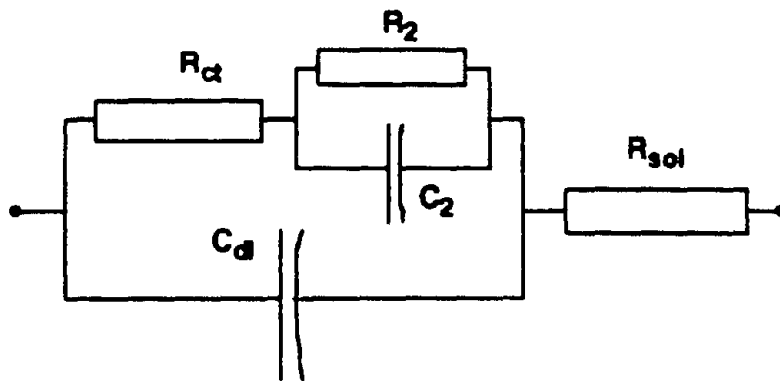
(c)

Figure 3. Equivalent circuits used for curve-fitting Eis results.
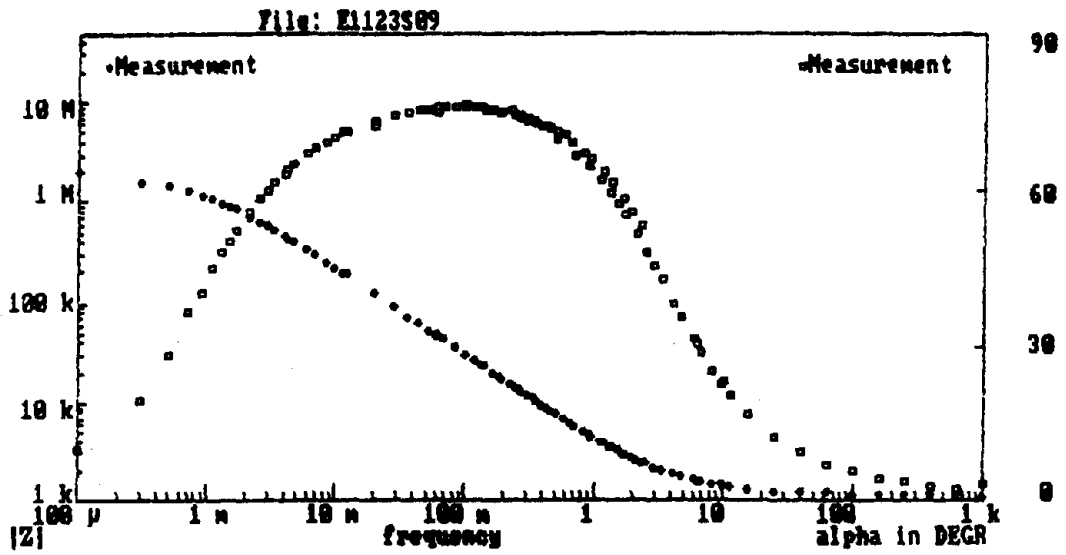
(a) Bode plot.
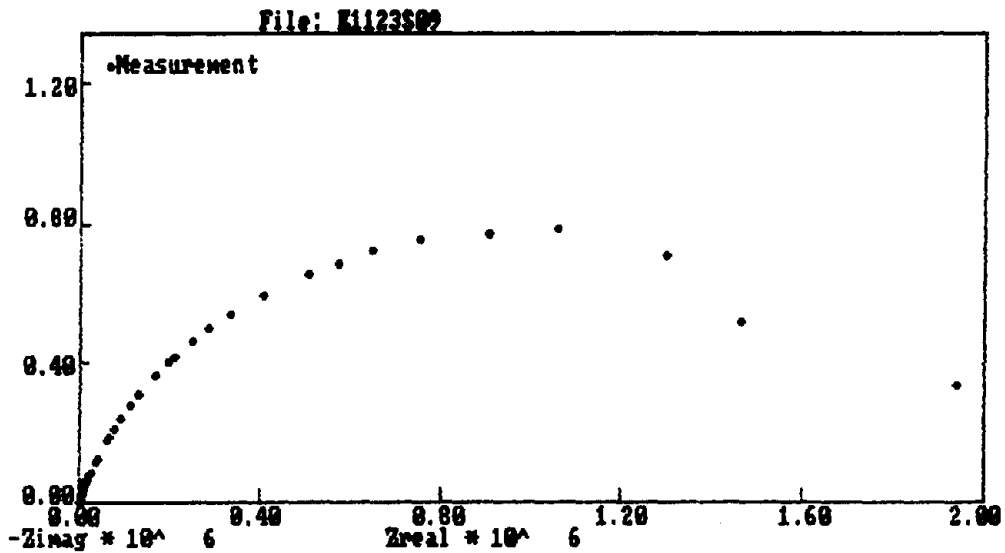
(b) Nyquist plot.

Figure 4. EIS spectra corresponding to the equivalent circuit in Figure 3a (specimen SS, solution #3, $E_m = -287$ mV/SCE).
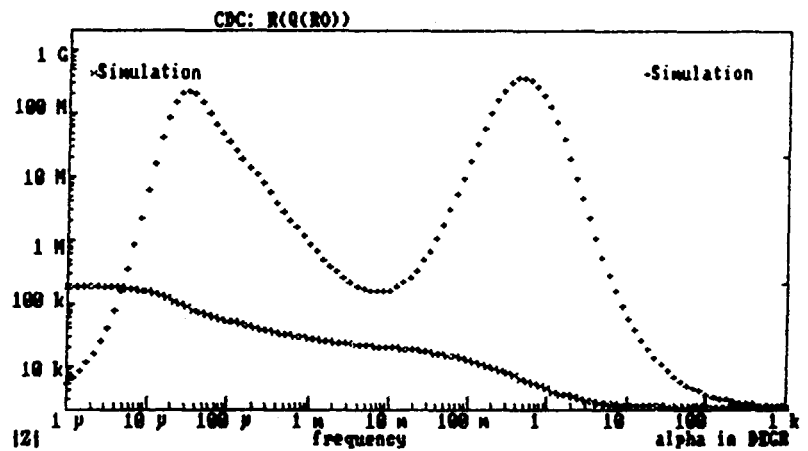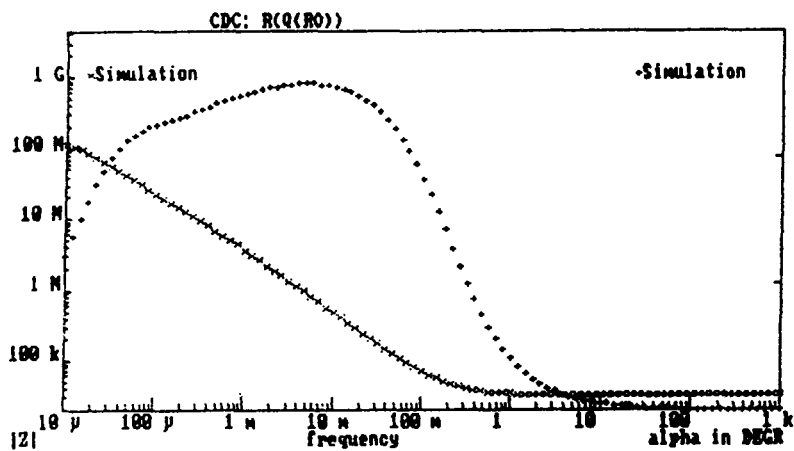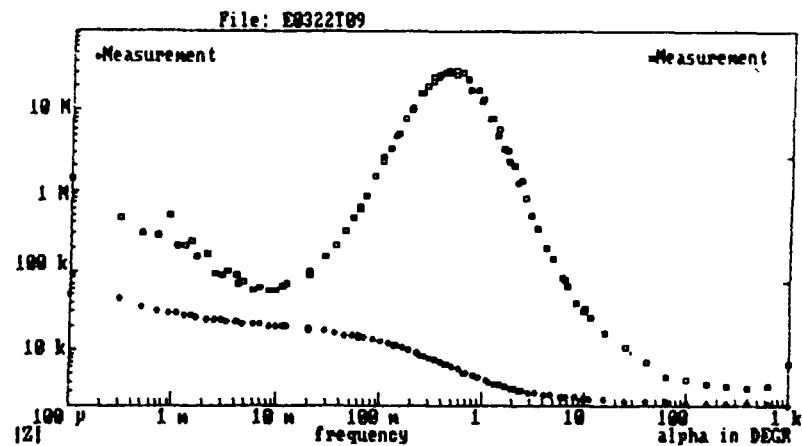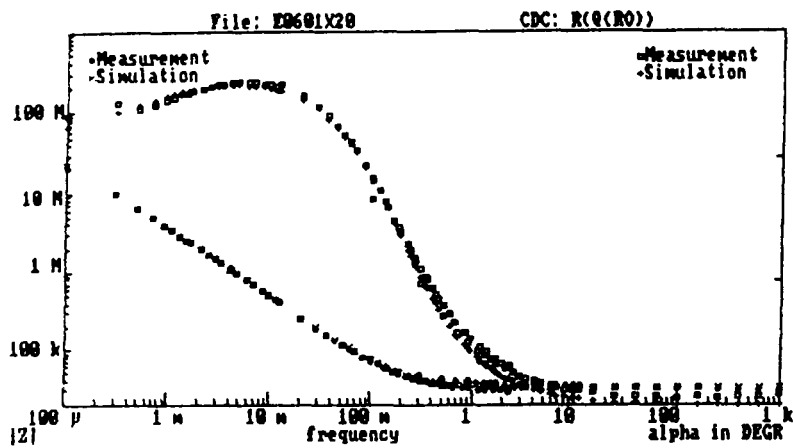
(a) Small separation of the time constants
(specimen XX, solution #6, E_m=-85 mV/SCE).

(b) Large separation the time constants
(specimen TT, solution #4, E_m=-437mV/SCE).

Figure 5. Experimental and simulated Bode plots corresponding to the equivalent circuit in Figure 3b.

(a) Experimental plot.
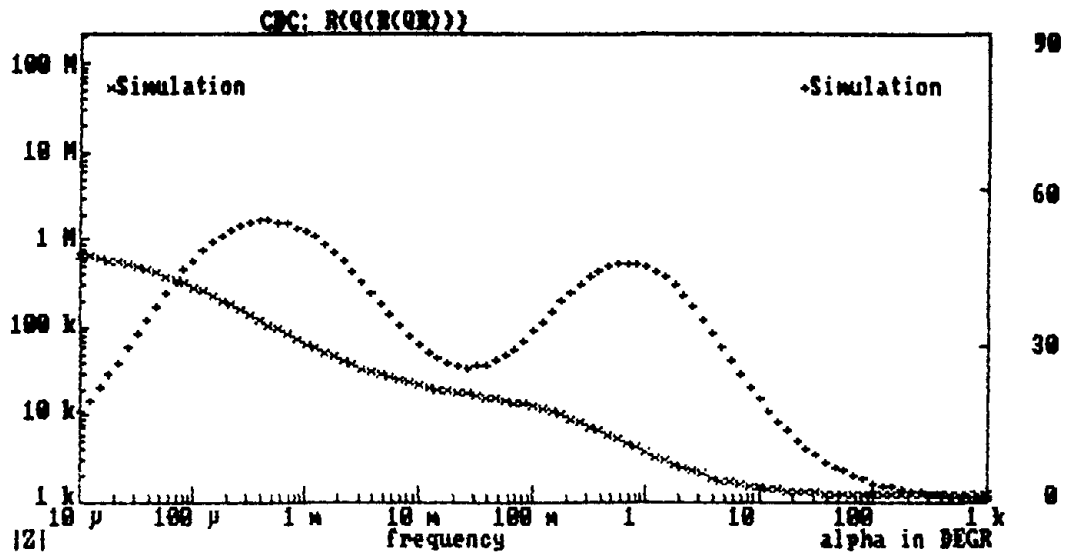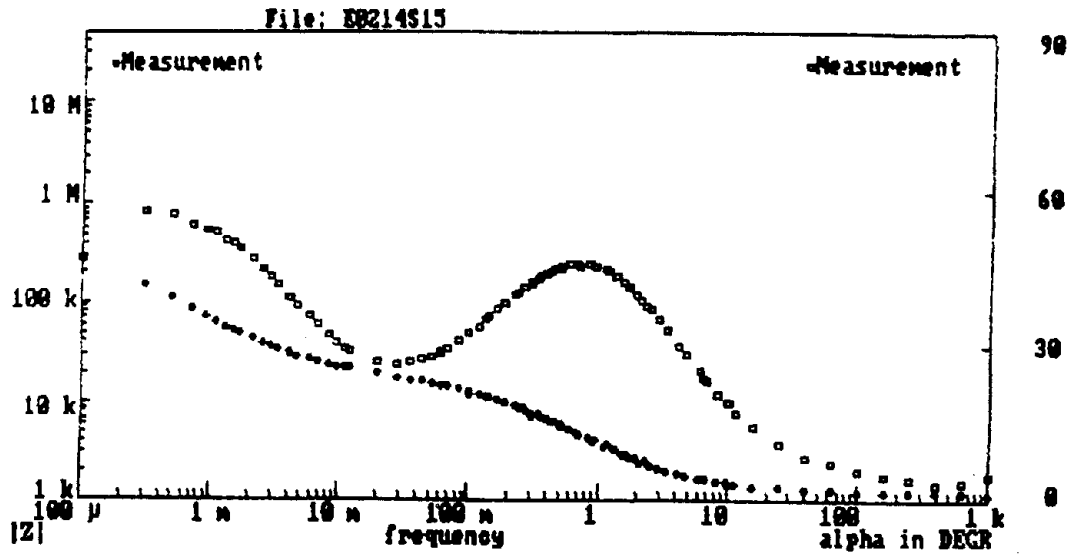
(b) Simulated plot.

Figure 6. Experimental and simulated Bode plots corresponding to the equivalent cicruit in Figure 3c (specimen SS, solution #3, E =-367 mV/SCE).
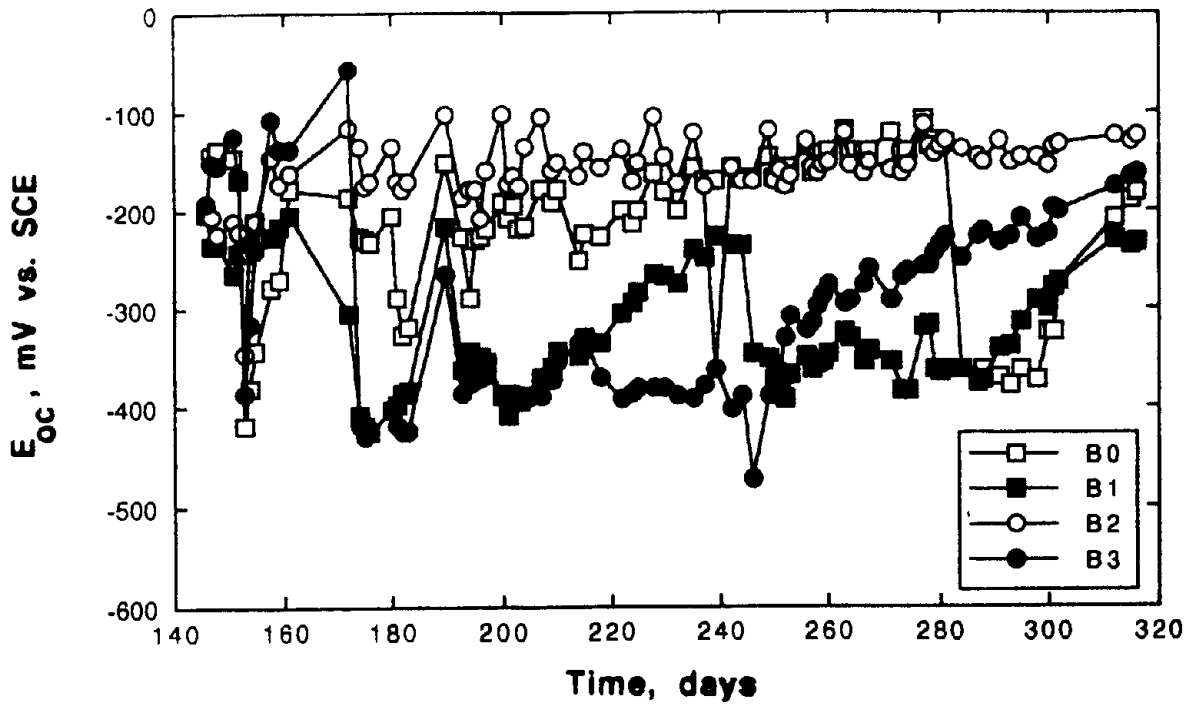
(a) Solution #2, Cl⁻-contaminated concrete.
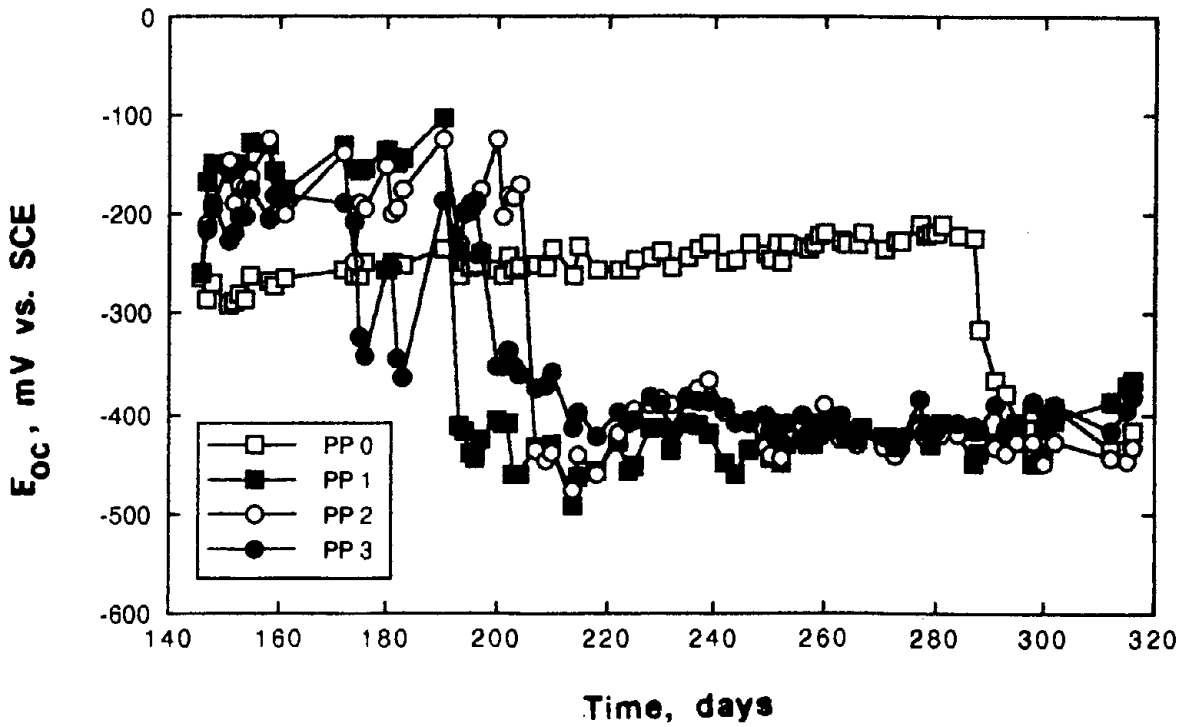
(b) Solution #2, Cl⁻-free concrete.

Figure 7. Open circuit potentials of rods not shortcircuited (solution #2).
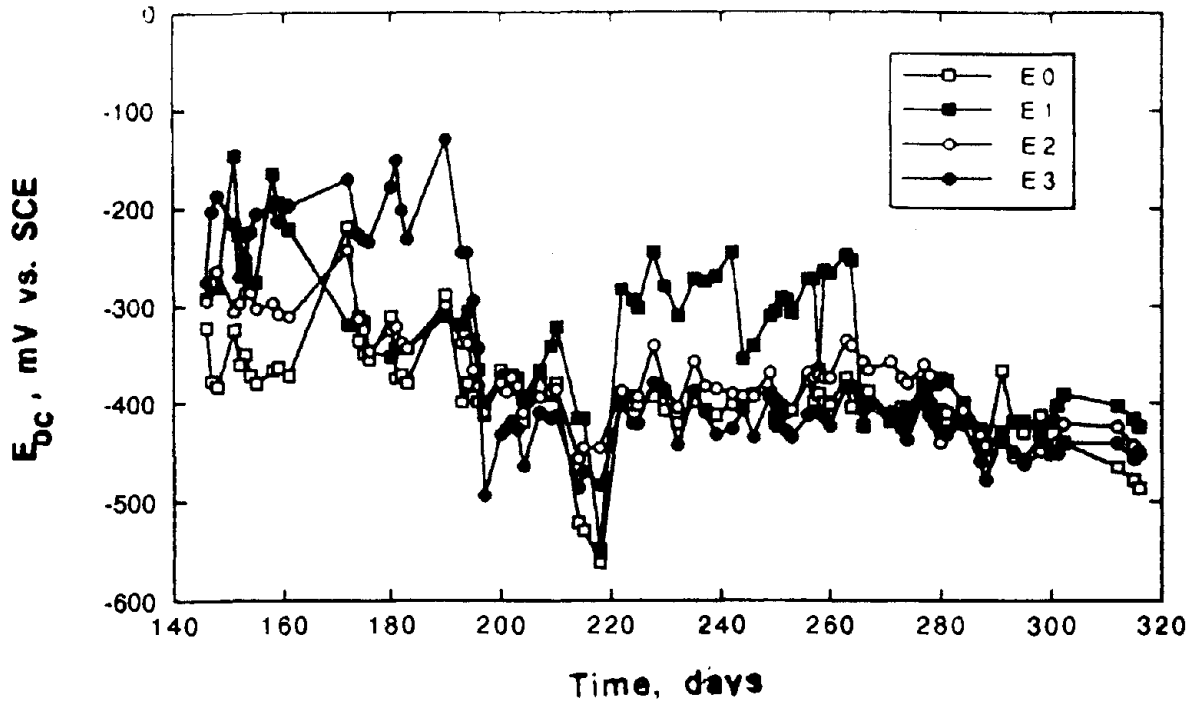
(a) solution #4, Cl⁻-contaminated concrete.
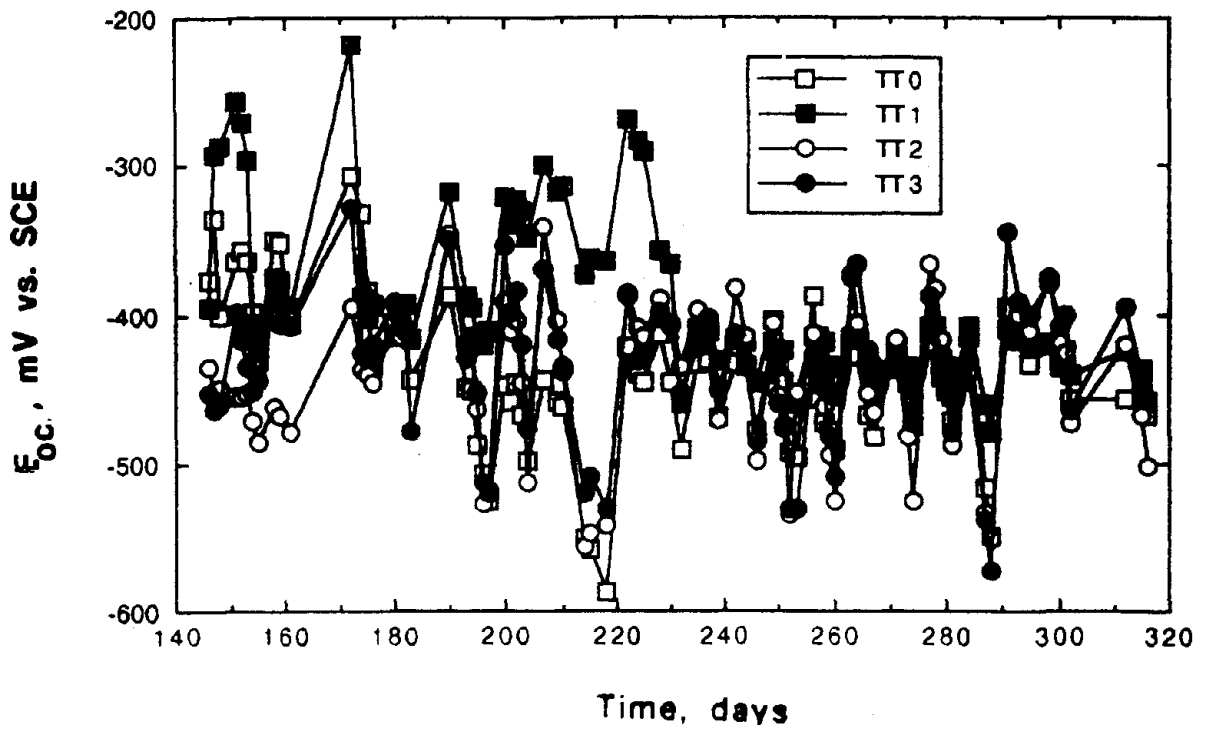
(b) solution #4, Cl⁻-free concrete.

Figure 8 . Open circuit potentials of the rods not shortcircuited (solution #4).
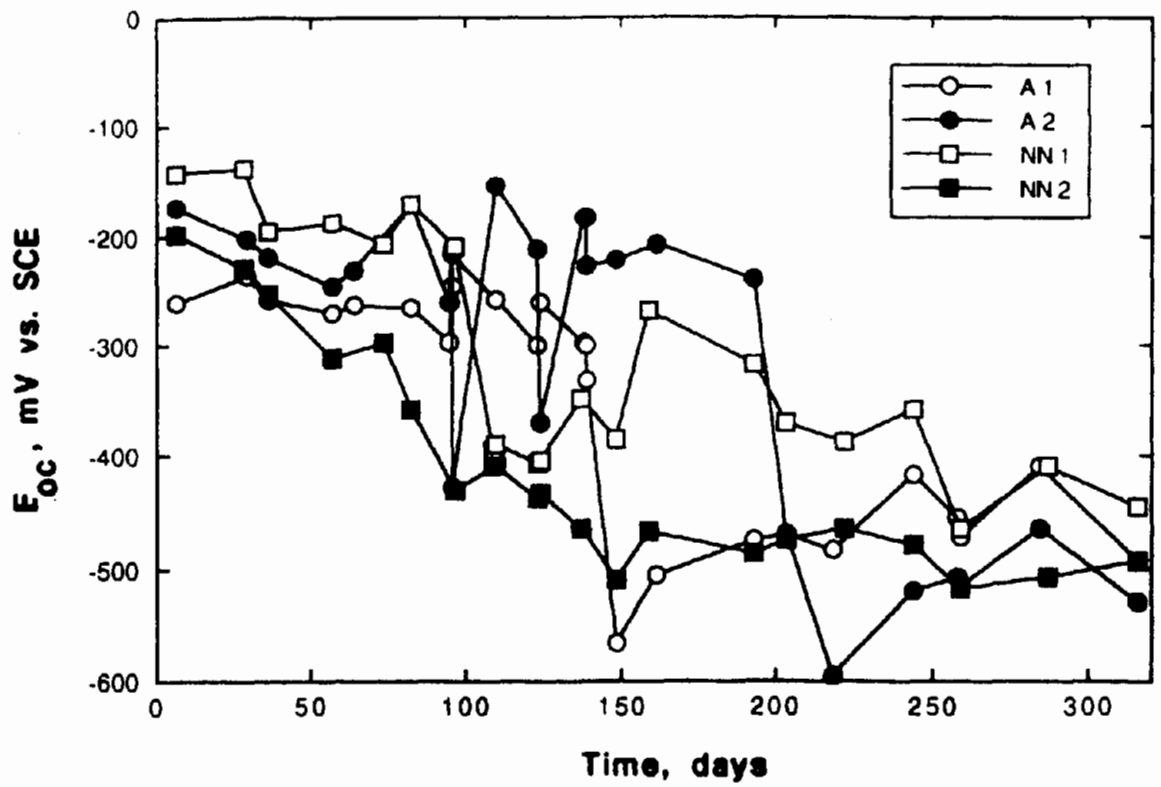
(a) solution #1.
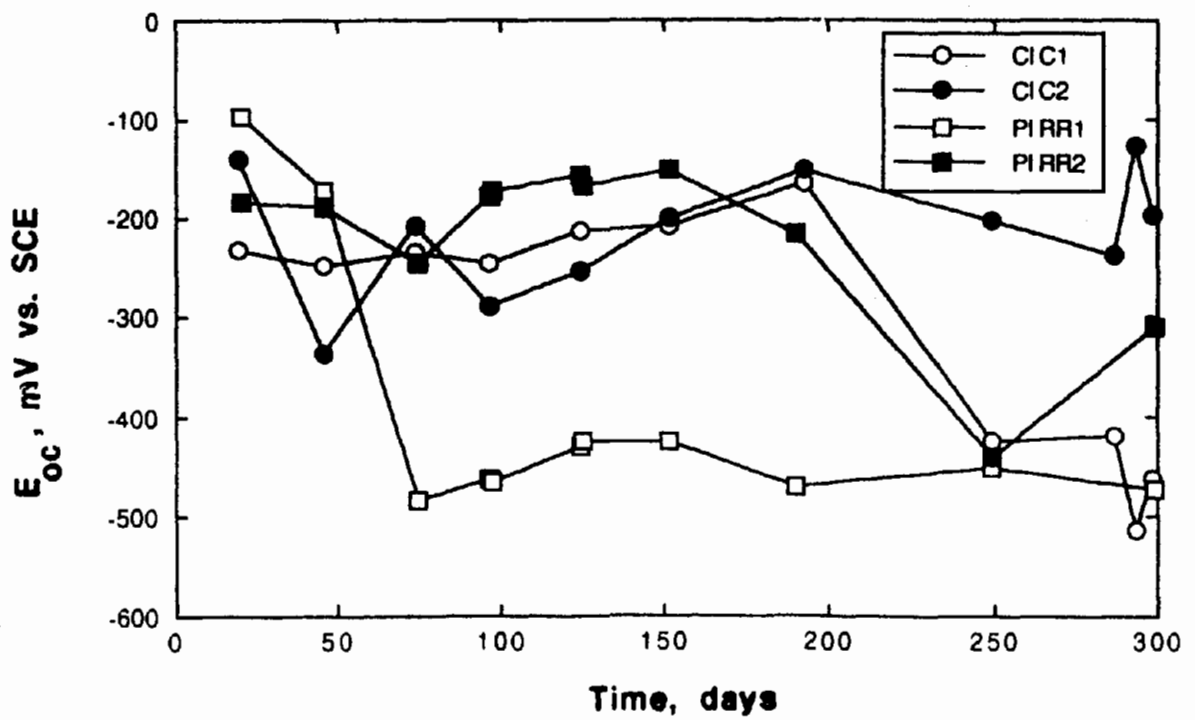
(b) solution #2.

Figure 9. Open circuit potentials of rods 1 and 2 after breaking the short circuit for at least 3 hours (squares: Cl⁻-free concrete, circles: Cl⁻-contaminated concrete) (solutions #1 and #2).

31
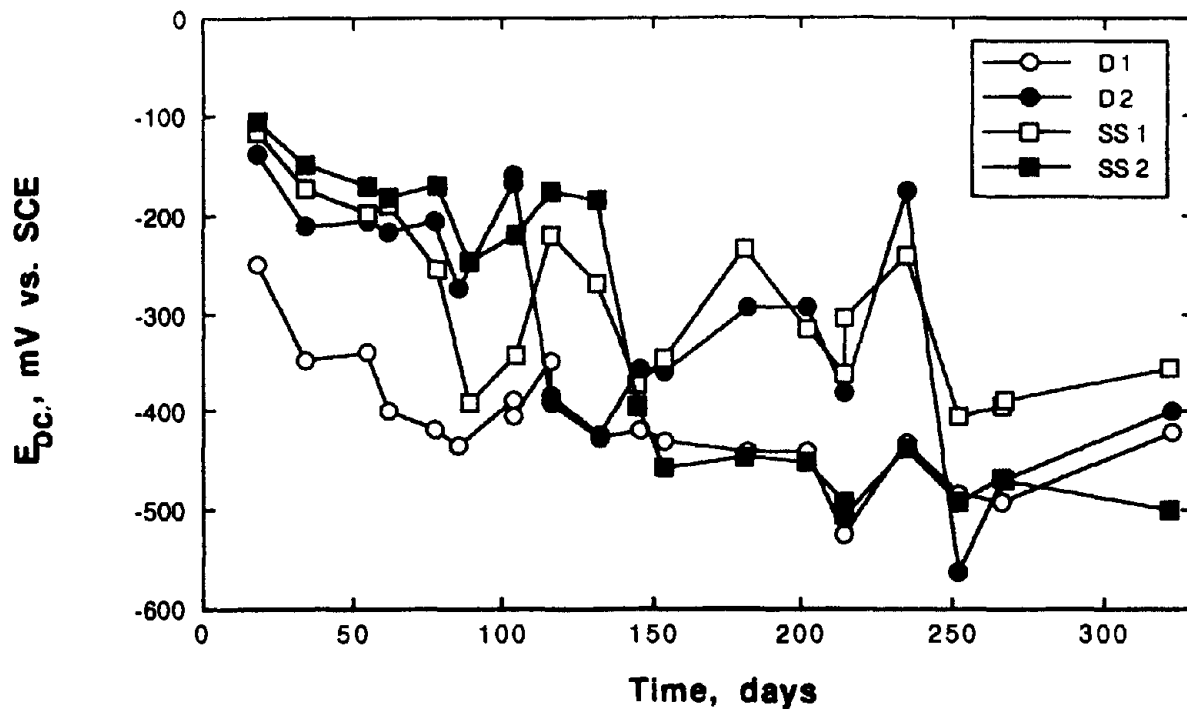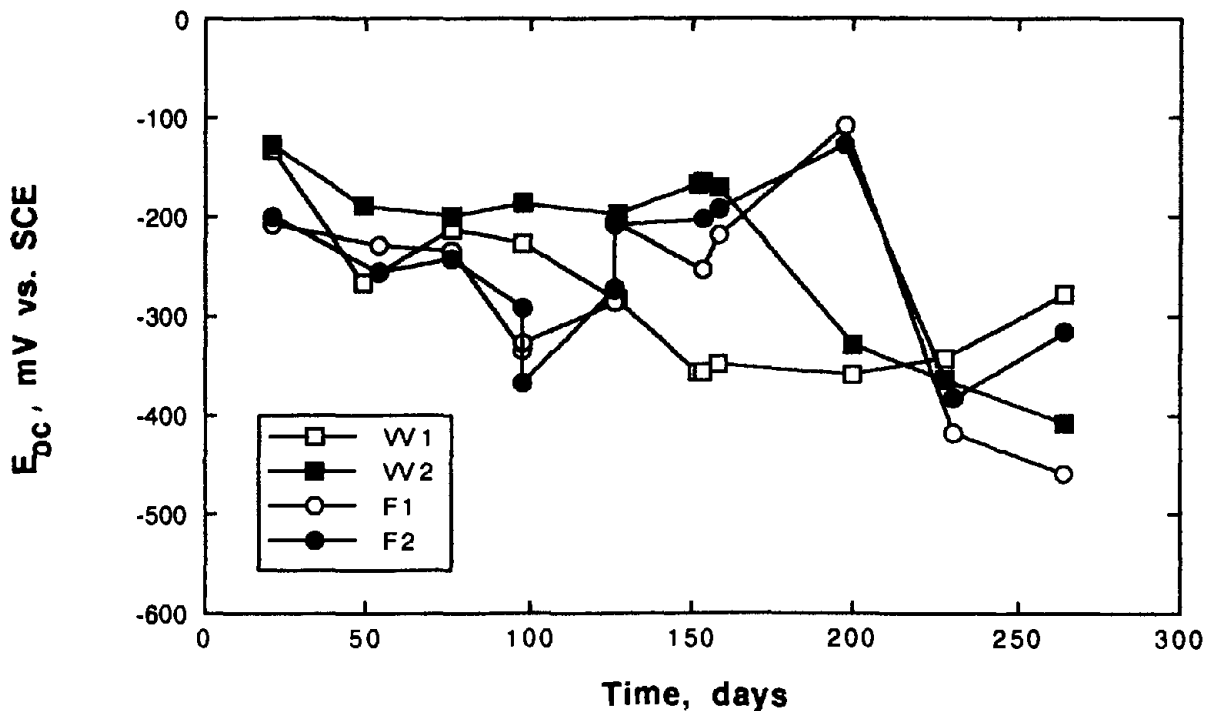
(a) Solution #3.

(b) Solution #4.

Figure 10. Open circuit potentials of rods 1 and 2 after breaking the short circuit for at least 3 hours (squares: C^--free concrete, circles: Cl^--contamiinated concrete) (solutions #3 and #4)

32
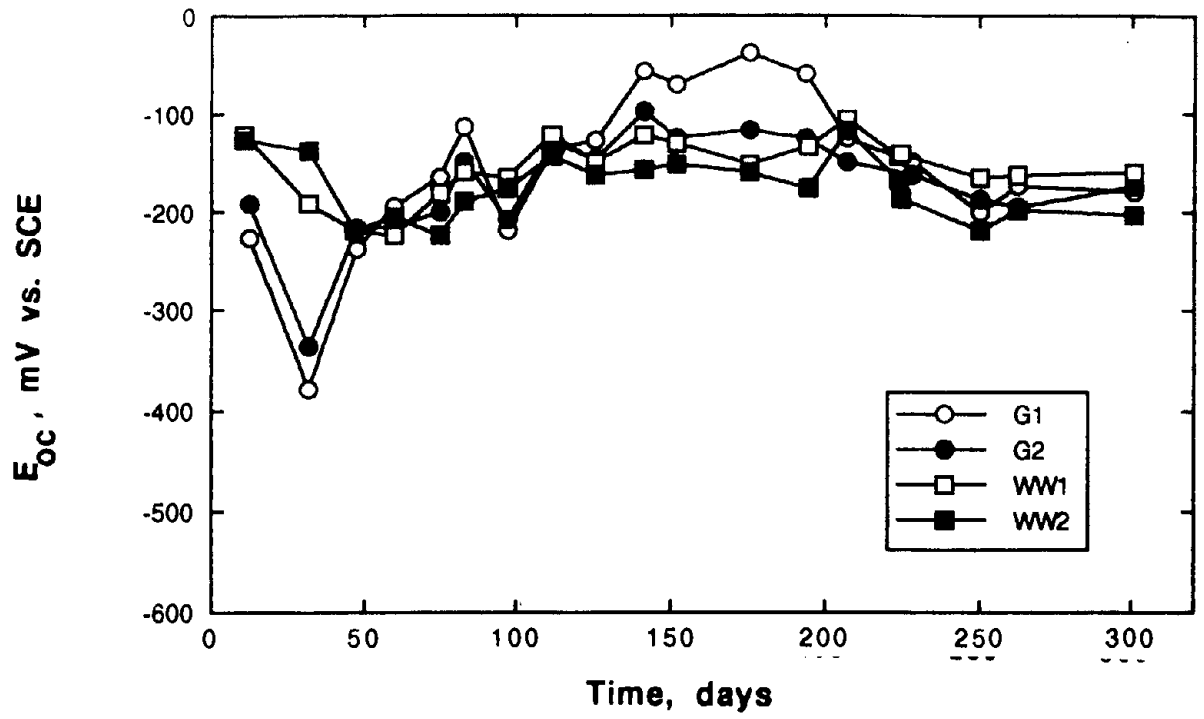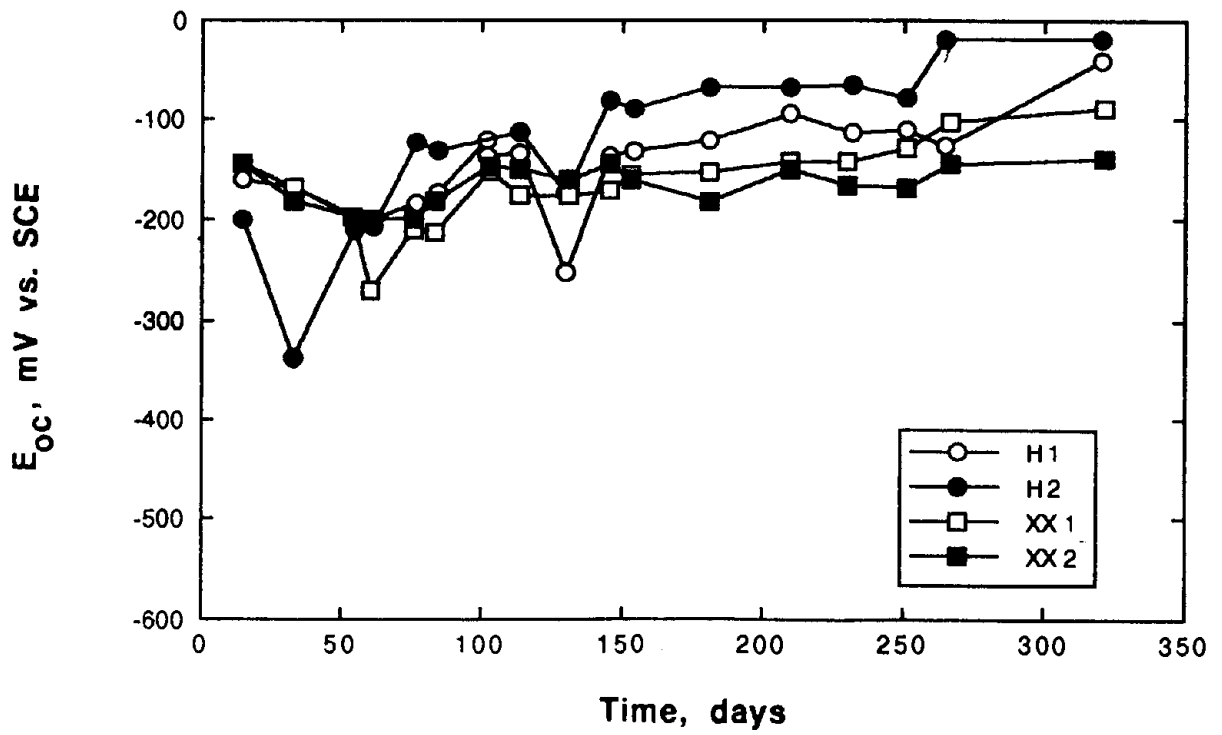
(a) Solution #5.

(b) Solution #6, CMA.

Figure 11. Open circuit potentials of rods 1 and 2 after breaking the short circuit for at least 3 hours (squares: Cl^--free concrete, circles: Cl^--contaminated concrete) (solutions #5 and #6)

33
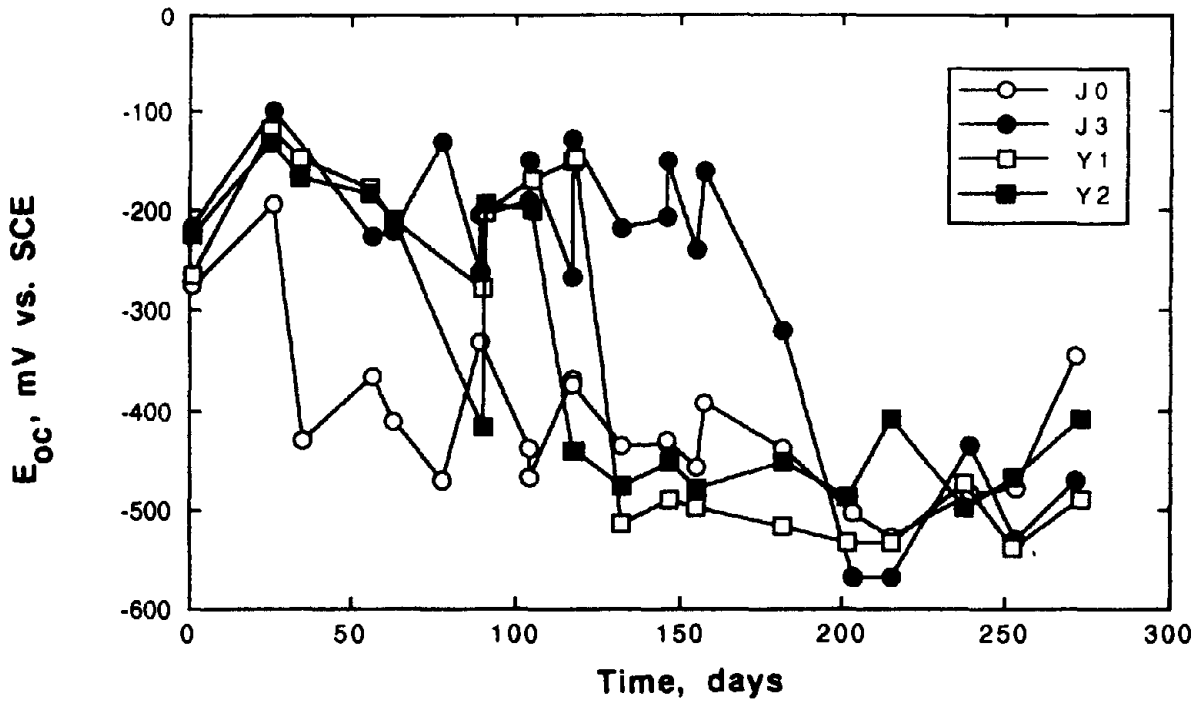
(a) Solution #7, NaCl.
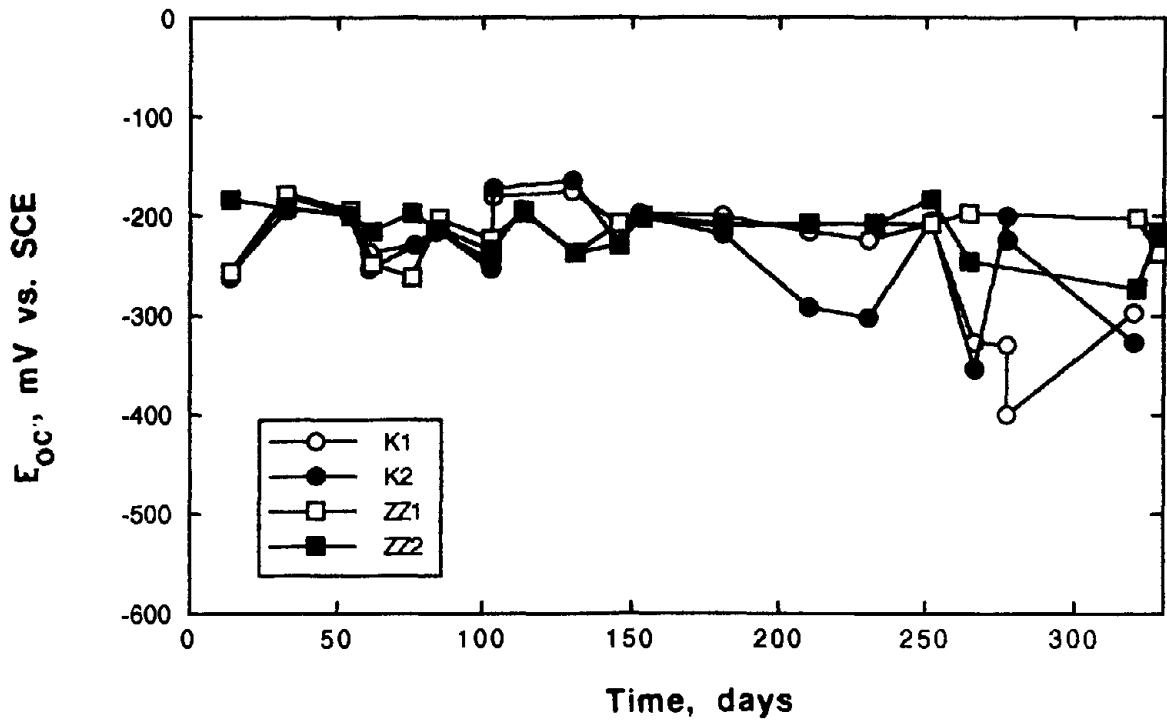
(b) Solution #8, "pore".

Figure 12. Open circuit potentials of rods 1 and 2 after breaking the short circuit for
At least 3 hours (squares: Cl^--free concrete, circles: Cl^--contaminated concrete)
(solutions #7 and #8).

34
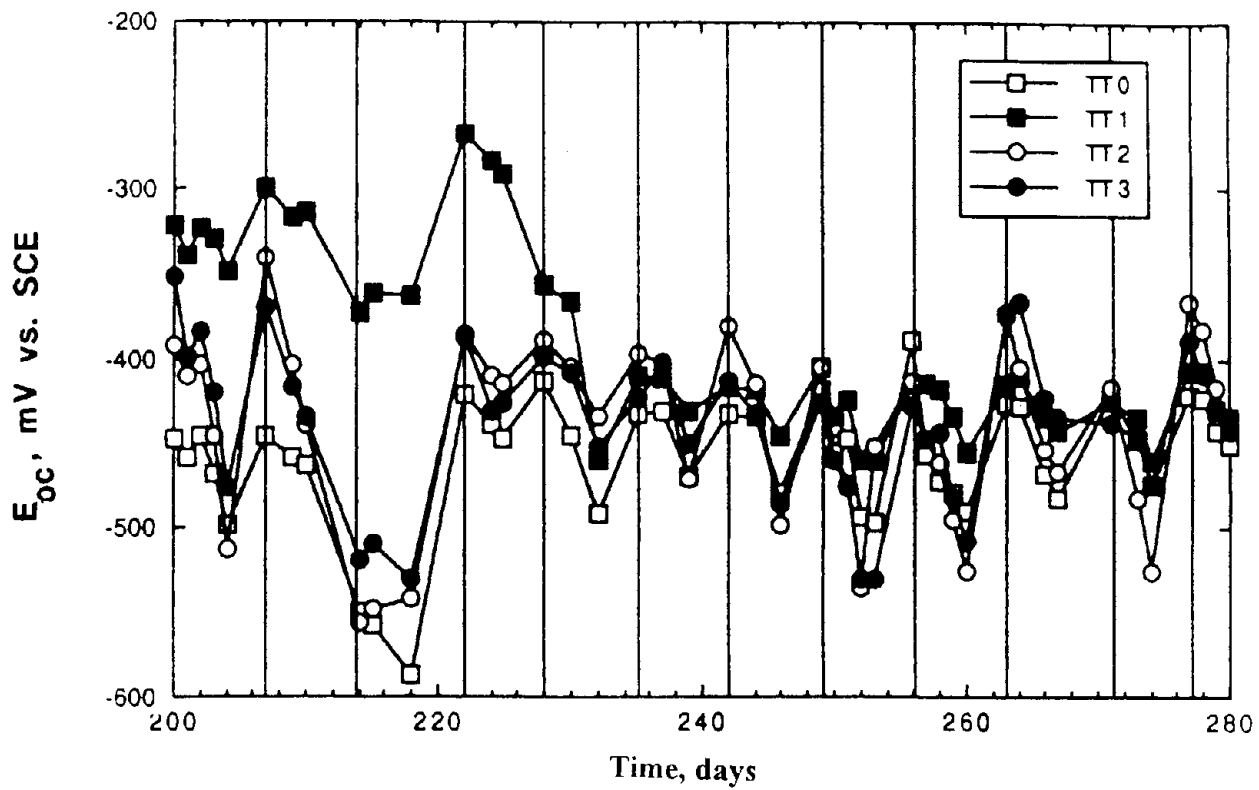
Figure 13. Expanded view of part of Figure 8b (solution #4).
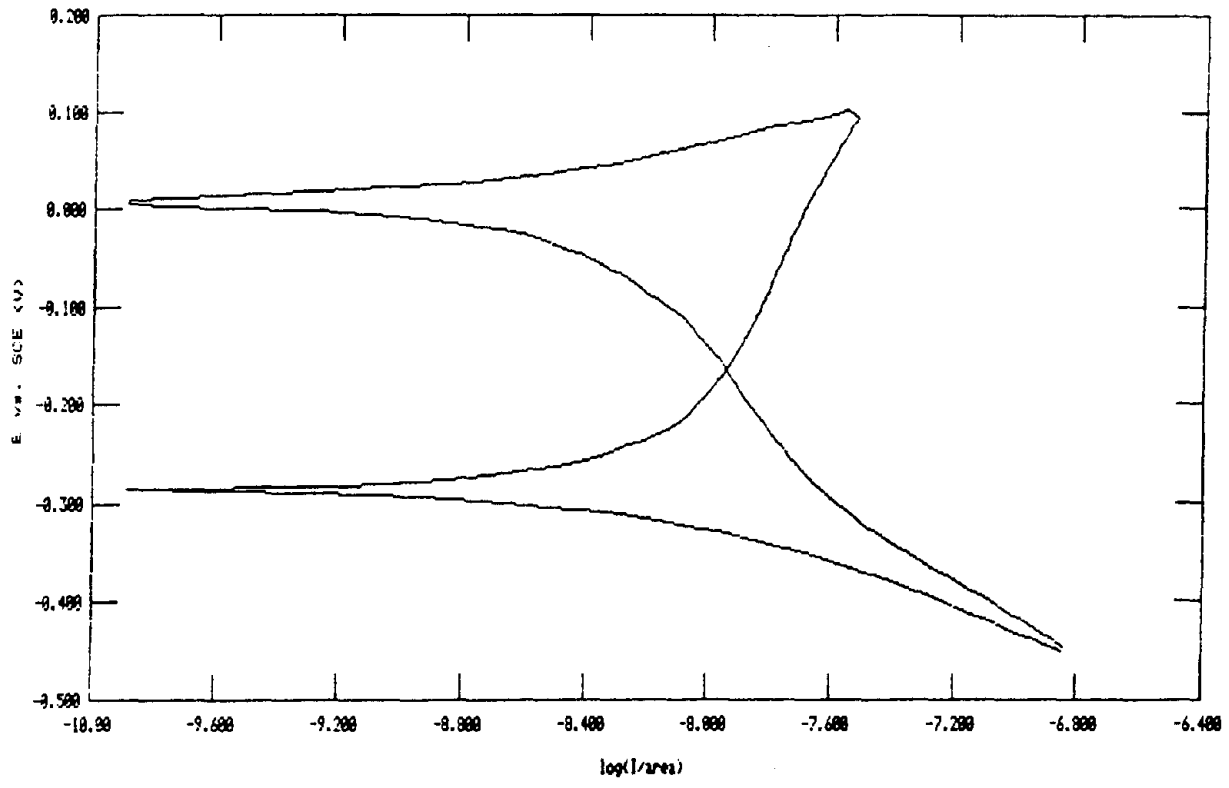
Figure 14. Potentiodynamic scan at 0.2 mV/s taken on specimen H, solution #6,
Cl⁻-contaminated concrete.
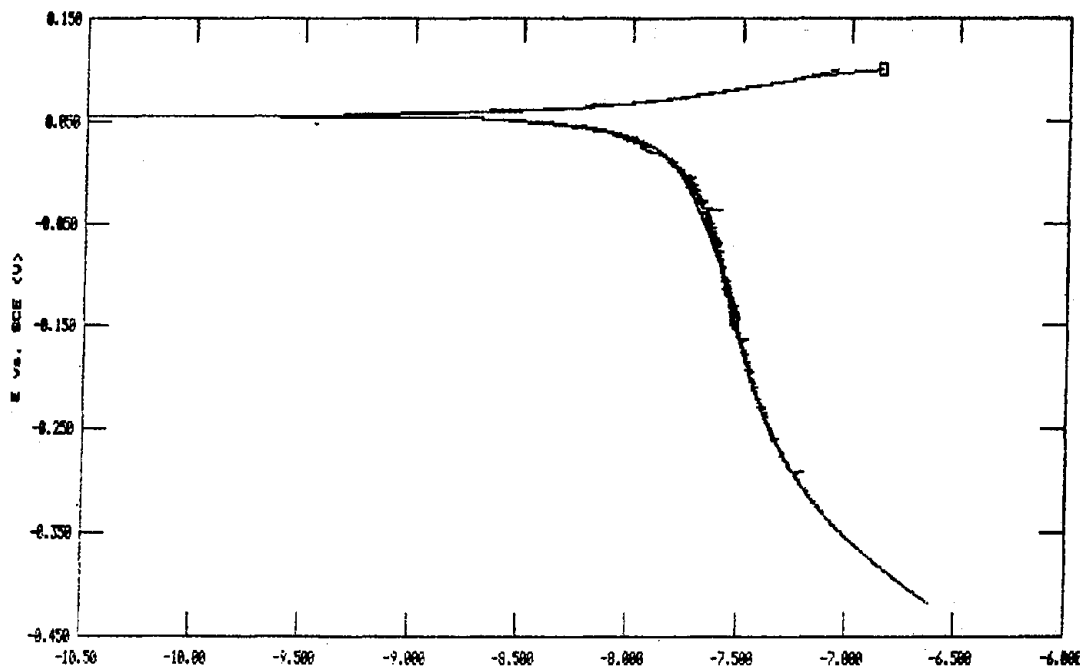
(a) Negative-going scan.
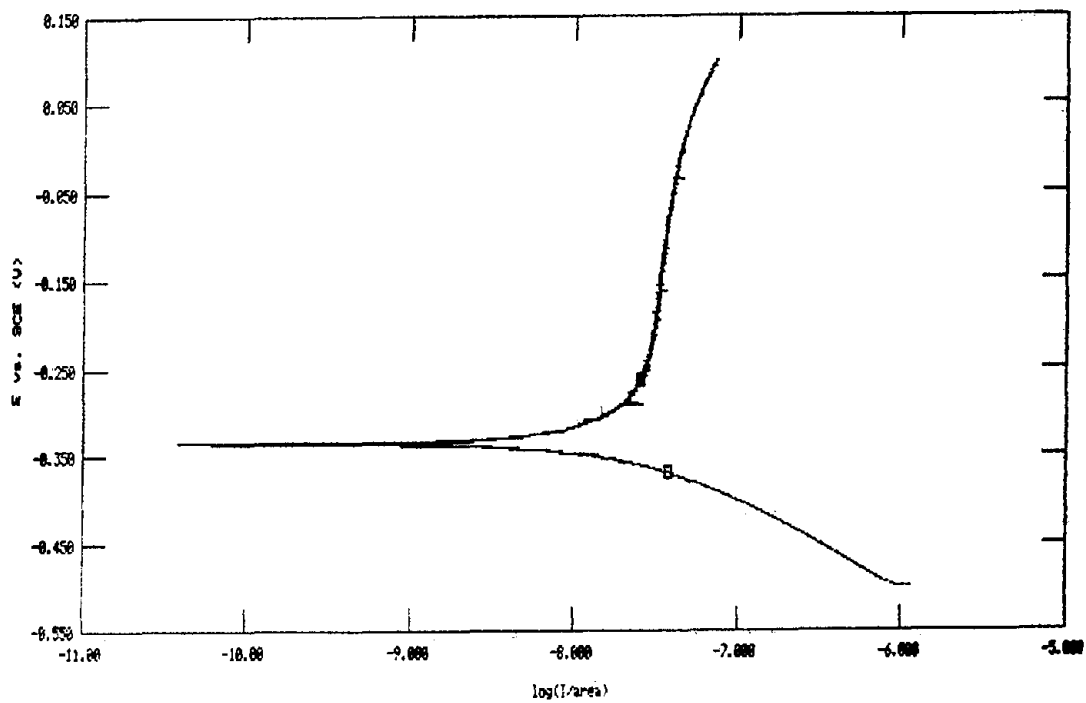
(b) Positive-going scan.

Figure 15. Potentiodynamic scans at 0.5mV/s taken on specimen G, solution #5, Cl⁻-contaminated concrete.

37
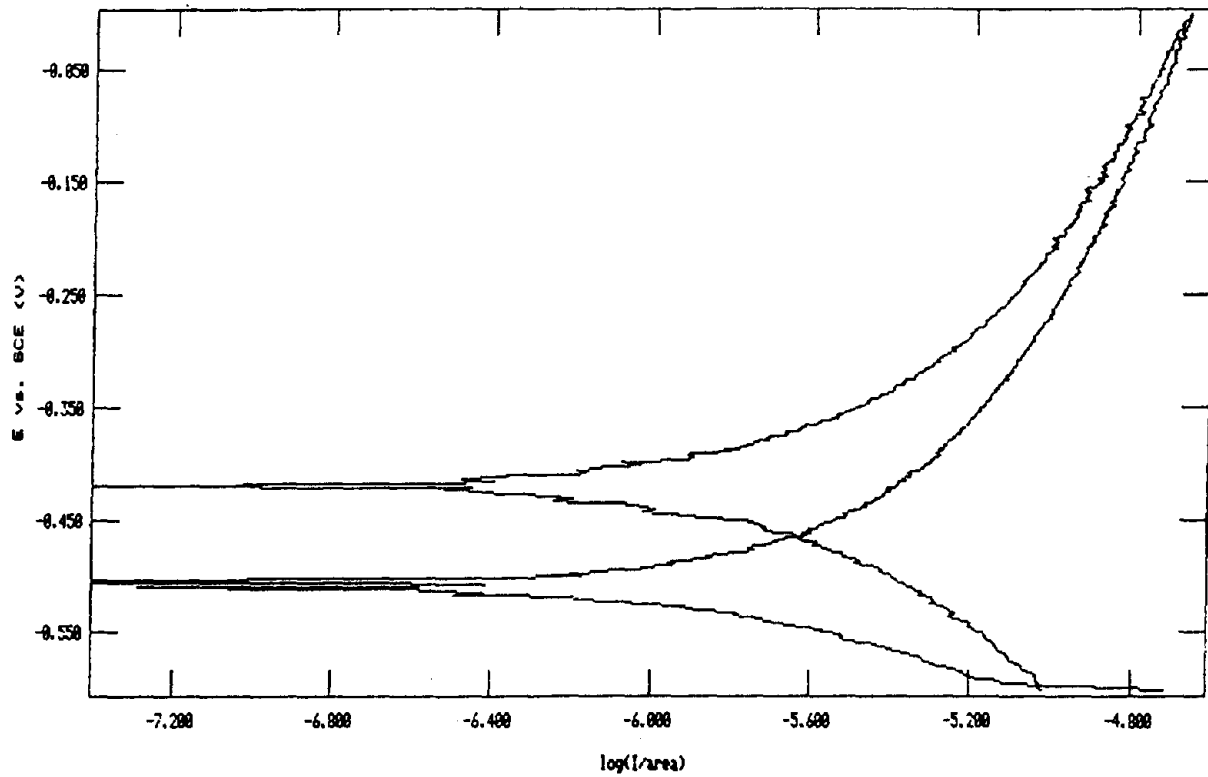
Figure 16. Potentiodynamic scan at 1 mV/s taken on specimen C, solution #2, Cl⁻-contaminated concrete.
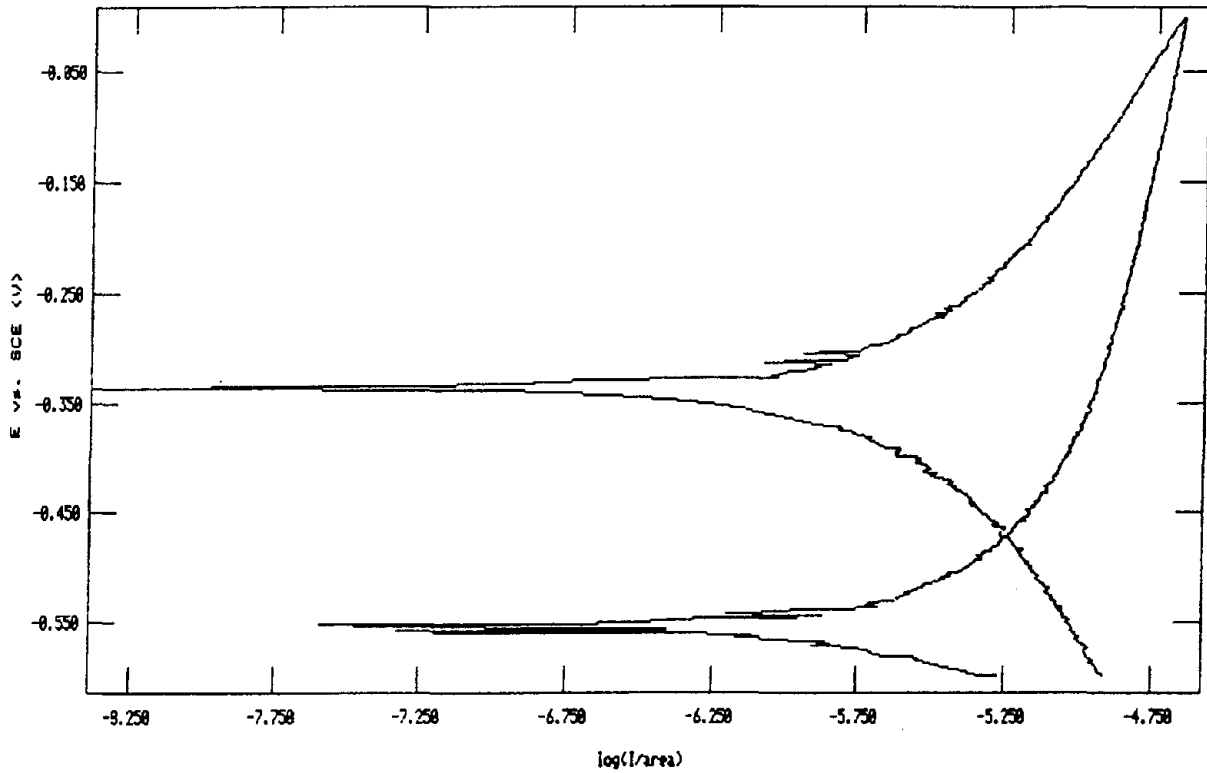
Figure 17. Potentiodynamic scan at 0.5 mV/s taken on specimen D, solution #3, Cl⁻-contaminated concrete.
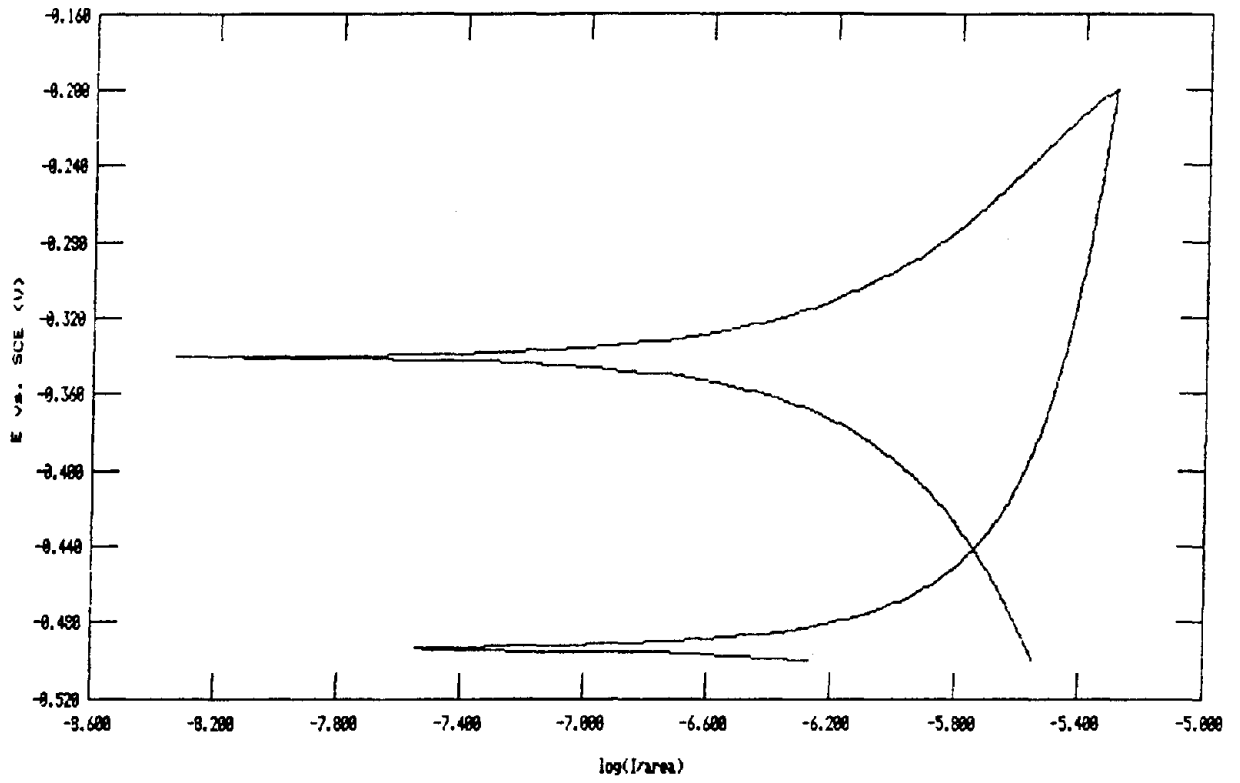
Figure 18. Potentiodynamic scan at 2 MV/s taken on specimen NN, solution #1,
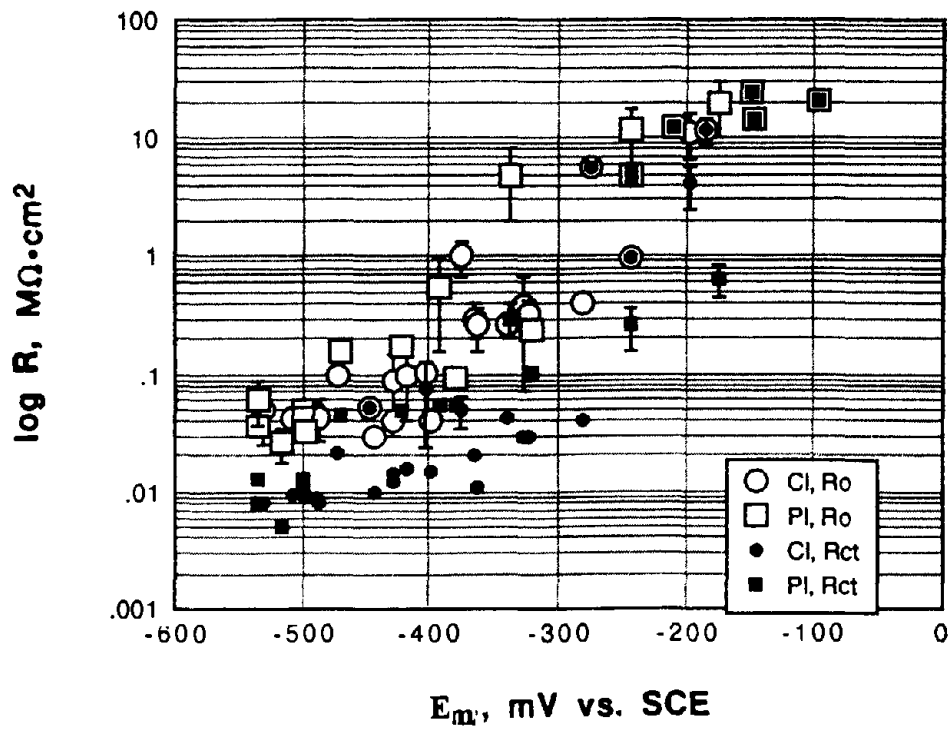Cl⁻-free concrete.

(a) log R_0 and log R_{ct} vs. time
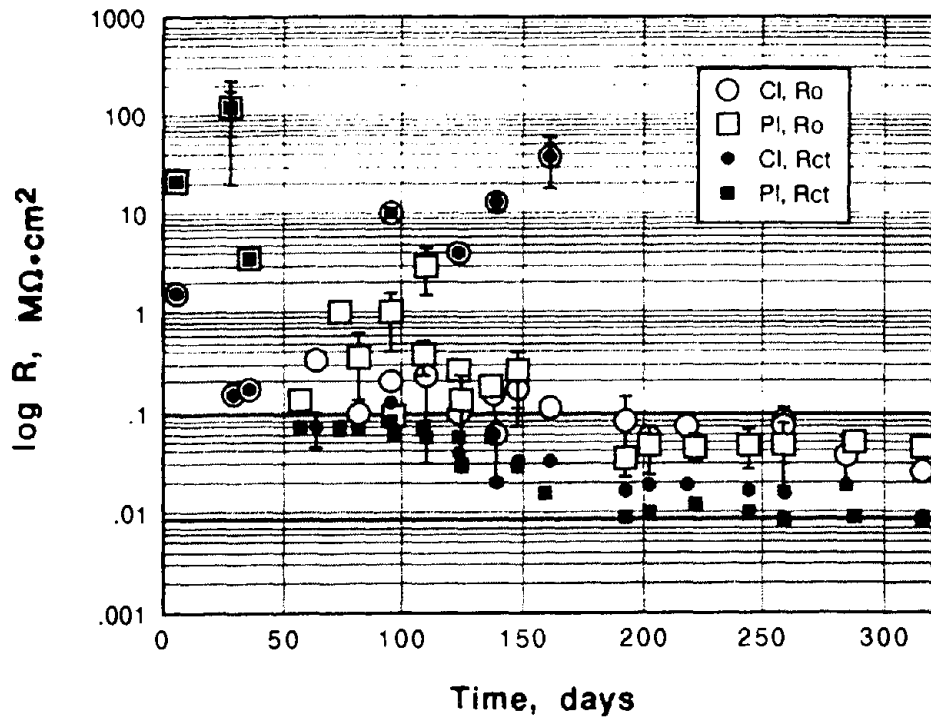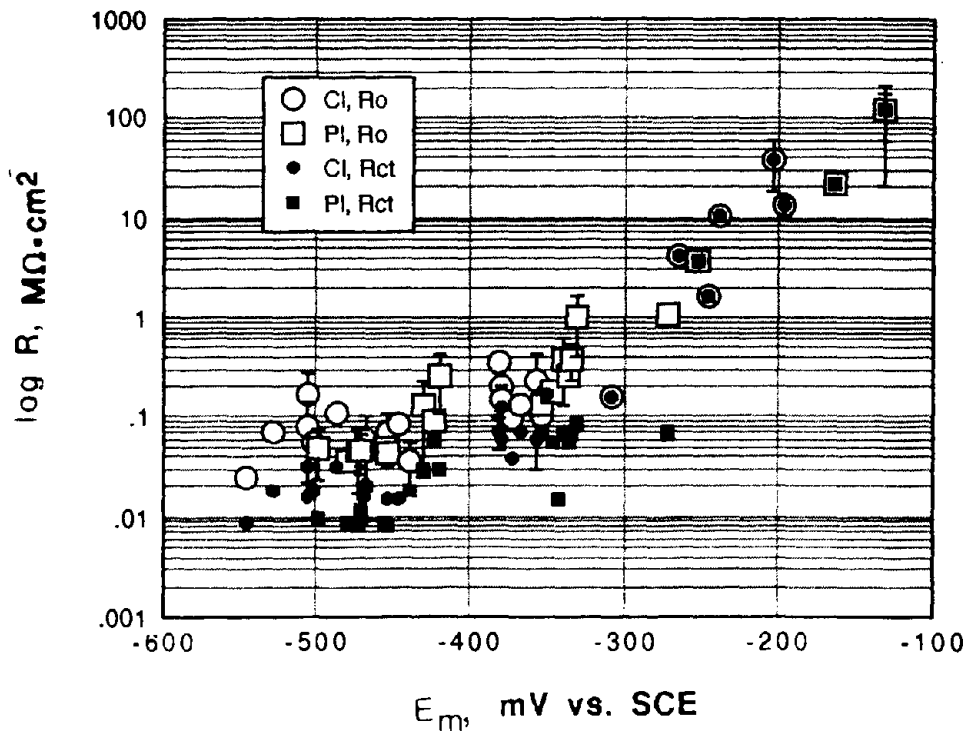
(b) log R_0 and log R_{ct} vs. E_m

Figure 19. Solution #1 (squares: Cl-free concrete, circles: Cl⁻-contaminated concrete).

41

(a) log R_O and log R_{ct} vs. time
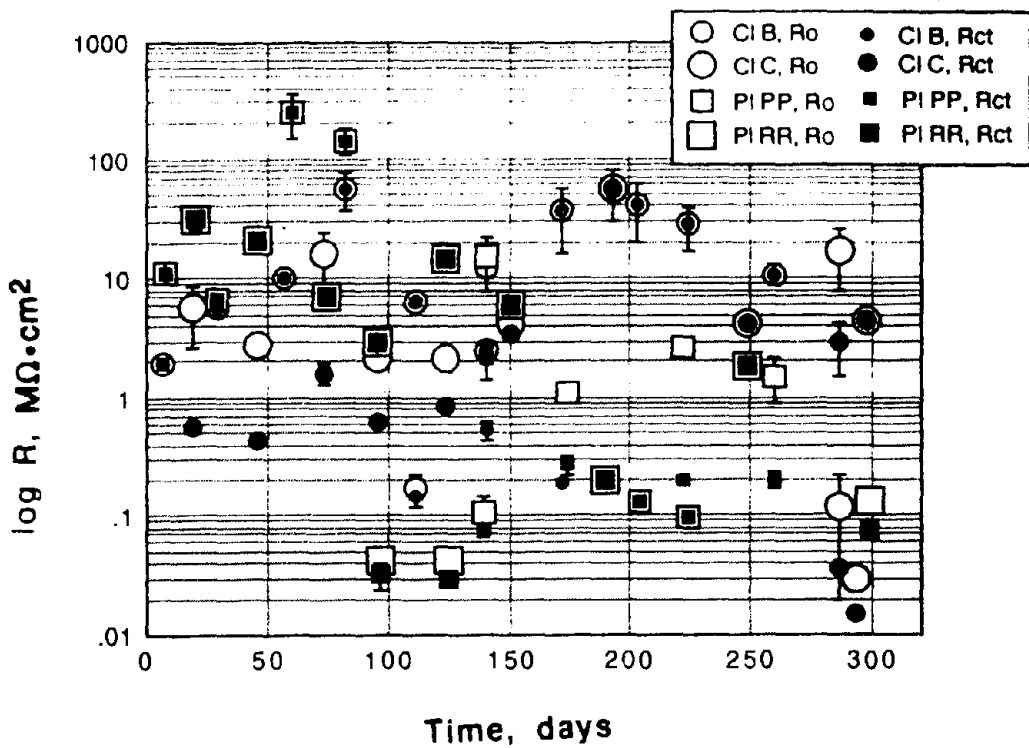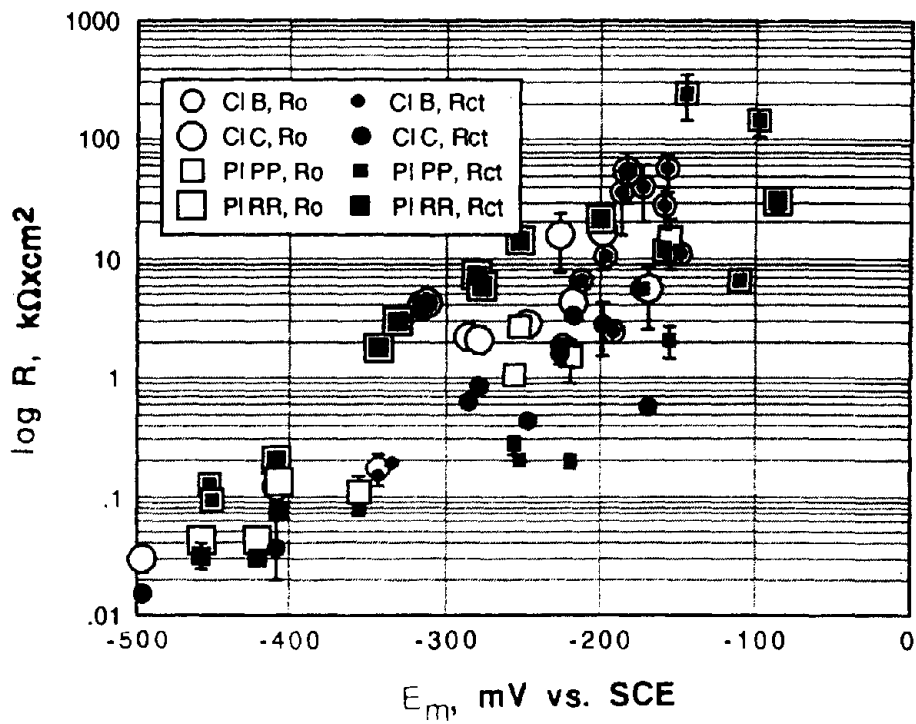
(b) log R_O and log R_{ct} vs. E_m

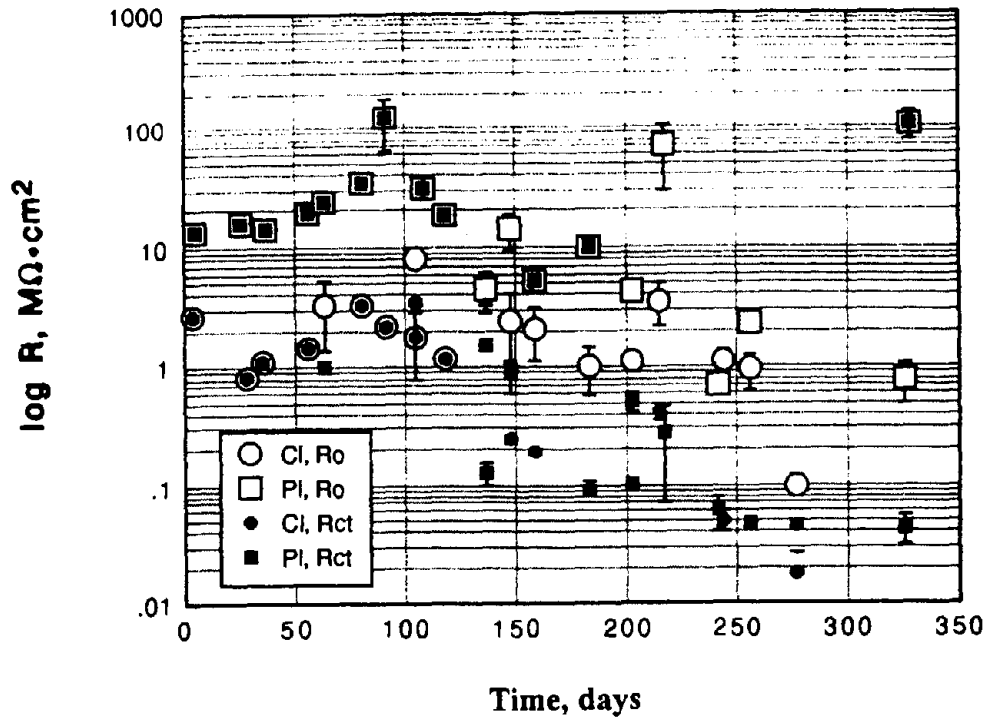Figure 20. Solution #2 (squares: Cl⁻-free concrete, circles: Cl⁻-contaminated concrete).

42

(a) log R_O and log R_{ct} vs. time
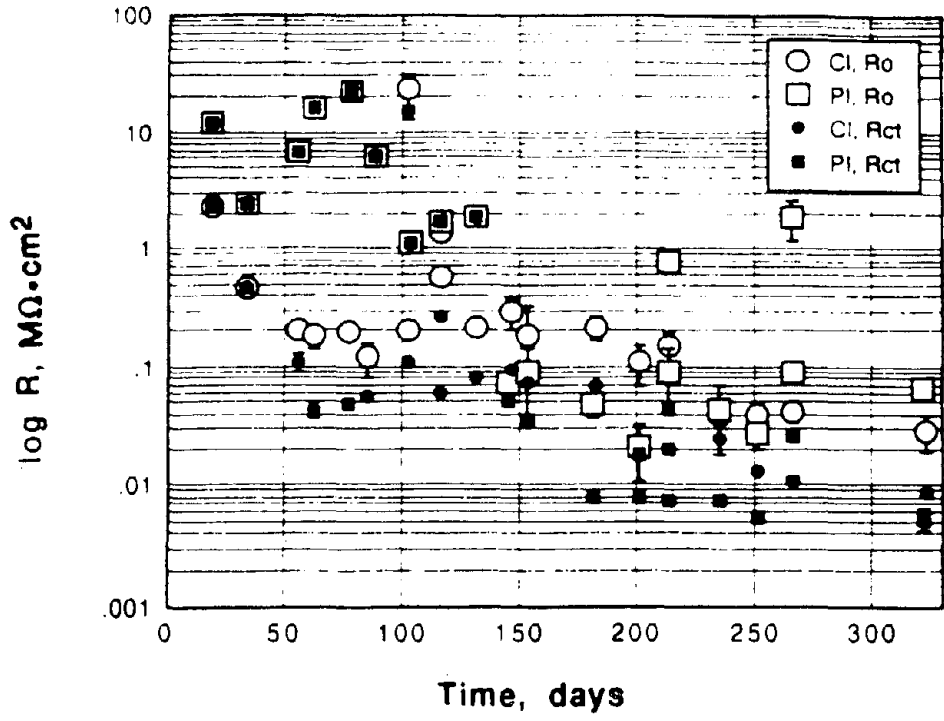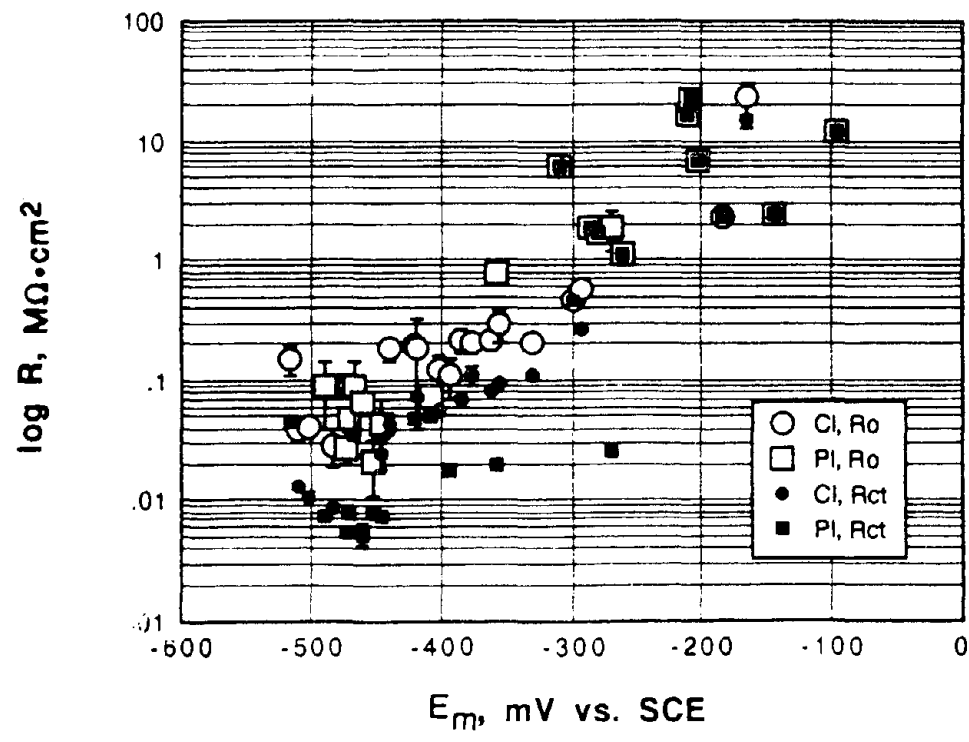
(b) log R_O and log R_{ct} vs. E_m

Figure 21. Solution #3. Squares: Cl-free concrete. Circles: Cl-contaminated concrete

(a) log R_O and log R_{ct} vs. time
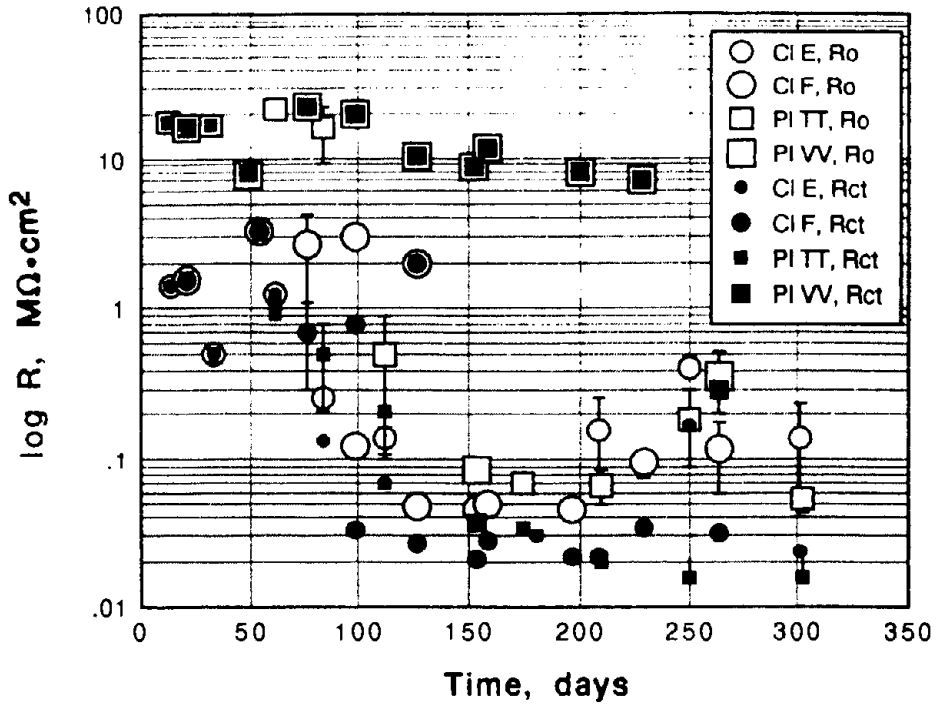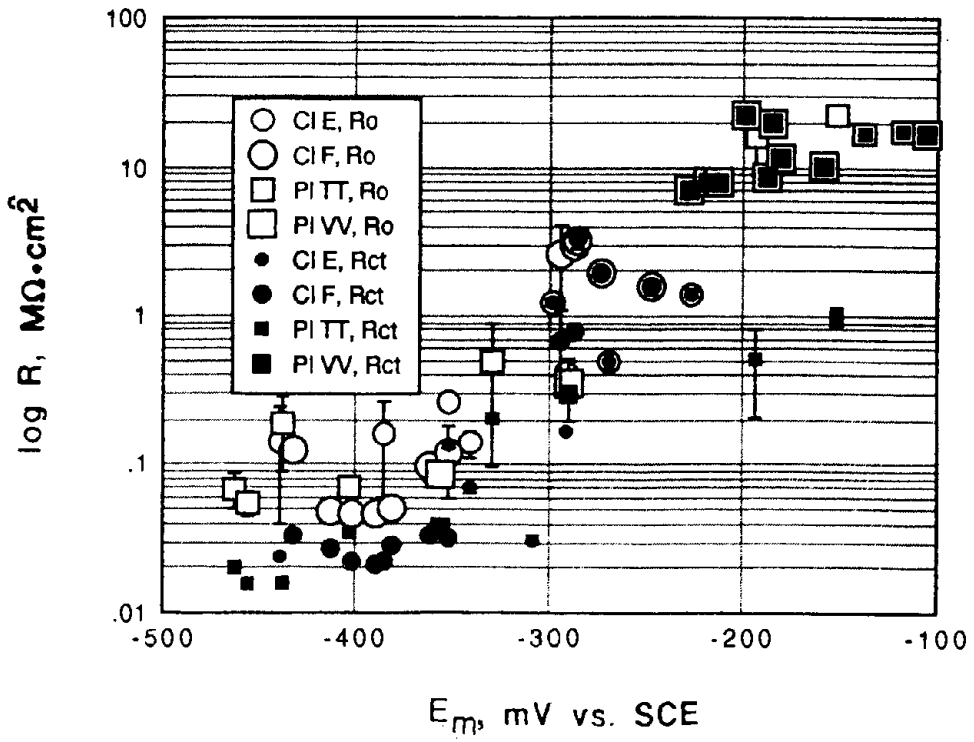
(b) log R_O and log R_{ct} vs. E_m

Figure 22. Solution #4 (squares: Cl^--free concrete, circles: Cl^--contaminated concrete).

44

(a) log R_O and log R_{ct} vs. time.
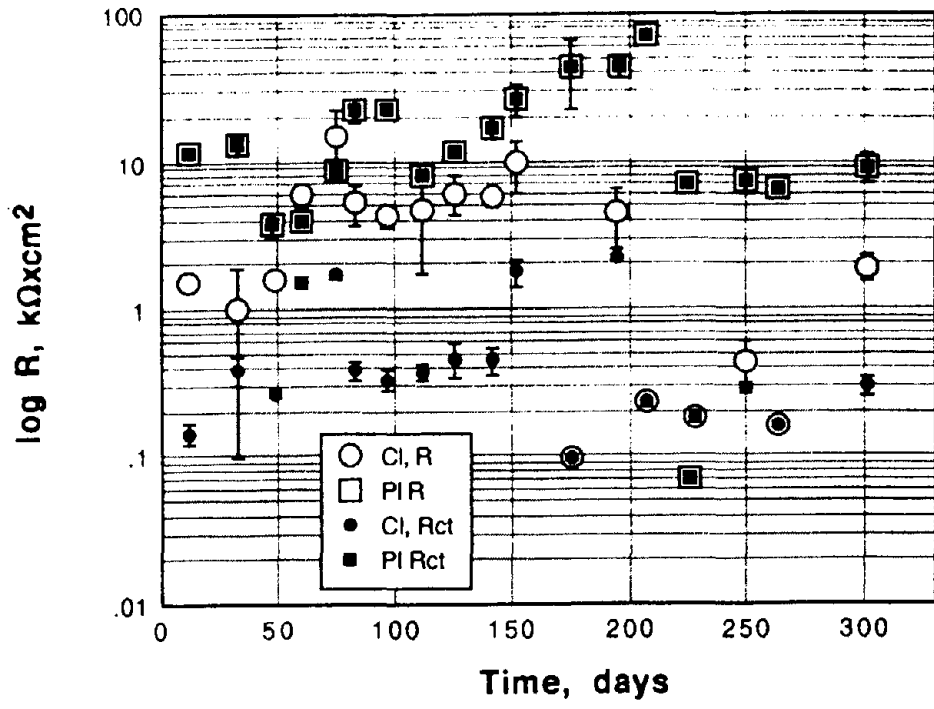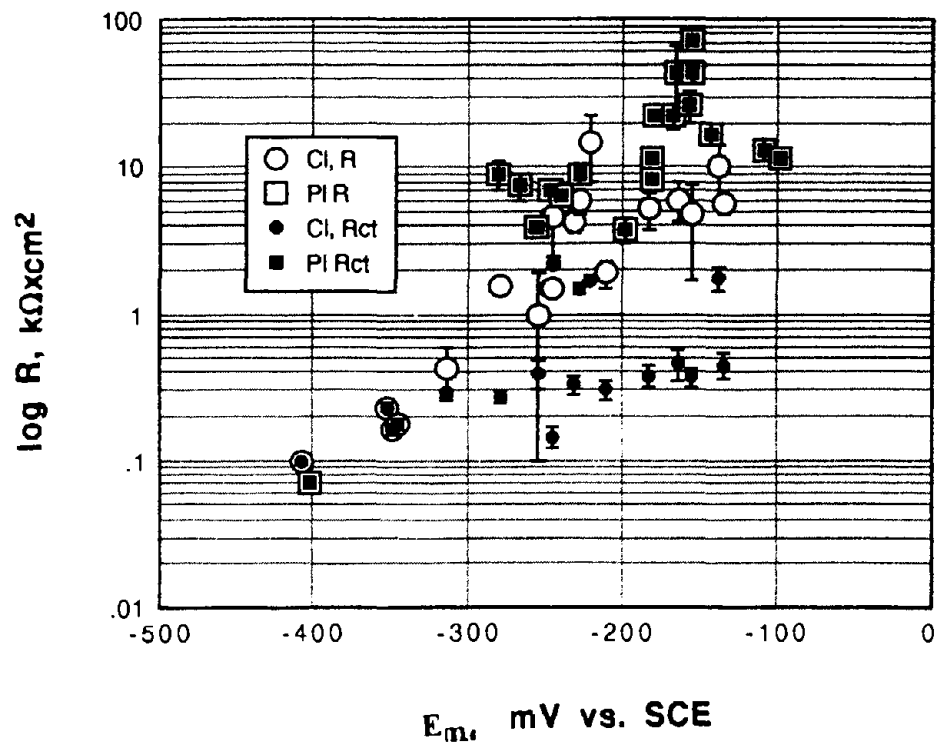
(b) log R_O and log R_{ct} vs. E_m.

Figure 23. Solution #5 (squares: Cl^--free concrete, circles: Cl^--contaminated concrete).

45

(a) log R_O and log R_{ct} vs. time.
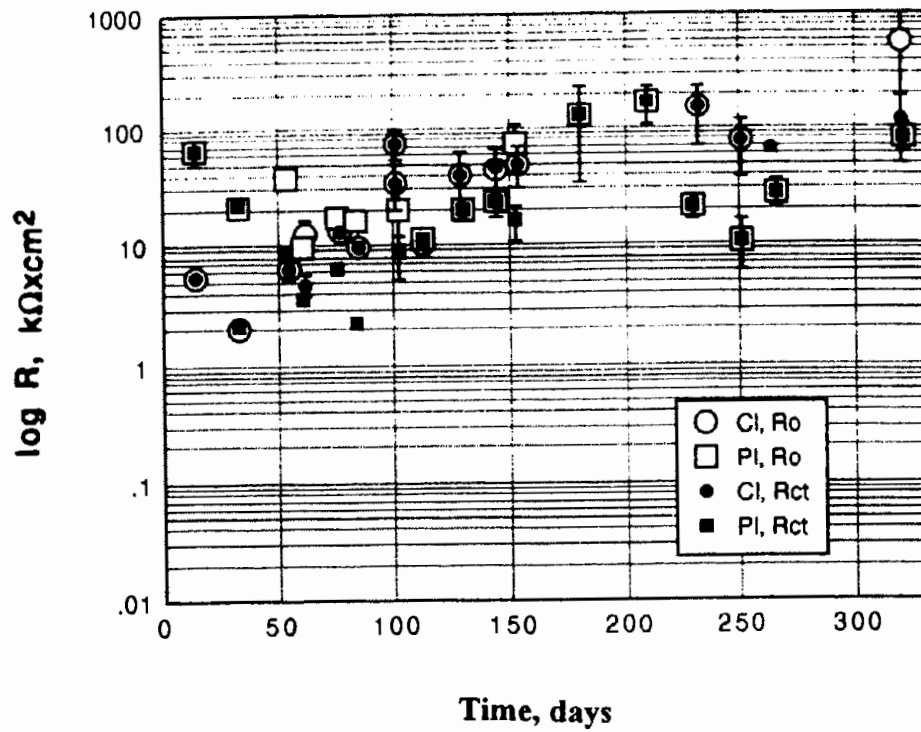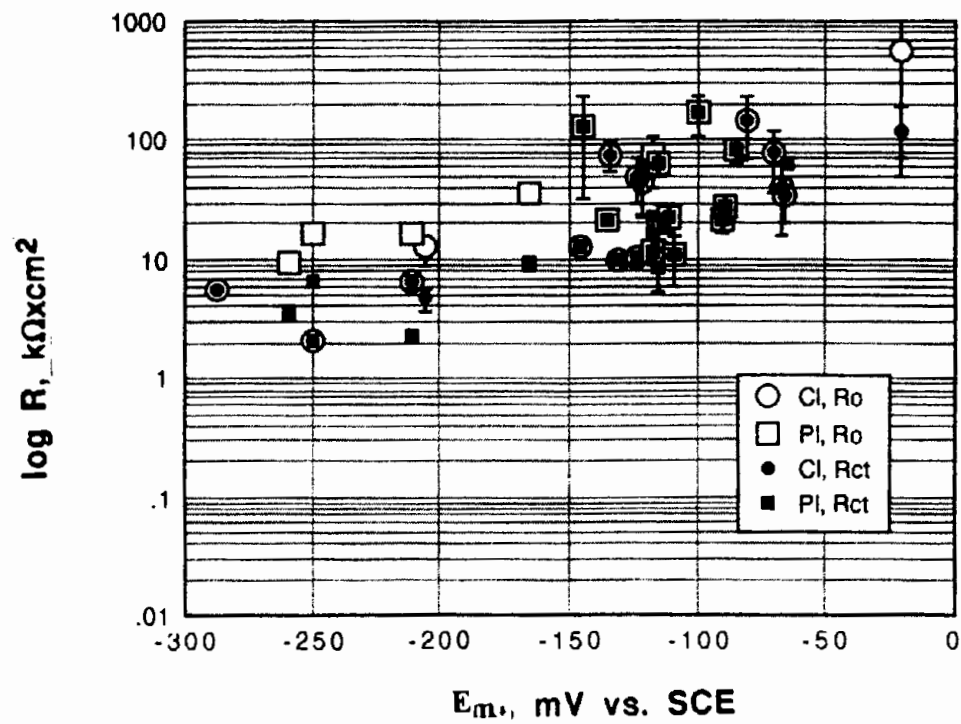
(b) log R_O and log R_{ct} vs. E_m.

Figure 24. Solution #6, CMA (squares: Cl⁻-free concrete, circles: Cl⁻-contaminated concrete).

(a) log R_0 and log R_{ct} vs. time.
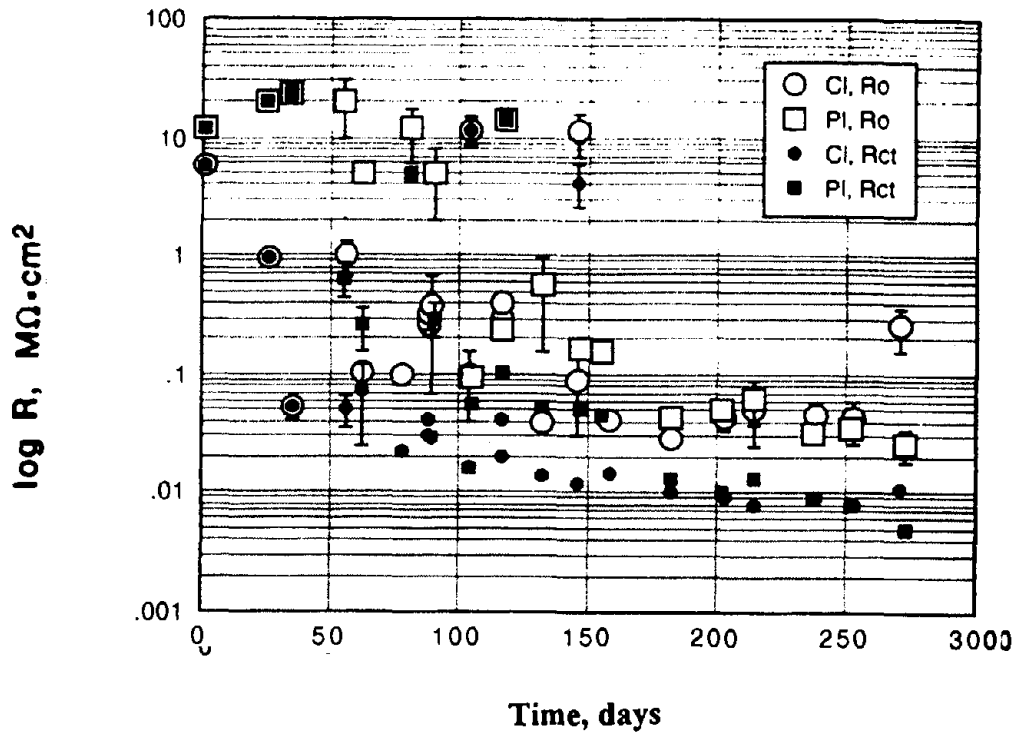
(b) log R_0 and log R_{ct} vs. E_m.

Figure 25. Solution #7, NaCl (squares: Cl^--free concrete, circles: Cl^--contaminated concrete).

47

(a) log R_O and log R_{ct} vs. time
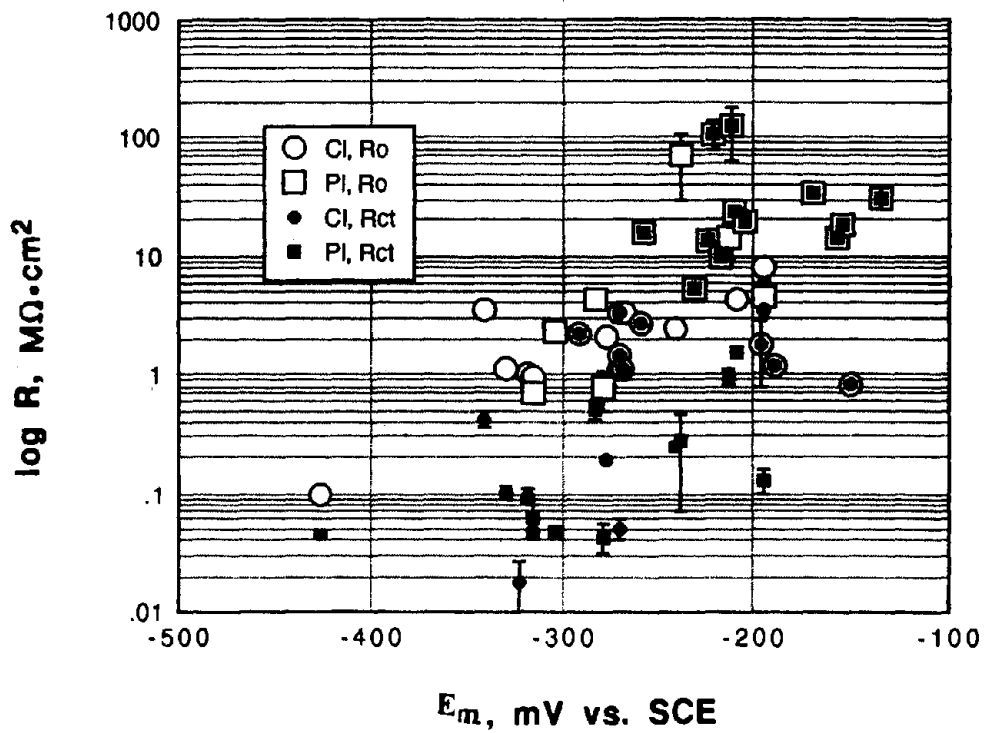
(b) log R_O and log R_{ct} vs. E_m.

Figure 26. Solution #8 (squares: Cl -free concrete. circles:
Cl -contaminated concrete).

48
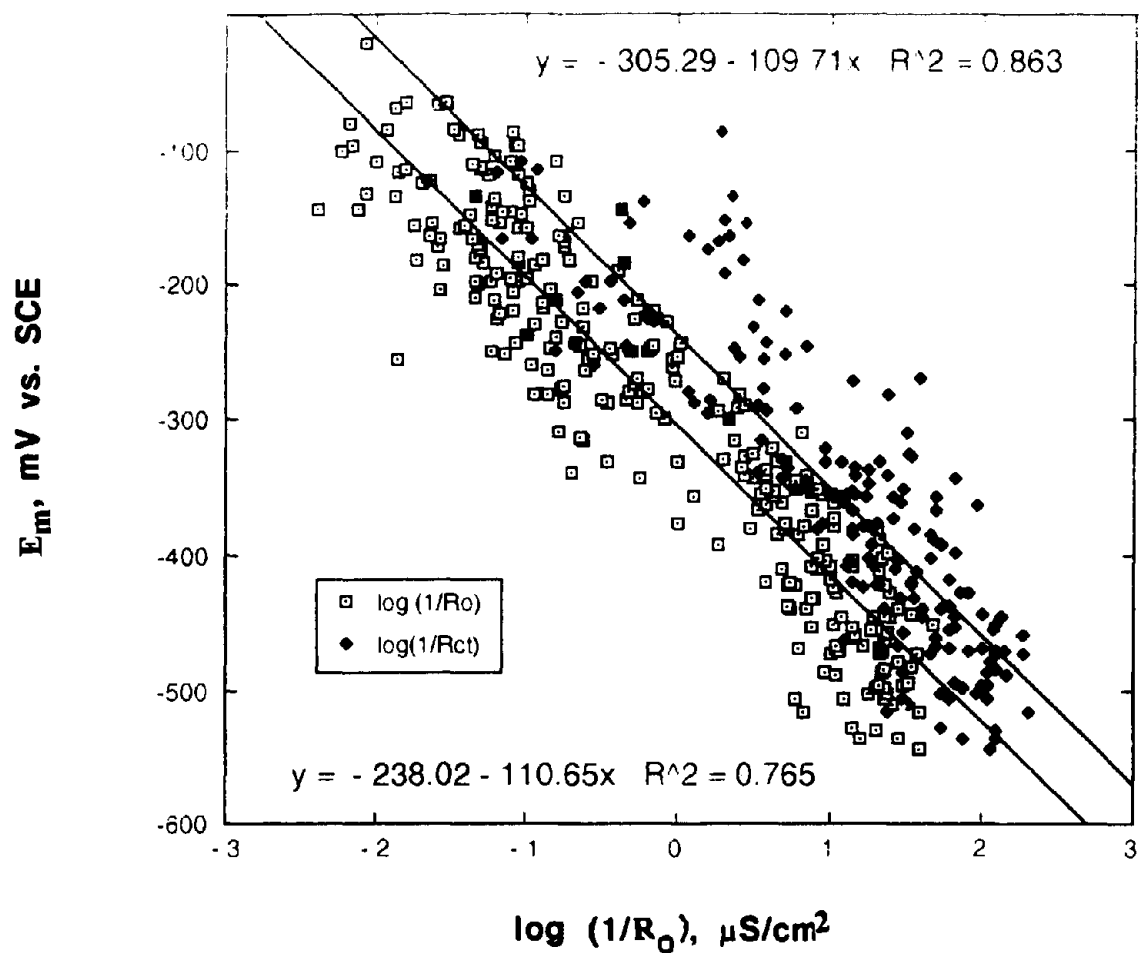
Figure 27. Relationship between electrode potential and electrode admittance from EIS (cumulative plot for all solutions except #8).
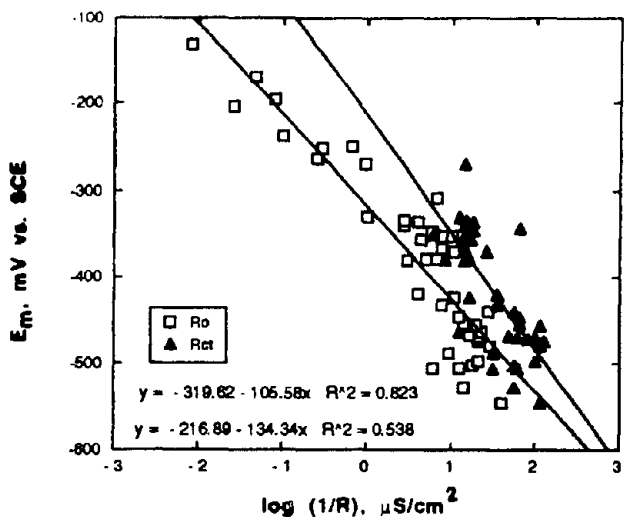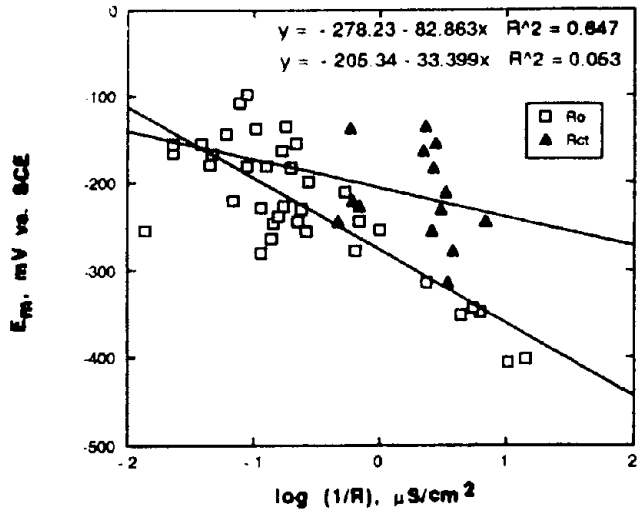
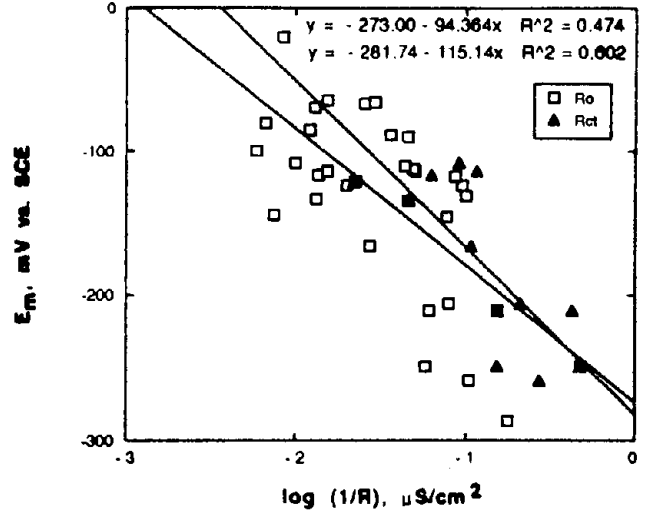(a) solution #1.
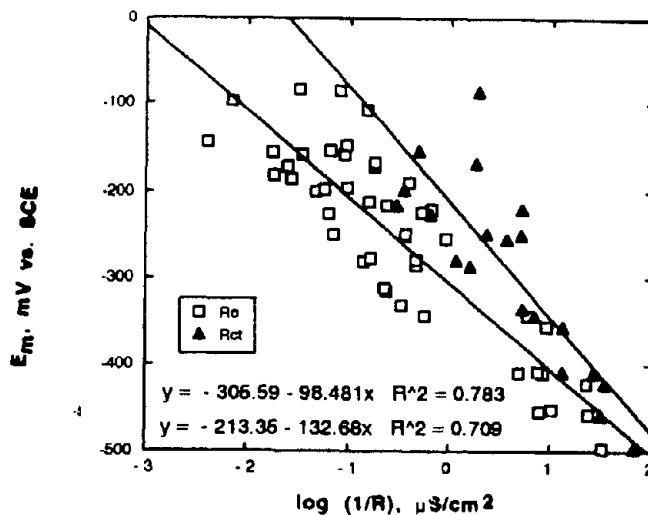
(b) solution #2.
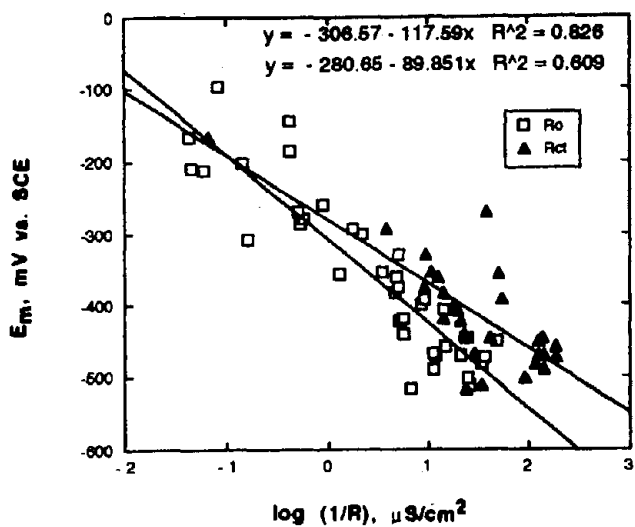
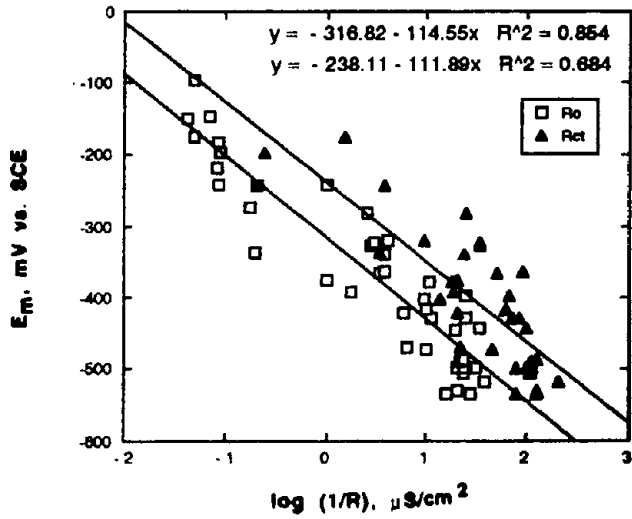(c) solution #3.
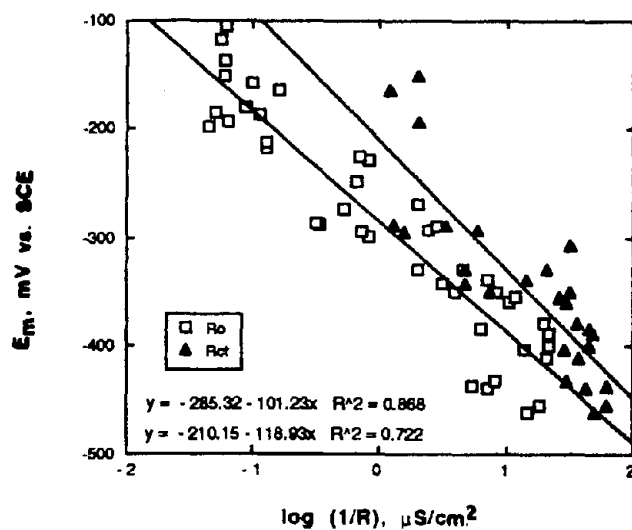
(d) solution #4.

Figure 28. Relationship between electrode potential and electrode admittance from EIS (open squares: R_O, filled triangles: R_{ct})(solutions #1 - #4).

Figure 29.   Relationship between electrode potential and electrode admittance from EIS (open squares: R_0, filled triangles: R_{ct} (solutions #5 - #8).
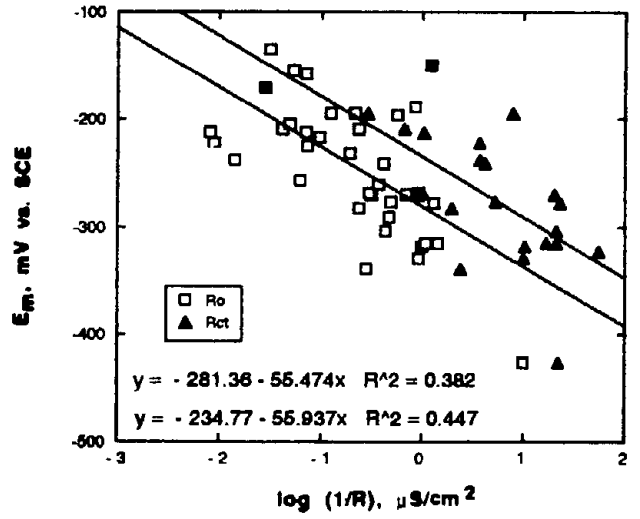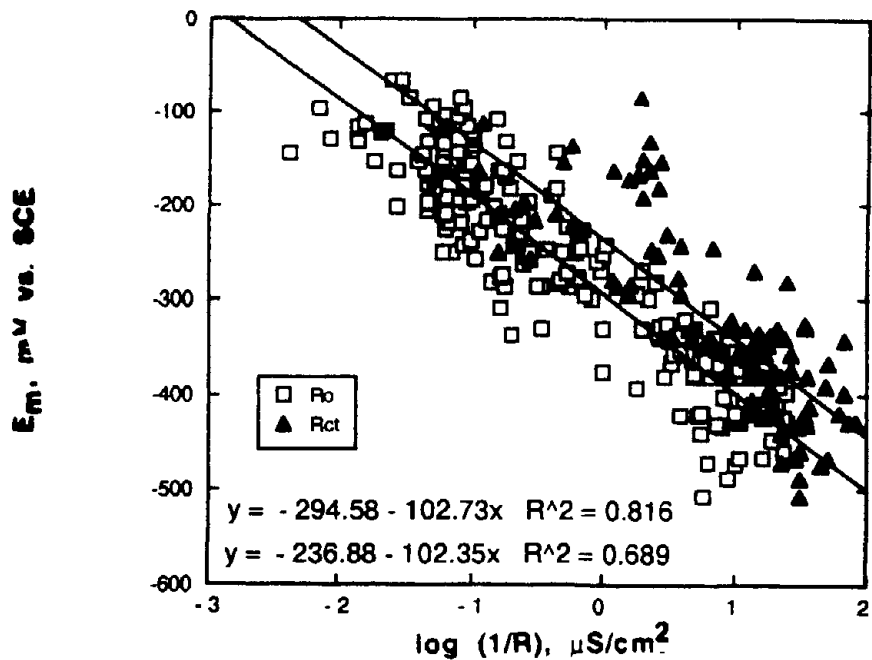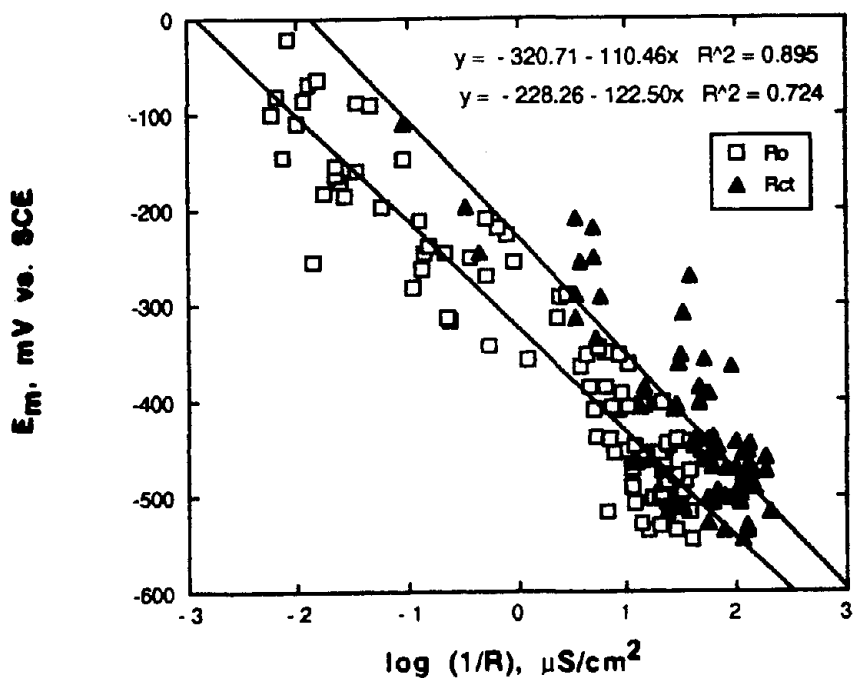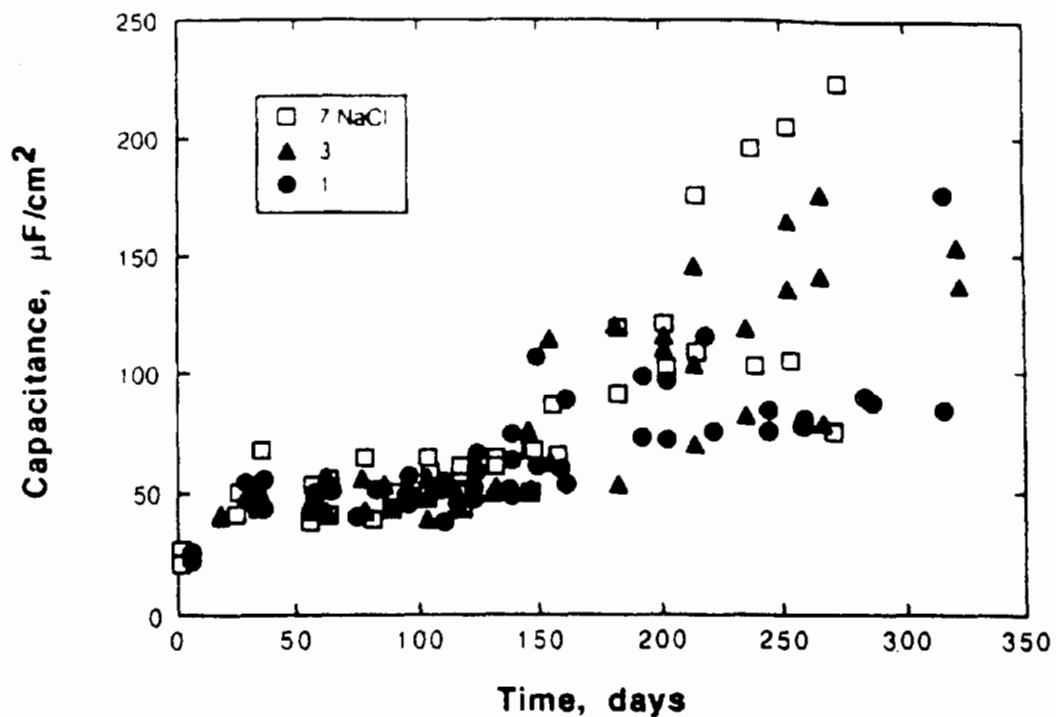
(a) First half of testing time.

(b) Second half of testing time.

Figure 30. Electrode potential vs. electrode admittance, dividing the data into two parts, according to testing time; all solutions except #8 (open squares: R_0, filled triangles: R_{ct}).

(a) Solutions #7, #3, and #1.
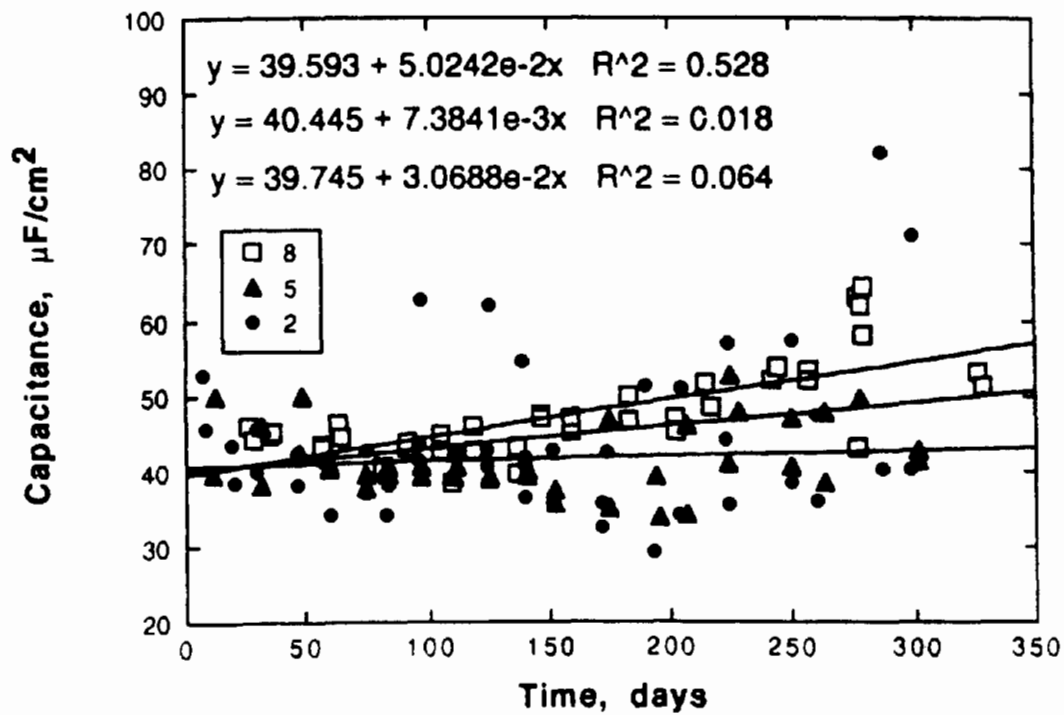
(b) Solutions #8, #5, and #2.

Figure 31. Double-layer capacitance vs. time (solutions #1 - #3, #5, #7, #8).

53
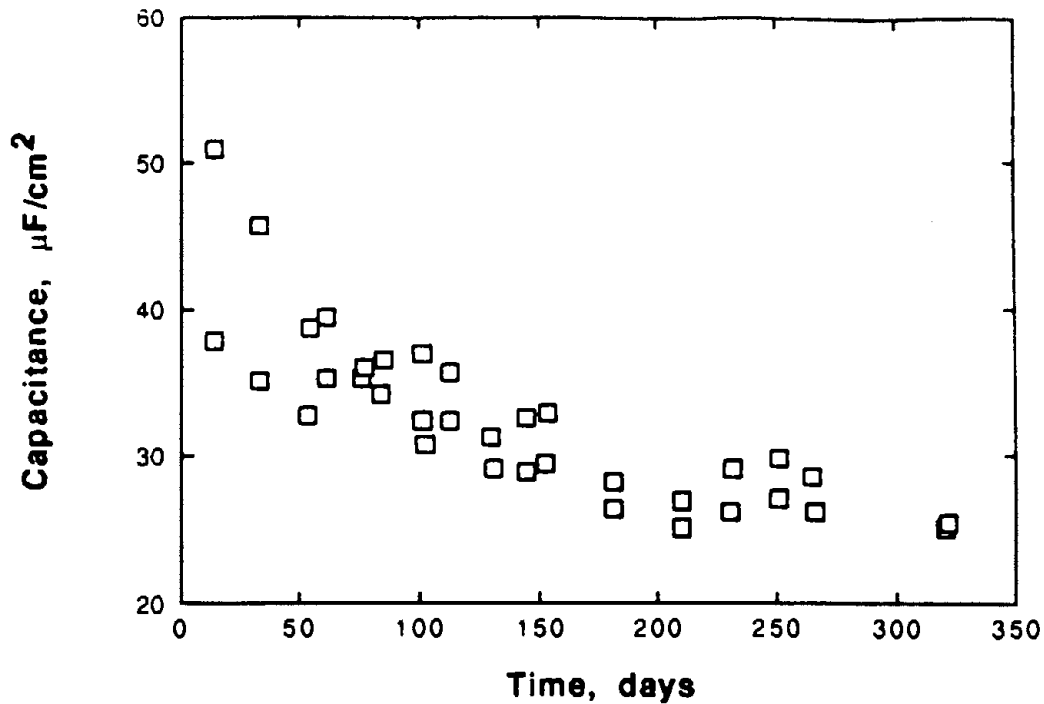
(a) Solution #6, CMA.
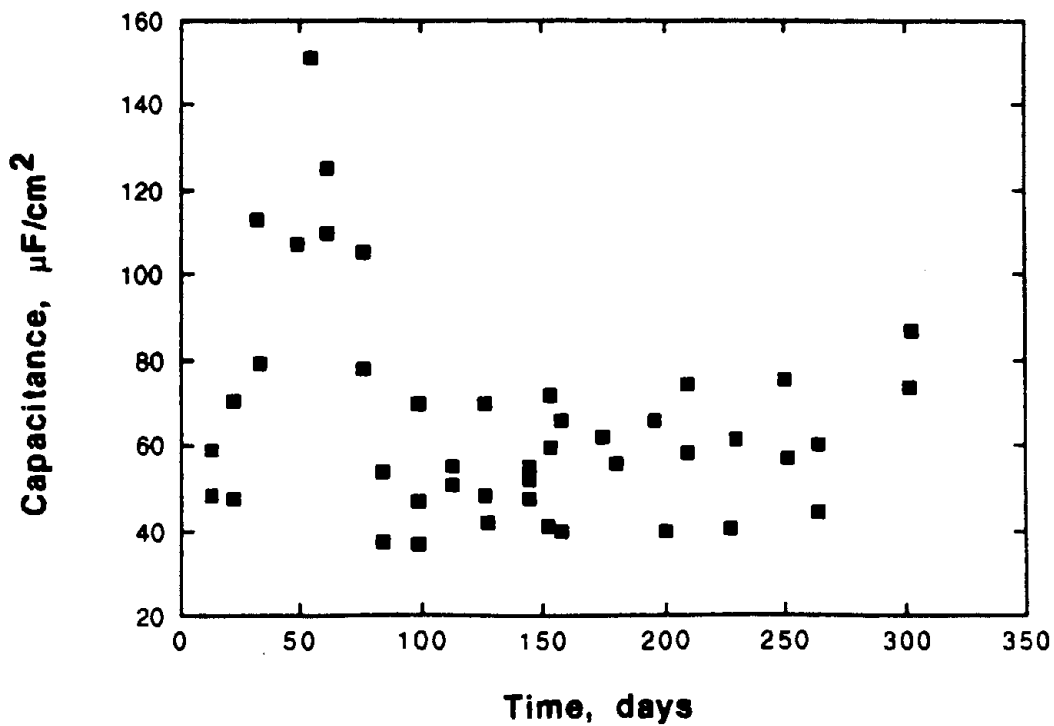
(b) Solution #4.

Figure 32. Double-layer capacitance vs. time (solutions #6 and #4).
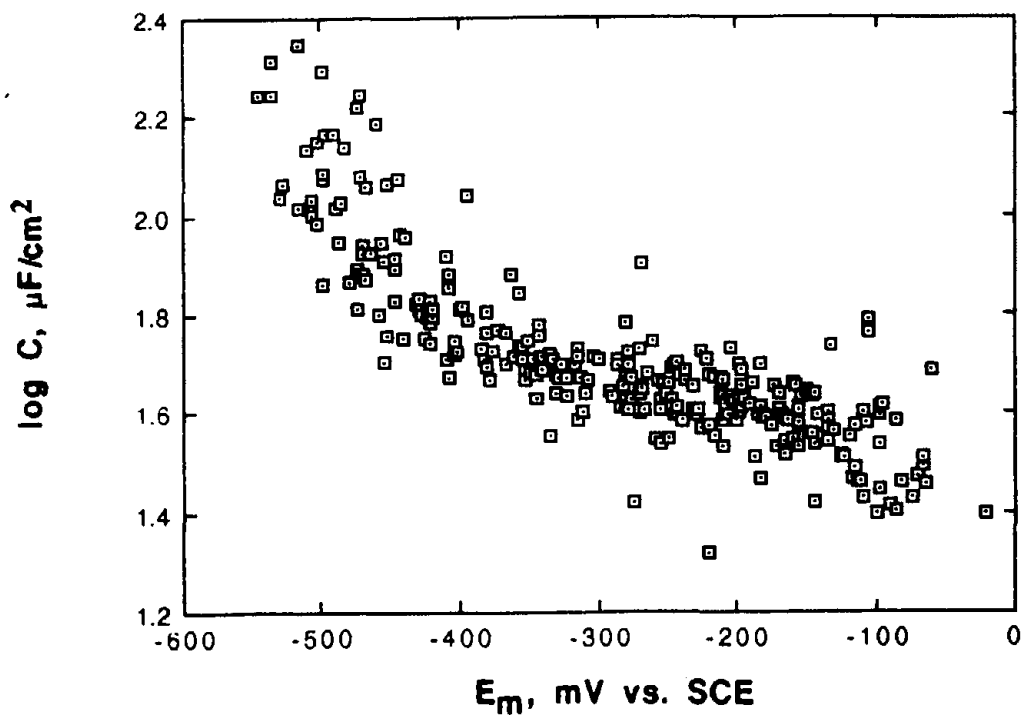
Figure 33. Cumulative plot: Log C vs E .
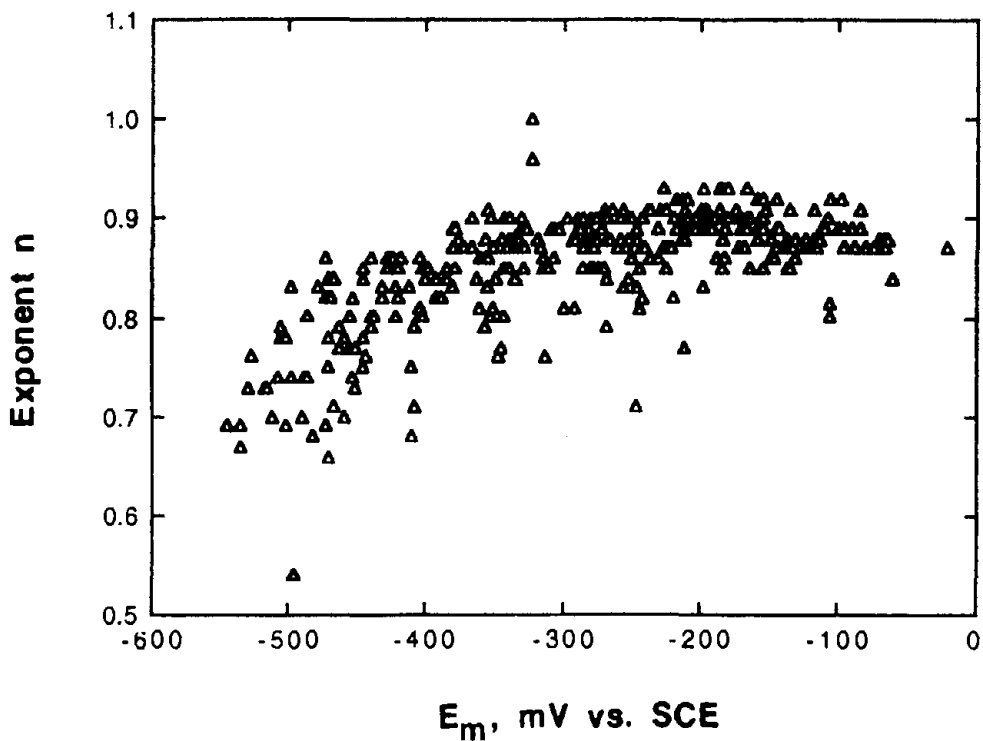
Figure 34. Cumulative plot: Exponent n vs. E .
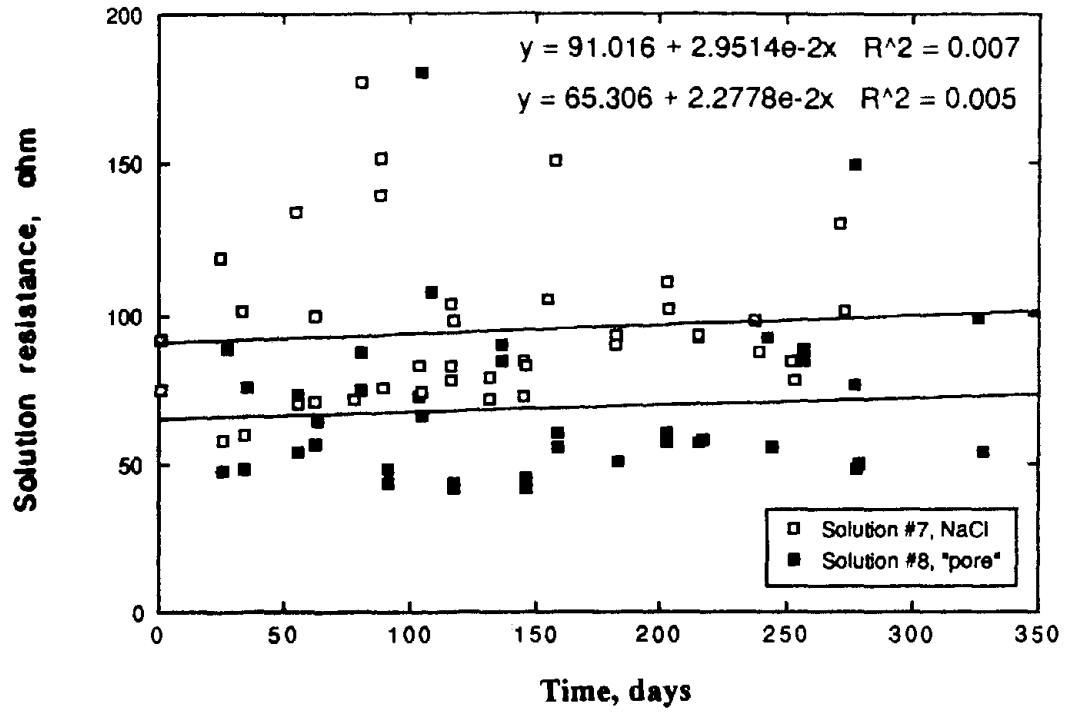
Figure 35. Changes in the electrical resistance of concrete with time (solutions #7 and #8).
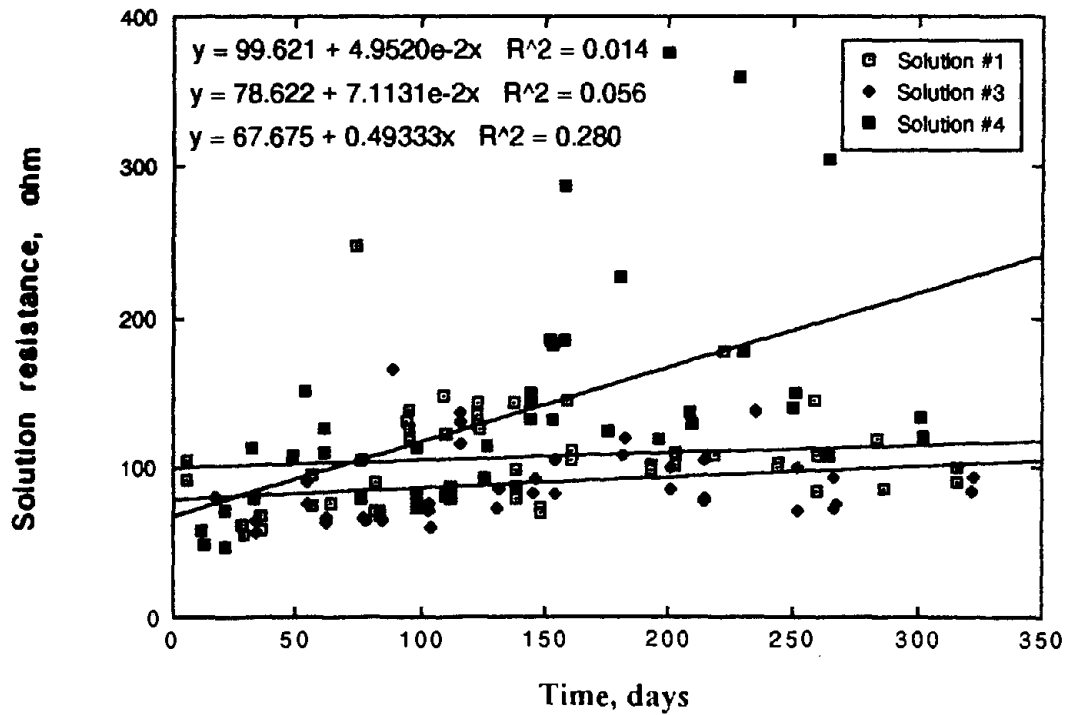
Figure 36. Changes in electrical resistance of concrete with time (solutions # 1, #3, and #4).

56
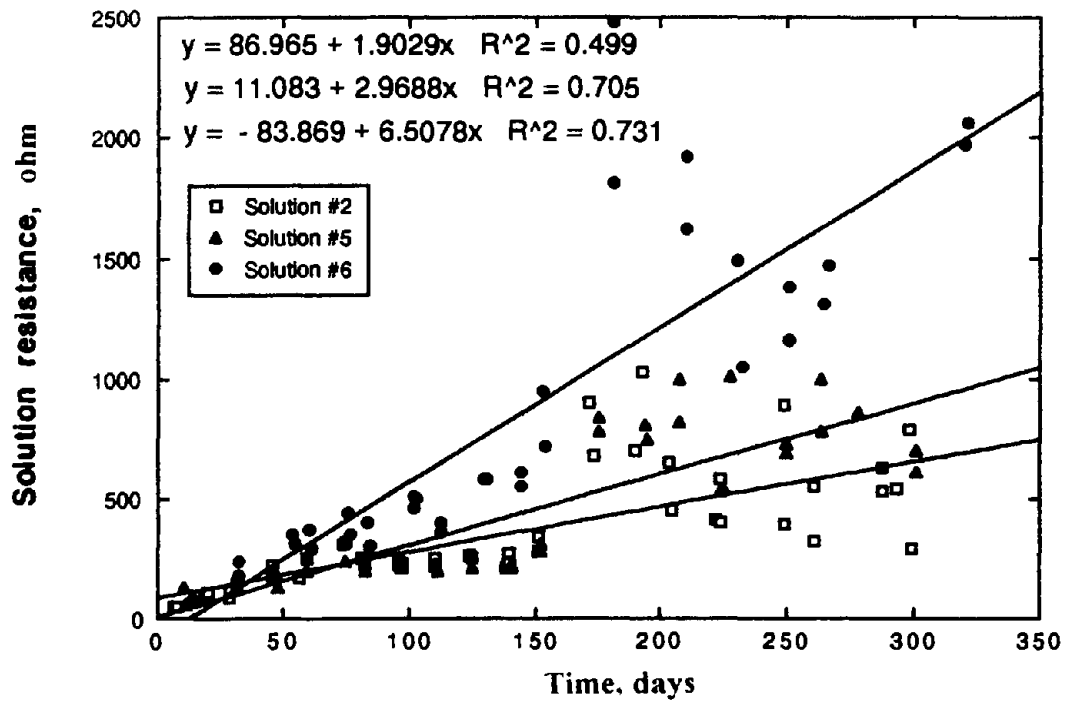
Figure 37. Changes in the electrical resistance of concrete with time (solutions #2, #5, and #6).
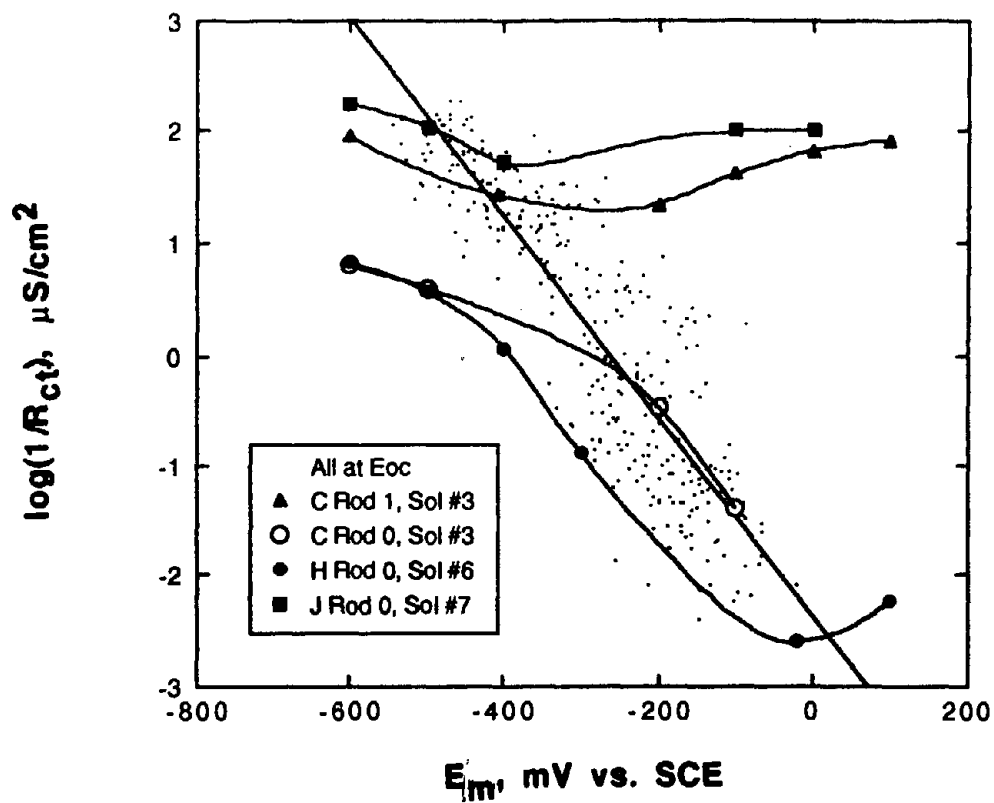
Figure 38. Effect of R_{ct} of polarizing electrodes away from E_{oc}.
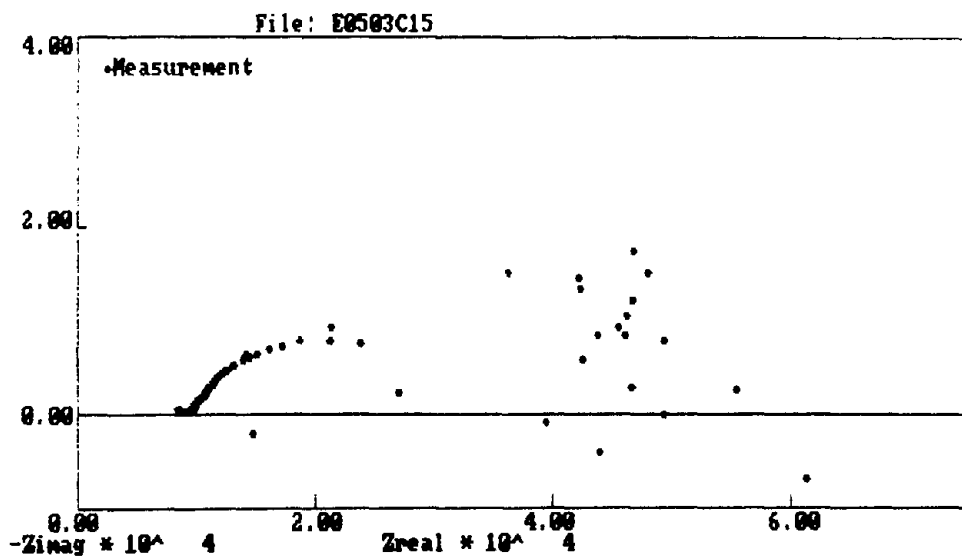
Figure 39. Nyquist plot taken at 0 mV/SCE on rod 1 of specimen C, solution #2
Cl⁻-contaminated concrete, E_{oc}= -496 mV/SCE,

(a) Experimental Nyquist plot.

(b) Simulated Nyquist plot.

(c) Experimental Bode plot.

(d) Simulated Bode plot.
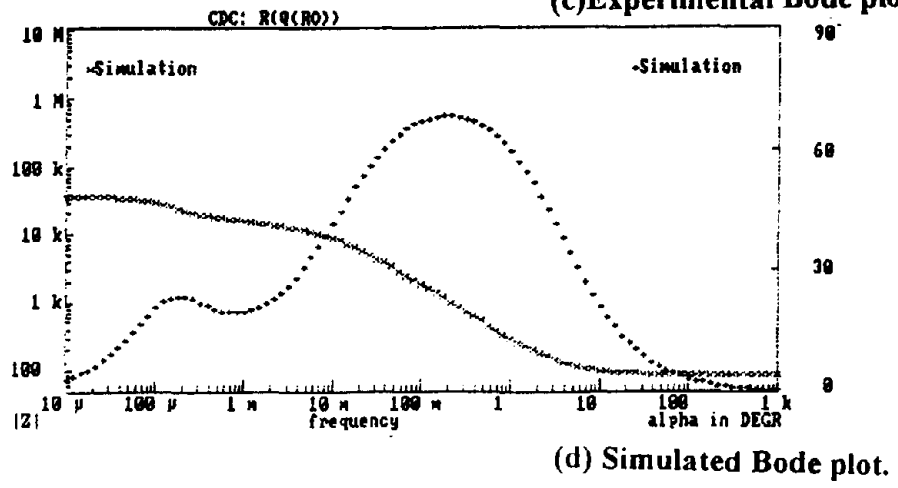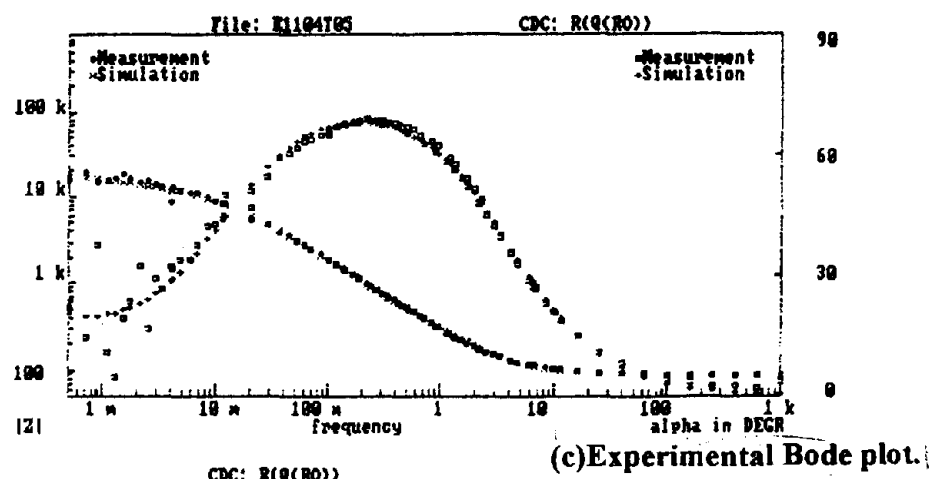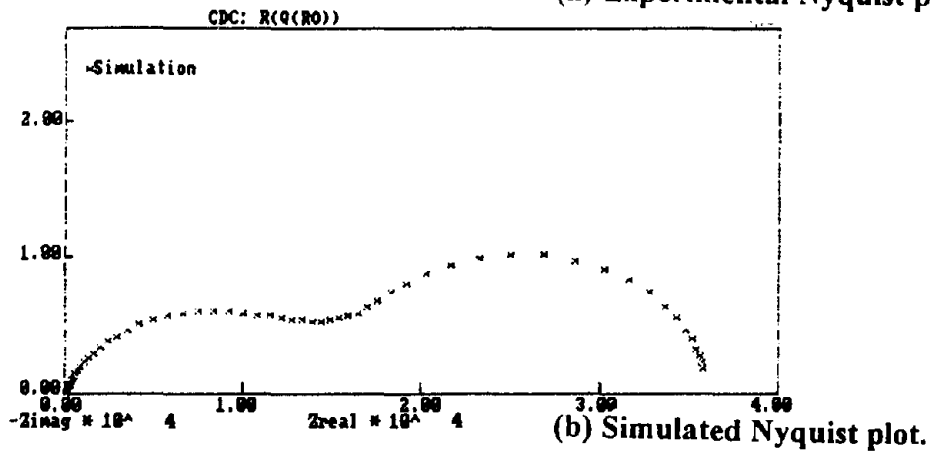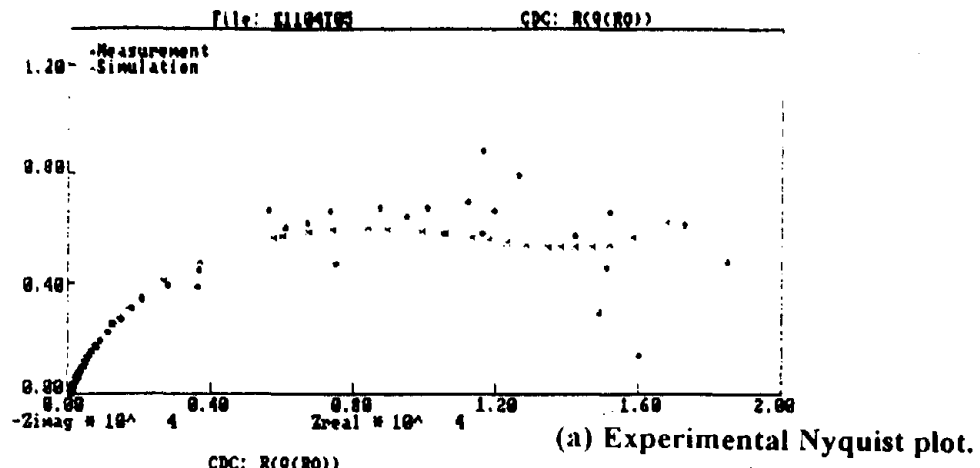
Figure 40. EIS experimental and simulated plots from curve-fitting results
(specimen TT, solution #4, Cl⁻-free concrete).

File: E1215F08

•Measurement

1.50

1.00

0.50

0.00

-Zimag * 10^ 3   Zreal * 10^ 3

(a) Experimental Nyquist plot.

CDC: R(Q(RO))

-Simulation

2.00

1.00

0.00

-Zimag * 10^ 3   Zreal * 10^ 3

(b) Simulated Nyquist plot.

File: E1215F08

•Measurement   •Measurement

1 M

100 k

10 k

1 k

100

|Z| frequency   alpha in DEGR

(c)Experimental Bode plot.

CDC: R(Q(RO))

-Simulation   -Simulation

10 M

1 M

100 k

10 k

1 k

100

|Z| frequency   alpha in DEGR
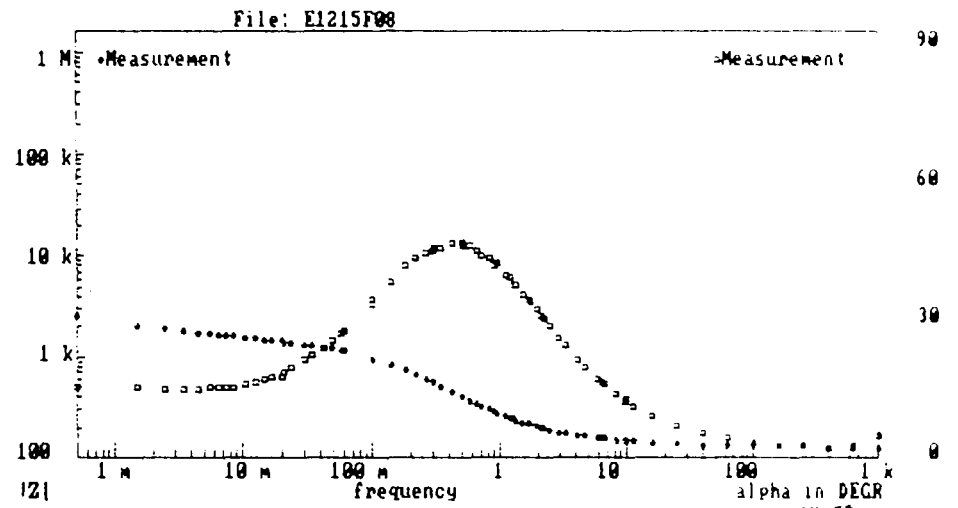
(d) Simulated Bode plot.

Figure 41. EIS experimental and simulated plots from curve-fitting results (specimen F,
solution #4, Cl⁻-contaminated concete).
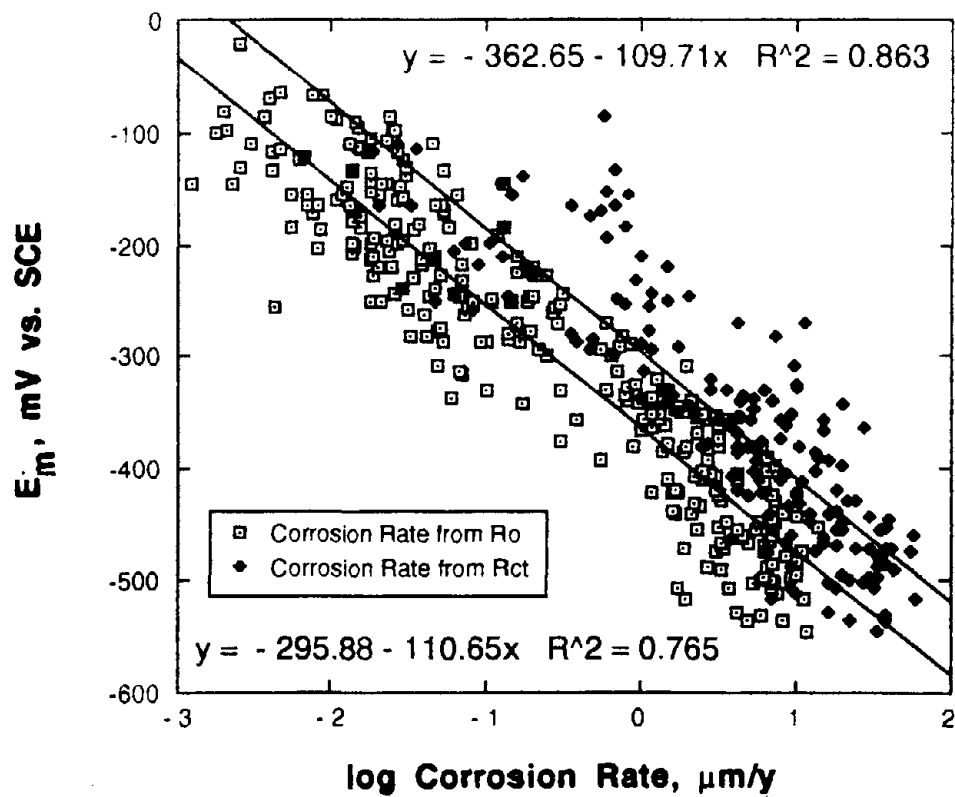
Figure 42. Corrosion rate in micrometers per year as a function of electrode potential calculated from EIS. Cumulative plot for all solutions except #8.
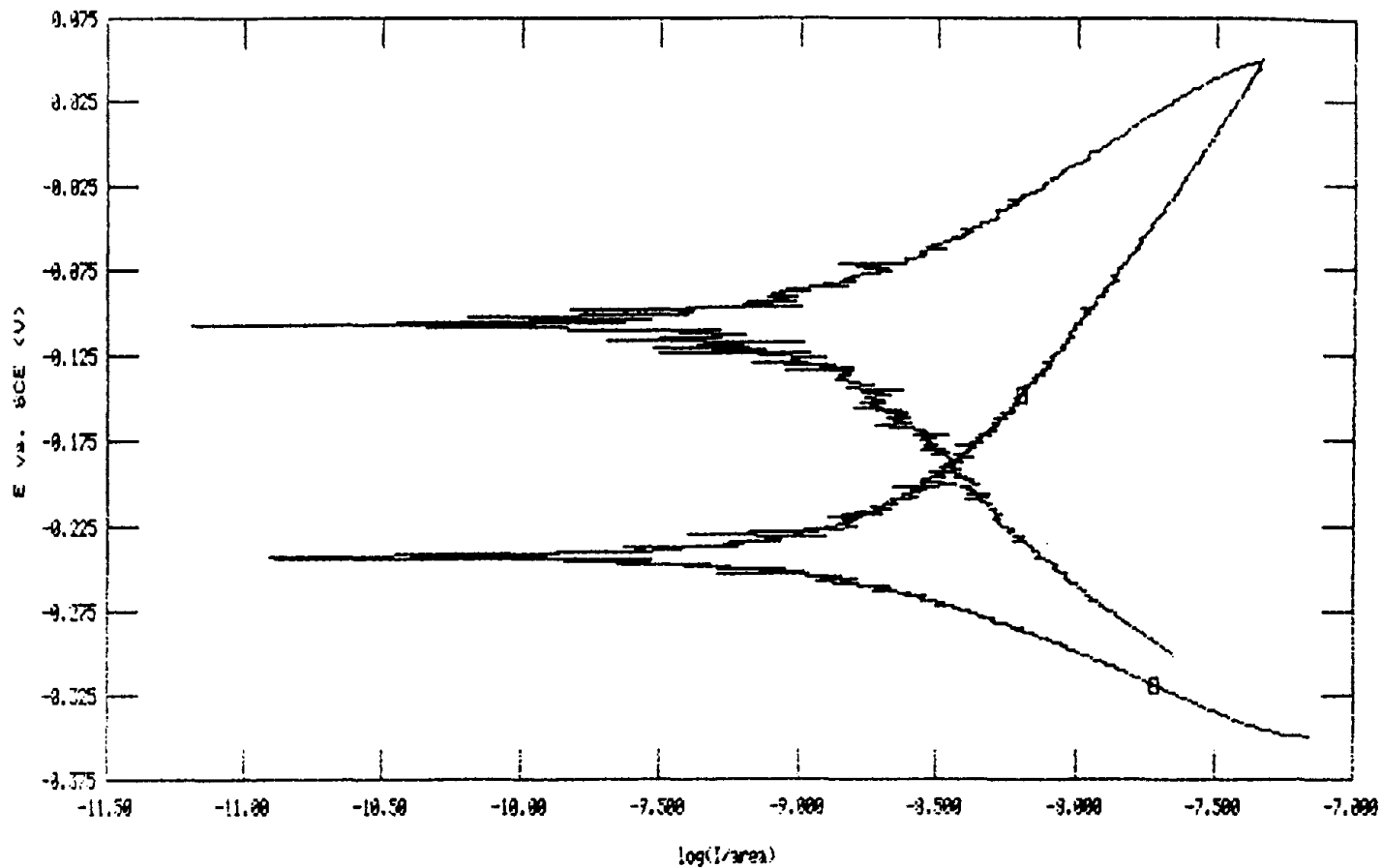
Figure 43. Potentiodynamic scan at 0.0 mV/s taken on rod 1 of specimen K, solution #8, Cl -contaminated concrete.

$y = 3.4354e\text{-}3 + 7.2530e\text{-}3x \quad R^2 = 0.328$

$y = -0.85285 + 4.0890e\text{-}3x \quad R^2 = 0.113$

$y = -0.64272 + 1.0180e\text{-}2x \quad R^2 = 0.592$

$y = -0.65991 + 7.8916e\text{-}3x \quad R^2 = 0.350$

$y = -0.41441 + 6.3501e\text{-}4x \quad R^2 = 0.004$

$y = -0.79175 - 3.8719e\text{-}3x \quad R^2 = 0.405$

$y = -0.27450 + 1.0308e\text{-}2x \quad R^2 = 0.468$

□	#1, "Rct"
■	#2, "Rct"
○	#3, "Rct"
●	#4, "Rct"
△	#5, "Rct"
▲	#6, "Rct"
◆	#7, "Rct"
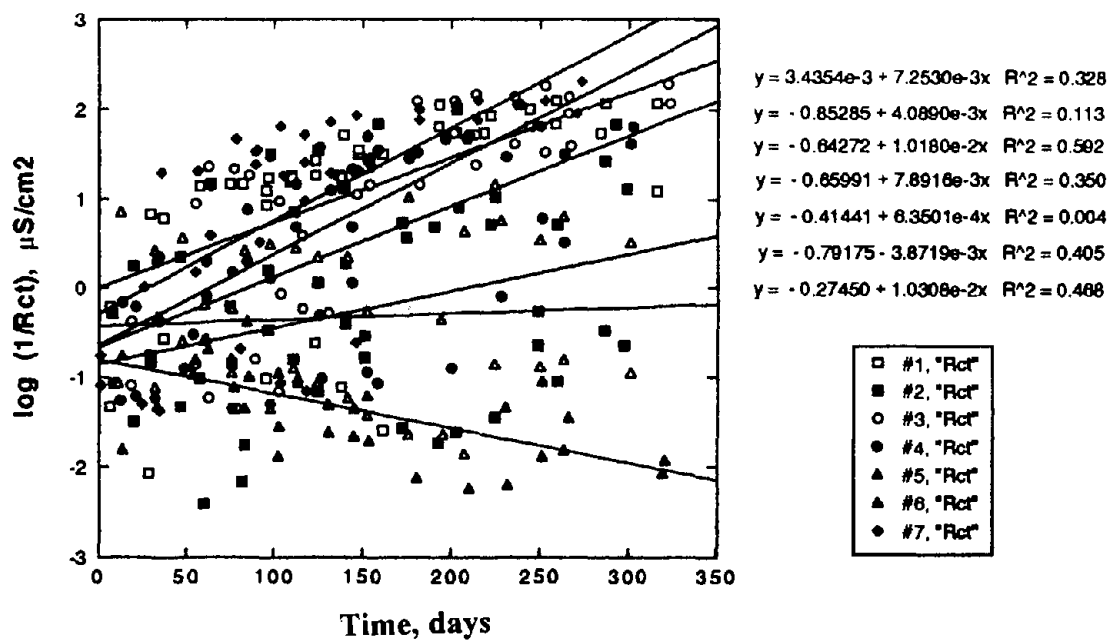
Figure 44. Trend with time of the charge transfer admittance.
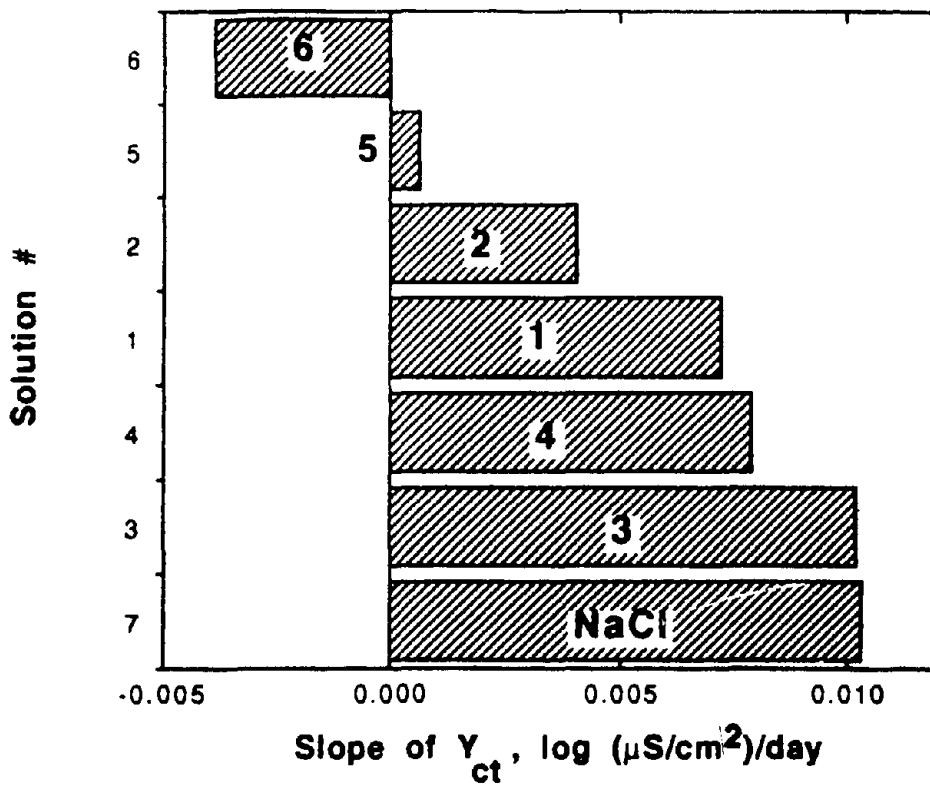
Figure 45. Ranking of the solutions tested in order of increasing corrosivity.

APPENDIX B. TABLES

Table 1. Composition of the solutions used in the measurements.

N	Main constituents	Form	Conc.	Inhibitor	pH of sol.
1	NaCl	solid	13 g/L	Mg phosphate	7.0
2	$MgCl_2$	liquid	30 g/L	citrate	9.3
3	NaCl	solid	13 g/L	?	6.1
4	NaCl 83% $MgCl_2$ 10%	solid	13 g/L	PCI™	6.8
5	$MgCl_2$	liquid	35 g/L	PCI™	6.0
6	30% $Ca(Ac)_2$+ 70% $Mg(Ac)_2$	solid	100 g/L	none	9.7
7	NaCl		0.2 mol/L	none	6.8
8	KOH $Ca(OH)_2$		0.25 mol/L saturated	none	13.3

Table 2. Chloride analysis results.

Solution #	Cl^-, mol/L
1	0.204
2	0.201
3	0.218
4	0.200
5	0.193

Table 3. Schedule of immersion and removal of concrete samples.

N	Immersion	Removal	Notes
1	Wed. 7/16	Fri. 7/23	8 days in
2	Mon. 7/26	Fri. 7/30	
3	Mon. 8/2	Fri. 8/6	
4	Mon. 8/9	Fri. 8/13	
5	Mon. 8/16	Fri. 8/20	
6	Mon. 8/23	Fri. 8/27	no measure
7	Mon. 8/30	Fri. 9/3	
8	Tue. 9/7	Fri. 9/10	short week
9	Mon. 9/13	Fri. 9/17	1 week out
10	Mon. 9/27	Fri. 10/1	
11	Mon. 10/4	Fri. 10/8	
12	Tue. 10/12	Fri. 10/15	short week
13	Mon. 10/18	Fri. 10/22	
14	Mon. 10/25	Fri. 10/29	
15	Mon. 11/1	Fri. 11/5	
16	Mon. 11/8	Fri. 11/12	
17	Mon. 11/15	Fri. 11/19	
18	Mon. 11/22	Fri. 11/26	
19	Mon. 11/29	Fri. 12/3	
20	Mon. 12/6	Fri. 12/10	
21	Mon. 12/13	Fri. 12/17	
22	Mon. 12/20	Thu. 12/23	out till 1/3/94
23	Mon. 1/3	Fri. 1/14	
24	Tue. 1/11	Fri. 1/28	short week
25	Fri. 1/21	Fri. 2/4	6 d. out, 8 d. in
26	Mon. 1/31	Fri. 2/4	
27	Mon. 2/7	Thu. 2/10	short week
28	Mon. 2/14	Fri. 2/18	short week
29	Tue. 2/22	Fri. 2/25	
30	Mon. 2/28	Fri. 3/4	
31	Mon. 3/7	Fri. 3/11	
32	Mon. 3/14	Fri. 3/18	
33	Mon. 3/21	Fri. 3/25	
34	Mon. 3/28	Fri. 4/1	
35	Mon. 4/4	Fri. 4/8	short week
36	Tue. 4/12	Fri. 4/15	
37	Mon. 4/18	Fri. 4/22	
38	Mon. 4/25	Fri. 4/29	
39	Mon. 5/2	Fri. 5/6	
40	Mon. 5/9	Fri. 5/13	5 d. out, 9 d. in
41	Thu. 5/19	Fri. 5/27	
42	Tue. 5/31	Fri. 6/3	
43	Mon. 6/6	Fri. 610	

Table 4. Specimens used in the tests.

Chloride-free concrete		Chloride-contaminated concrete	
Designation	Solution #	Designation	Solution #
NN	1	A	1
PP	2	B	2
RR	2	C	2
SS	3	D	3
TT	4	E	4
VV	4	F	4
WW	5	G	5
XX	6	H	6
YY	7	J	7
ZZ	8	K	8

Table 5. Preliminary measurements on dry specimens.

	Min Freq. mHz	R_{sol} Ω	Capacitance		Open Circuit Potential	
			C_{dl}, $\mu F/cm^2$	n	Rod# vs.Rod#	E_{oc} mV
A	5	577	17.8	0.90	0 vs.3	13
D	50	529	17.5	0.85	0 vs. 3	1
	50	540	16.7	0.86	2 vs. 3	-16
E	5	427	20.4	0.89	0 vs. 3	-5
F	50	433			0 vs. 3	13
K	50	522	20.1	0.83	0 vs. 3	-8
NN	50	457			0 vs. 3	9
PP	5	413	19.1	0.90	0 vs. 3	3
RR	50	480	21.5	0.84	0 vs. 3	-11
SS	50	422			0 vs. 3	-4
TT	5	459			0 vs. 3	5
XX	50	464			0 vs. 3	1
YY	50	480			0 vs. 3	1
ZZ	5	417	21.5	0.90	0 vs. 3	-18

Table 6. Weight of concrete samples in grams.

	Dry 5/14/93	Wet 12/3/93	Dry 12/6/93	Wet 12/23/93	Dry 1/3/94
A	576.9	608.0	596.1	607.5	588.5
B			584.0	590.7	579.0
C	569.0			586.0	574.9
D	566.0			595.5	576.3
E	557.7	587.0	575.1		567.8
F	559.6				
G	567.5		579.2		573.6
H	564.0	587.9	569.0		
J	547.8			576.7	557.5
K	556.3	585.7	580.8	585.7	562.7
NN	562.9			592.0	573.8
PP	555.8		566.0	573.6	561.2
RR	555.8				562.1
S S	555.0				564.2
TT	558.7			586.9	567.8
VV	561.8				568.9
WW	555.5				
XX	570.2		584.8	591.3	582.5
YY	556.5			583.9	564.9
ZZ	559.8			585.8	565.5

Table 7. Values from potentioidynamic scans obtained by curve fitting.

Spec	Sol #	Scan dir.	E(I=0) mV/SCE	i_{corr} nA/cm^2	β_a mV/dec	β_c mV/dec	R_p kΩxcm^2
NN	1	Up	-494	651	98	32	1.2
		Down	-341	712	152	193	3.3
C	2	Up	-481	3380	600	327	1.8
		Down	-415	4120	575	563	1.9
D	3	Up	-554	2900	192	205	0.7
		Down	-337	2087	163	295	1.4
SS	3	Up	-450	54	89	36	13
		Down	-415	143	38	131	3.6
G	5	Up	-334	15.7	?	89	89
		Down	-56	14	52	240	107
H	6	Up	-287	8.4	740	124	420
		Down	7	3.7	131	370	860
K	8	Up	-270	5.7	?	250	405
		Down	-222	1.6	88	69	432

Table 8. Intercept and slope of the electrode admittance with potential
$\log(Y)=a + b^*E$.

Sol	1/R$_o$			1/R$_{ct}$		
	a	b	R^2	a	b	R^2
1	-320	-107	0.82	-217	-134	0.54
2	-306	-98	0.78	-213	-133	0.71
3	-307	-118	0.83	-281	-90	0.61
4	-285	-101	0.87	-210	-119	0.72
5	-278	-83	0.65	-205	-33	0.05
6	-273	-94	0.47	-282	-115	0.60
7	-316	-115	0.85	-238	-112	0.68
all 7	-305	-110	0.86	-238	-111	0.77
8	-281	-355	0.38	-235	-56	0.44

Table 9. Effect of varying RE on R_{sol} and C_{dl}.

Spec.	Sol. #	WE	RE	R_{sol} Ω	C_{dl} $\mu F/cm^2$	Ratio $(R_{sol})x/(R_{sol})_{SCE}$
G	5	0	SCE	858	43.6	1
		0	3	446	44.1	0.52
		0	2	505	43.4	0.59
XX	6	0	SCE	2068	25.1	1
		0	3	1167	25.4	0.56
		0	2	1344	25.2	0.65

Table 10. Values of EIS parameters obtained from rods 0 and 1 of specimen C at different potentials (solution #2, Cl^--contaminated concrete).

Rod 0	Rod 1	E_m mV/SCE	R_o $M\Omega xcm^2$	R_{ct} $k\Omega xcm^2$	C_{dl} $\mu F/cm^2$	n
	•	100	0.036	12	55	0.81
•		0	17.6	-	34.1	0.88
	•		0.05	17	55.5	0.87
	•		0.1?	14	70.6	0.73
	•		?	13	75.2	0.74
	•		?	15	87.6	0.65
•		-100	24.3	-	34.1	0.88
	•		0.039	24	61.4	0.79
	•		-	17	100	0.61
•		-199	17	2900	40.2	0.83
	•	-200	0.074	45	66.8	0.74
•		-312	4.4	-	40.1	0.85
	•	-409	0.12	37	82.7	0.68
	•	-496	0.03	15	146	0.54
•		-500	0.25	-	74.5	0.73
•		-600	0.16	-	133	0.57
	•		?	11	220	0.48

REFERENCES

[1] D.T. Ireland, in *Chemical Deicers and the Environment*, F.M. D'Itri, editor, p. 403, Lewis Publishers, Boca Raton, FL (1992).

[2] R.L. McCrum, ibid., p. 363.

[3] D.G. John, P.C. Searson, and J.L. Dawson, *Brit. Corr. J.*, Vol. 16, p. 102 (1981).

[4] P. Lay, P.F. Lawrence, N.J.M. Wilkins, and D.E. Williams, *J. Appl. Electrochem.*, Vol. 15, p. 755 (1985).

[5] F. Wenger and J. Galland, *Electrochim. Acta*, Vol. 35, p. 1573 (1990).

[6] K.K. Sagoe-Crentsil, F.P. Glasser, and J.T. Irvine, *Brit. Corr. J.*, Vol. 27, p. 113 (1992).

[7] M.I. Jafar, J.L. Dawson, and D.G. John, in *Electrochemical Impedance: Analysis and Interpretation*, J.R. Scully, D.C. Silverman, and M.W. Kendig, eds., p. 284, ASTM, Philadelphia (1993).

[8] E. Escalante and S. Ito, in *Corrosion Rates of Steel in Concrete*, N.S. Berke, V. Chaker, and D. Whiting, eds., p. 86, ASTM, Philadelphia (1990).

[9] B.L. McFarland and K.T. O'Reilly, in *Chemical Deicers and the Environment*, F.M. D'Itri, ed., p. 193, Lewis Publishers, Boca Raton, FL (1992).

[10] U. Bertocci and R.E. Ricker, in *Computer Modeling In Corrosion*, R.S. Munn, ed., p. 143, ASTM, Philadelphia (1992).
U. Bertocci and R.E. Ricker, in *Electrochemical Impedance: Analysis and Interpretation*, J.R. Scully, D.C. Silverman, and M.W. Kendig, eds., p. 284, ASTM, Philadelphia (1993).

[11] F. Wenger and J. Galland, *Mat. Sci. Forums*, Vols. 44 and 45, p. 375 (1989).

[12] T.J. Hakkarainen, ibid., p. 347.

[13] Danish Corrosion Centre, *Effect of CMA on Corrosion Properties of Rebars in Concrete*, December 1990.

[14] E. Escalante, in *Corrosion of Reinforcement in Concrete*, C.L. Page, K.W.J. Treadaway, and P.B. Bamforth, eds., p.281, Elsevier, London (1990).

[15] J. Flis, S. Sabol, H.W. Pickering, A. Sehgal, and K. Osseo-Asare, *Corrosion*, Vol. 49, p. 601 (1993).